Field Emission Properties of a Silicon Tip Array

FUNG YUN MING

A Thesis Submitted in Partial fulfilment
of the Requirements for the degree of
Master of Philosophy
in

Department of Electronic Engineering

April 2001

Abstract of thesis entitled:

Field Emission Properties of a Silicon Tip Array

Submitted by FUNG YUN MING

For the degree of Master of Philosophy in Department of Electronic Engineering

at The Chinese University of Hong Kong in April 2000

Abstract

Field emitter arrays are very popular in the field of vacuum micro-electronic devices, and field emitters are fabricated by various methods. In this thesis, new methods were adopted to fabricate field emitters in order to decrease the fabrication time, and to improve field emission properties by using different surface treatments and coating materials of different work function.

In part I of this thesis, three fabrication methods were studied. These were; a two-step anodization method, a texturing etching method and the formation of porous silicon. For the two step anodization of silicon different concentrations of HF solutions were used. The turn-on voltage for a wide range of tip profiles was found to be in the region of 27V/μm, much lower than that obtained by conventional wet. In addition, different shaped field emitters having good uniformity and reproducibility were fabricated on <111> and <100> silicon. The current densities were achieved about 100 $\mu A/cm^2$. For the second method, texturing etching was used to form randomly distributed silicon field emitters without any masking pattern. The turn-on voltage and current density were in the range of 24-38V/μm and 500 $\mu A/cm^2$ respectively. The third method was the formation of porous silicon (PS). This has a high density of very sharp asperities, each of which can behave as a site

for field emission. A dramatic improvement in the emission properties was observed. The turn-on voltage of PS layers and the overall current density of field emitters were about 12-25 V/μm and 100-500μA/cm^2 respectively.

In part II of this thesis, the influence of amorphous carbon (a-C) coatings on porous silicon (PS) and single crystal silicon surface by DC magnetron sputtering was studied. The field emission properties were further improved by deposition of a-C. The turn-on voltage and current density were in the range at 10-17V/μm and 900 μA/cm^2 respectively. Besides, we found that silicon carbide (SiC) synthesized by ion implantation of carbon both by modification of work function and by sputter etching the surface can improve the field emission properties of textured surfaces. The turn-on voltage and current density were in the range of 10-19V/μm and 100 μA/cm^2. In addition the a-C and SiC layers improved the stability of field emission with time, especially on PS surfaces.

摘要

在真空微電子的研究裏，場致電子發射器是一個非常熱門的題目. 本論文的主要研究目的是找尋不同的方法來減少制備場致電子發射器的時間，並找尋不同的涂覆材料來改善場發射器的表面功函數．

在本文的第一部分，採用了陽極氧化、織構化的方法和採用多孔硅的表面來制備場致發射器．在陽極氧化的方法下，採用了兩種不同濃縮度的刻蝕來制備場致發射器．其電子場發射的閥值電壓爲 27V/μm，而採用傳統制備方法制備的場致發射器，其閥值電壓爲 35V/μm．在<111> 和 <100>硅片上，能夠制備不同形狀的場致發射器．其電流密度爲 100 μA/cm^2．在織構化的方法下，能夠制備隨機分散的場致發射器，無需掩蔽圖案來設定場致發射器的形狀．其閥值電壓和電流密度分別大約爲 24-38 V/μm 和 100 μA/cm^2．至於多孔硅這種物質，它擁有高密度而且突出的峰，對於改善場發射有很明顯的幫助．其閥值電壓和電流密度分別大約爲 16-25 V/μm 和 500 μA/cm^2．

在本文的第二部分，主要是探討非晶碳涂覆在多孔硅和碳化硅涂覆在隨機分散的場致發射器對場發射的特性的影響．透過直流磁控濺射的方法，把非晶碳涂覆在硅和多孔硅上，以多孔硅的高密度而且突出的峰來增加非晶碳的粗糙面，藉此來增加場發射的機會．其閥值電壓和電流密度分別大約爲 10-17 V/μm 和 900 μA/cm^2．最後，透過金屬真空弧離子源的方法，把碳化硅涂覆在隨機分散的場致發射器，藉此來減少隨機分散的場發射器的功函數．

Acknowledgement

I would like to thank my supervisor, Professor I.H. Wilson, head of the Department of Electronic Engineering. Professor Wilson has taught me a lot, his generous guidance, encouragement, and patience are essential to my research study and thesis.

I would like to thank Professor J.B. Xu and Professor S.P. Wong for their support and advice.

I would like to thank Dr. W.Y. Cheung for his technical assistance in all experiments, measurements, and every necessary thing. I would like to thank Dr. W.Y. Cheung and Dr. B. Sundaravel for their suggestions on my thesis. I would like to thank Dr. D. H. Chen for his help on translating the thesis abstract.

I was very lucky to work with the largest research term in Electronic Engineering Department, the Chinese University of Hong Kong, the Solid State Laboratory. I would like to thank my colleagues Dr. W.Y. Cheung, Dr. N. Ke, Dr. D.H. Chen, Dr. B. Sundaravel, Dr. E.Z. Luo, Mr. L. Pang, Mr. S. Lin, Dr. G.D. Hu, Dr. Z.Q. He, Mr. W.K. Chan, Mr. M. F. Chiah, Mr. R. Venugopal, Miss H. Y. Guo, Mr. W. F. Lau, Miss P.S. Chung, Mr. C.H. Ng, Miss Y. Gao and Mr. H.J. Peng for their help, suggestions and advice on my research.

Of course, I wouldn't be here if it wasn't for the love and patience of my wonderful parents, sister and brother. Also, I would like to thank Miss Alman Wong and all my friends for their help and support. I would like to thank the Graduate School and Electronic Engineering Department, the Chinese University of Hong Kong, for providing the Graduate studentship and financial support for conference attendance.

TABLE OF CONTENTS

List of Figure Captions

List of Table Captions

Chapter 1 Introduction

Introduction

Field emitter arrays (FEAs) are very popular in the field of vacuum microelectronic devices. FEAs have been applied in flat panel field emission displays (FED) which are being pursued aggressively by a number of companies worldwide as an alternative to liquid crystal displays (LCDs).

FED technology's performance in video, graphics, text and multimedia applications offer countless opportunities to improve today's electronic products and enable tomorrow's. An advantage of FED technology is its high packing density and lightweight. It provides a powerful combination of bright and crisp images with very fast response times, low power requirements and wide viewing angles. For these reasons, it makes an ideal platform for a wide variety of electronic products.

FEAs are electron sources that have the form of arrays of sharp tips. When an electrode is biased to a sufficiently large positive potential with respect to the tips, electron emission takes place from the tip to vacuum via electron tunneling through the solid-vacuum potential barrier at the surface of a solid. This phenomenon is known as field emission.

The field emission effect has been investigated since the beginning of this century. The concept of field emitter was introduced in the early sixties when Shoulders proposed devices based on microfabricated field emission sources [1]. The concept was put in practice by Spindt in 1968 [2]. The Spindt-type emitters came to denote metal FEAs fabricated via evaporation of the material through a shrinking aperture. Silicon-based microfabricated FEAs were demonstrated in 1972 by Thomas et al. [3]. These arrays were ungated FEAs. A method for incorporating

the gate was proposed by Smith et al [4]. In the eighties Gray introduced the concept of an integrated microfabricated vacuum transistor based on gated silicon FEAs. The gated FEAs were fabricated by using etching and oxidation sharpening techniques, and their electrical characteristics was reported [5-8].

The emission characteristics of a field emitter strongly depends on the geometry and work function of the material. The best value of emission currents at a reasonable external field (in the range of a few hundred volts) can be obtained with the following parameters. Emitter material with low work function (ϕ), high emitter density micrometric size of the emitter with height (h), radius(R) and h/R >>1 and nanometer size of the apex tip radius.

The goal of this work is to improve the field emission properties of silicon field emitters by using different fabrication methods and coating of the emitter surface with different materials with various work functions.

Three different new fabrication methods are optimized to improve the size and density of the silicon field emitters. (i) A two step anodization method is explored in order to simplify the fabrication process. (ii) An anisotropic texturing method is used to improve the density and size of emitters. (iii) The formation of porous silicon on low resistivity n-type silicon is utilized to fabricate the nanometer sized tips for field emission.

The coating of the silicon field emitter with low work function materials has been investigated. The deposition of amorphous carbon (a-C) film on silicon and porous silicon by using DC magnetron sputtering and the implantation of SiC into the silicon emitter by using Metal Vapour Vacuum Arc (MEVVA) ion implantation was found to improve the field emission properties of the silicon field emitter.

Chapter 2 Theory and Applications

Theory and Application

2.1 Principle of field emission

2.1.1 The Fowler-Nordheim Theory

The application of quantum mechanics to the emission of electrons from metal surface under the action of strong applied electric fields is enshrined in the "Fowler-Nordheim Equation" [9].

The assumptions made are as follows:

1. The cathode surface is a perfectly smooth conducting plane.
2. The force on an electron outside the cathode surface is the sum of the forces due to the charge induced on the surface (i.e., the image force) and that due to the externally applied electric field.
3. A conduction electron can travel the distance from the surface to an external point where its potential energy is equal to the kinetic energy of its state inside the metal by "tunneling" through the classically forbidden region where the potential energy is larger than the initial kinetic energy. The probability of tunneling is given by quantum theory. The electron is then accelerated by the external electric field and can be collected by the anode.

The image force F on an electron of charge $-e$ at a distance x from a conductive plane is given by

$$F = -e^2 / 4\pi\xi_o (2x)^2 \qquad \text{Eq. 2.1}$$

where ξ_o is the absolute permittivity of vacuum. This force attracts the electron to the surface. If an external electric field E is applied in the opposite direction, the total force is given by

$$F = Ee - e^2/16\pi\xi_o x^2 \qquad \text{Eq. 2.2}$$

If the energy associated with the velocity component of an electron moving in a direction perpendicular to a surface is designated ε, then the current escaping from a unit area of the surface is given in general by

$$J = e\int_{-\infty}^{+\infty} N(T,\varepsilon)D(E,\varepsilon,\phi)d\varepsilon \qquad \text{Eq. 2.3}$$

where $N(T, \varepsilon)d\varepsilon$ is the number of electrons incident upon the surface per unit area per second with velocity component perpendicular to the surface in the associated energy range ε to $\varepsilon + d\varepsilon$, when the crystal is at temperature T; $N(T, \varepsilon)$ is called the supply function. $D(E, \varepsilon, \phi)$ is called the transmission function and it is the probability of an electron with kinetic energy ε penetrating a potential barrier of work function ϕ with the applied external field E.

The supply function for conduction electrons may be calculated using the quantum statistical theorem that for a free electron, each volume h^3 of phase space can contain only two states, combined with the Fermi-Dirac probability that each state of energy ε is occupied when the system is at temperature T [10] and is given by

$$N(T,\varepsilon) = \{4\pi mkT/h^3\}\ln[1+\exp(-\varepsilon/kT)] \qquad \text{Eq. 2.4}$$

where m is the mass of the electron, h is Planck's constant, and k is Boltzmann's constant. As $T \to 0$, $\exp(\varepsilon/kT)$ becomes >> 1 and $\log[1+\exp(\varepsilon/kT)] \to \varepsilon/kT$

Hence $N(0,\varepsilon) = (4\pi m\varepsilon/h^3)$ Eq. 2.5

For field emission at T=0, it has been shown [11] that the transmission function is given by $D(\varepsilon) \sim \exp[-2\kappa(\varepsilon)]$ Eq. 2.6

where $\kappa(\varepsilon) = (2\pi/h)\int_0^{u_0} |p| du$ Eq. 2.7

p is the momentum at point u along the path, and u_o is the value of u where the potential energy = e and the electron is free to move under action of the external field.

Now $p^2 = 2m$ {(initial kinetic energy)-(the work done against the image force in reaching point u)+(the energy gained from the external field E)}

That is, for a plane cathode

$$p = \left\{2me\left[\varepsilon - \int_d^u e/(16\pi\xi_0 u^2)du + Eu\right]\right\}^{1/2} \quad \text{Eq. 2.8}$$

where d is the distance from the surface where the image force commences. The distance d is introduced as the distance the electron can move perpendicular to the surface without doing any work and at which the classical image force begins to act. The value of d needs to be finite if ϕ is to be finite. Note that p is imaginary when the image force potential energy is greater than the initial kinetic energy plus the energy gained from the external field. Fowler and Nordheim [9] are able to evaluate κ(ε) using (Eq. 2.8) in terms of a function $v(y)$ of the dimensionless variable

$$y = \{Ee/4\pi\xi_0\}^{1/2}/\phi \quad \text{Eq. 2.9}$$

where

$$\phi = \int_d^\infty e/(16\pi\xi_0 u^2)du = e/(16\pi\xi_0 d)V \quad \text{Eq. 2.10}$$

and ϕ is the work function with E=0 for electrons at energy ε inside the metal, leading to

$$D \sim \exp\left\{-4(2me^3)^{1/2} v(y)/[3(h/2\pi)eE]\right\} \quad \text{Eq. 2.11}$$

Putting (Eq. 2.5) and (Eq. 2.11) into (Eq. 2.3) and integrating yields the Fowler-Nordheim equation for field emission at zero temperature

$$J = \{e^3 E^2 8\pi h \phi_0 t^2(y)\} \exp\left[-8\pi(2m)^{1/2} \phi_0^{3/2} v(y)/3heE\right] \quad \text{Eq. 2.12}$$

Where $v(y)$ and $t(y)$ are the Nordheim elliptic functions of y using $\varepsilon = \varepsilon_f$, the Fermi energy, and ϕ_0 is the zero temperature, zero field work function for an electron at the Fermi energy. Computed values of these functions are available, but to a good approximation we may write $t^2(y)=1.1$ and $v(y)=0.95-y^2$, leading to

$$J = \left(1.5\times10^{-6} E^2/\phi_0\right) \exp\left\{10.4/\phi_0^{1/2}\right\} \exp\left\{-6.44\times10^7 \phi_0^{3/2}/E\right\} A/cm^2 \quad \text{Eq. 2.13}$$

2.1.2 Field emission from metals

In the field emission phenomenon, an electron is tunnelled through a potential barrier at the surface by applying a large electric field. Field emission is distinct from thermionic emission and photoemission in which electrons acquire sufficient energy via heating or energy exchange with photons, respectively, to overcome the potential barrier. The presence of the electric field makes the width of the potential barrier finite and therefore permeable to the electrons. Figure 2.1 presents a diagram of the electron potential energy at the surface of a metal.

The dashed line in Fig. 2.1 shows the shape of the barrier in the absence of an external electric field. The height of the barrier is equal to the work function of the metal, ϕ. The work function of the metal is the energy required for an electron moving from the Fermi level E_F of the metal to the vacuum level. The solid line in Fig. 2.1 corresponds to the shape of the barrier in the presence of the external electric field. The barrier becomes triangular in shape and the height of the barrier in the presence of the electric field E is smaller, with the lowering given by [12]

$$\Delta\phi = \left(\frac{eE}{4\pi\varepsilon_o}\right)^{\frac{1}{2}} \qquad \text{Eq 2.14}$$

where e is the elementary charge and ε_o is the permittivity of vacuum.

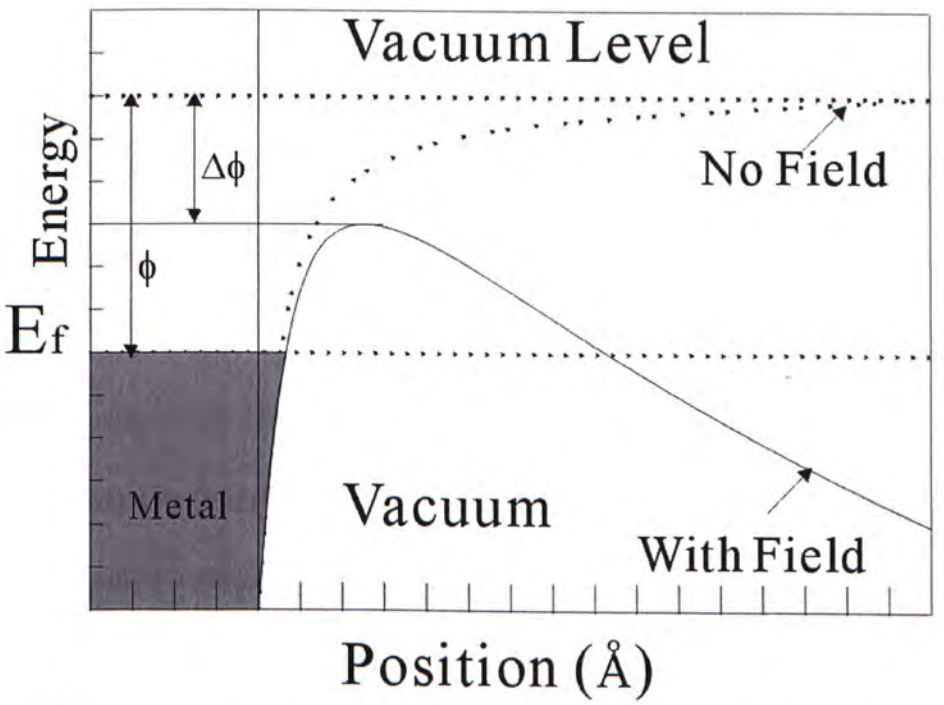

Figure 2.1. Diagram of the potential energy of electrons at the surface of a metal.

By using the shape of the energy barrier, the probability of an electron with a given energy tunneling through the barrier can be calculated. Integrating the probability function and then multiplying by an electron supply function in the available range of electron energies leads to an expression for the tunneling current density J as a function of the external electric field E. The tunneling current density can be expressed by Eq. (2.15) which is often referred to as the Fowler-Nordheim equation [13-15]

$$J = \frac{e^3E^2}{8\pi h\phi t^2(y)}\exp\left[\frac{-8\pi(2m)^{\frac{1}{2}}\phi^{\frac{3}{2}}}{3heE}v(y)\right] \qquad \text{Eq 2.15}$$

Where $y = \Delta\phi/\phi$ with $\Delta\phi$ given by Eq.(2.14) , h is planck's constant, m is the electron mass, and $t(y)$ and $v(y)$ are the Nordheim elliptic functions; to the first

approximation $t^2(y)$=1.1 and $v(y)=0.95-y^2$. Substituting these approximations in Eq.(2.15), together with Eq.(2.14) for y and values for the fundamental constants, one obtains [11]

$$J = 1.42x10^{-6}\frac{E^2}{\phi}\exp\left(\frac{10.4}{\phi^{\frac{1}{2}}}\right)\exp\left(\frac{-6.44\times10^7\phi^{\frac{3}{2}}}{E}\right) \qquad \text{Eq 2.16}$$

where J is in units of Acm^{-2}, E is in units of Vcm^{-1} and ϕ in units of eV. Plotting the $log(J/E^2)$ versus $1/E$ results in a straight line with the slope proportional to $\phi^{3/2}$.

2.1.3 Field emission from semiconductors

For the case when the external electric field penetrates into the interior of an n-type semiconductor and the surface states are neglected, $log(J/E^2)$ is shown to be a linear function of $1/E$, as for metals.

The work function ϕ in the Fowler-Nordheim equation is substituted by a quantity χ-δ, where χ is the electron affinity defined as the energy required for removing an electron from the bottom of the conduction band of the semiconductor to a rest position in the vacuum, and δ denotes the band bending below the Fermi level. These parameters are illustrated in Fig. 2.2.

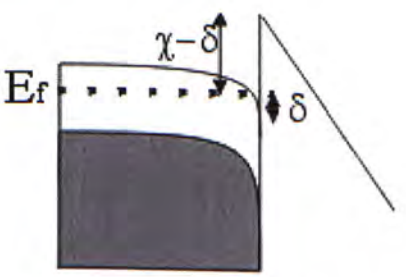

Figure 2.2. Diagram of the potential energy of electrons at the surface of an n-type semiconductor with field penetration into the semiconductor interior.

The linear dependence of $log(J/E^2)$ versus $1/E$ is expected only if the density of carriers flowing through the sample is much less than the current limiting density $J_{\lim} = en\mu_n E/\varepsilon$, where μ_n, is the electron mobility and n is the electron concentration in the bulk of the semiconductor [16-18]. At $J \approx J_{lim}$, the Fowler-Nordheim character of the relationship $J(E)$ passes into the Ohmic behaviour which results in the appearance of the saturation region in the emission current versus voltage curve [16]. Such saturation regions are observed experimentally for lightly doped n-type semiconductors and for p-type semiconductors [18-20].

2.1.3.1 Advantages and limitations of silicon

The followings are the advantages and limitations of silicon:

Advantages:

1. Any manufacturer with existing IC fabrication facilities can start making microtip arrays immediately.
2. Oxidation and other overcoating techniques have enabled turn on driving voltages of 10V or less to be obtained with silicon microtips.
3. When a large number of arrays have to be independently addressed, the driving circuitry can be fabricated on the same silicon surface and directly connected to the cathodes.

Limitations:

1. Size and coating of the substrate are limited by available wafer suppliers.
2. IC processing may not be compatible with the processes required for fabrication of the tips and the formation of the vacuum envelope.
3. The maximum current per tip obtained with silicon is limited.

2.1.4 Application of the Fowler-Nordheim Theory

Typically, the field emission current I is measured as a function of the applied voltage V and substitute $J=I/A$ and $E=\beta V$ in (Eq. 2.13), where A is the emitting area and β is the local field conversion factor at the emitting surface. Combining these relationships gives

$$I = aV^2 \exp(-b/V)$$

where

$$a = \left(1.56\times10^{-6} A\beta^2 / 1.1\phi_0\right)\exp\left\{10.4/\phi_0^{1/2}\right\}$$

$$b = -6.44\times10^7 \phi_0^{3/2} / \beta V$$

Anode current I as a function of corrected anode voltage V can be collected by computer automatically.

Plotting log (I/V^2) versus $1/V$ should yield a straight line. Indeed, linear "Fowler-Nordheim" plots are usually obtained over many orders of magnitude of current, indicating the general validity of the theory.

The I vs. V data are typically plotted in the Fowler-Nordheim coordinates, $log(I/V^2)$ vs. $1/V$, to test linearity of the relationship and determine the a and b parameters which are functions of the field enhancement factor β, emission area A, and the work function ϕ.

In addition to the parameters a and b, current density and turn-on voltage is also determined. FEA current density is defined as the anode current divided by the physical area which the array occupies. Turn-on voltage or threshold voltage is defined as the gate voltage for which the anode current of the order of μA is measured.

2.1.5 Factors influencing field emission efficiency

The field emission characteristics can be described by the Fowler-Nordheim theory. The field emission efficiency is proportional to the emission area, the field enhancement factor β at the emission site and work function ϕ of the emission surface.

From the Fowler-Nordheim theory [15], the field emission process is very sensitive to the initial state, and changes therein of the emitter tip surface. Factors influencing field electron emission include :

(1) The morphology of the surface,

(2) The material of the emitter tip,

2.2 Applications

The recent application of flat panel displays in multi-media portable electronics has spurred a renewed interest in developing field emission displays. FEDs are of most interest since they result in the most desirable aspects of a CRT such as emissive display, full color, gray scale, wide viewing angle and high resolution. In addition, this display is thin, light-weight, rugged, low power, wide operating temperature range, matrix addressed and will not generate radiation.

2.2.1 Operation of a Field Emission Displays

The cathode which is a part of the panel baseplate consists of an X-Y electrically addressable matrix of field emitter arrays. Each field emitter is located at the intersection of a row and a column conductor, with the row conductor serving as the gate electrode and the column conductor as the base. The locations where the rows and columns intersect define a pixel. Pixel area and number of tips are

determined by the desired resolution and luminance of the display. Typically, each pixel contains an FEA of 500-5000 tips. The emission current required for a pixel varies from 0.1 to 10μA, depending on factors such as the desired luminance of the display, phosphor efficiency and the anode voltage.

When a field emitter is addressed via applying suitable voltages to the base and gate conductors, electrons are emitted and accelerated towards the phosphor-coated transparent faceplate which serves as an anode as shown in figure 2.3. When electrons strike the phosphor layer, light is produced and then image is formed on viewer. FEDs employ physical support spacers between the faceplate and the baseplate to prevent collapse of the panel as a result of the gradient between the atmospheric pressure and the low pressure inside the panel. [21-24]

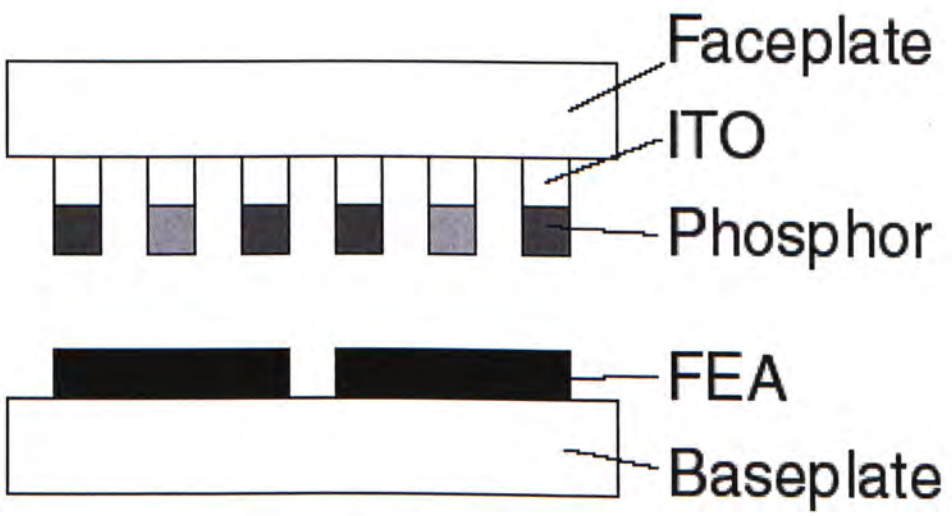

Figure 2.3. Schematic of the FED anode colors produced sequentially

2.2.2 Basic structure of an Field Emission Displays

In principle, a field emission display is similar to a conventional CRT. Electrons emitted from a material surface under high electric field are accelerated onto a phosphor screen to generate light. There are two basic display structures, diode and triode as shown in figure 2.4. Most of the field emission displays are driven in a matrix-addressed fashion with scan-a-line at a time scheme. This driving method applies a half of the operating voltage to off-pixels, called a half select. A diode display consists of simple cathode stripes on the back plate and phosphor coated ITO stripes on the front plate. The smallest features are on the order of pixel size, thus even printed wiring board (PWB) type lithography can be used. Obviously, the process for making this type of the display is extremely simple. These two plates are separated by a suitable distance approximately 10-30μm and the pixels are formed at the intersection of cathode and phosphor stripes [25].

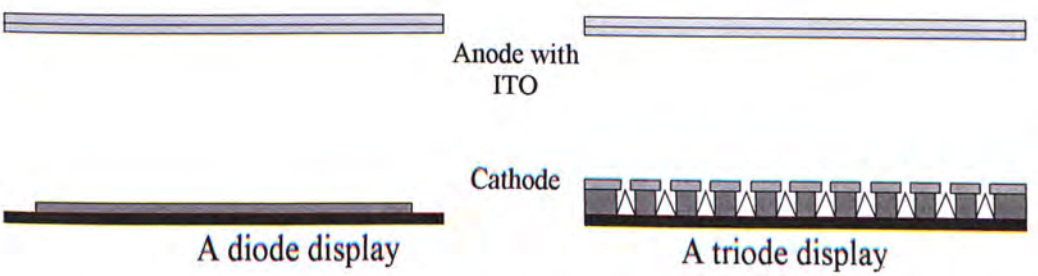

Figure 2.4. The basic structure of triode and diode field emission display

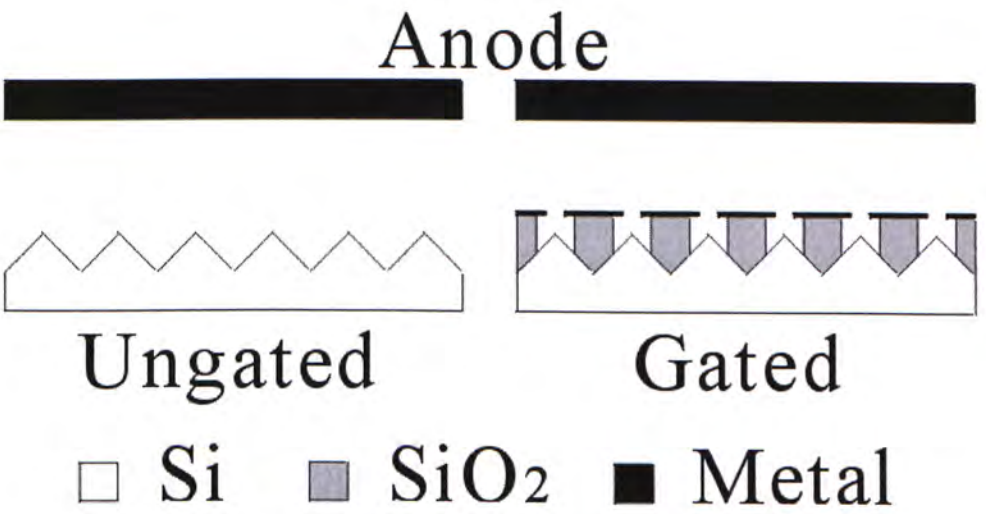

Figure 2.5. Schematic diagram of ungated and gated field emitter

The ungated field emitter constitutes the simplest form of microfabrication as shown in figure 2.5. Ungated field emitters are sharp tips, with the tip height and width, and the tip-to-tip spacing in the order of micrometers. It requires an external electrode to provide the electric field for field emission. Typically, this external electrode also serves as a collector of emitted electrons.

For a gated field emitter [26-29], the gate electrode that provides the field necessary for field emission is integrated into the device structure. This gate electrode is insulated from the cathode by a layer of a dielectric material. Due to the tip sharpness and the small distance between the tips and the gate (typically less than 1 μm), the gate bias required for field emission is typically only in the order of 100V.

The gated microtip field emission display [30, 31] is the most popular field emission display because of its advantages: low power, mature technology, low voltage and manufacturability. Compared to other field emission displays such as diode and monolithic diode. In this triode field emission display, electrons extracted by applying a positive potential to the gate, is accelerated to bombard the phosphor layer on the anode. The phosphor excited by bombardment of electrons emits light.

This display uses a large number of very fine microtip cold cathodes as the sources of electrons. Micron size microtips and concentric grids are necessary to achieve enhanced electric field.

Electrons are generated at room temperature without the heating necessary in conventional CRTs. In fact, emitters use "cold cathode" technology. It consumes only a small fraction of the power used by the traditional CRT's hot cathode and FED does not require the shadow mask used in conventional CRTs, which can waste up to 80% of the power. Conventional CRTs consist of a large bell-shaped tube while the FED uses a flat tube which has a thickness of only 3.5 millimeters.

2.2.3 Parameters relevant to applications

The FED performance parameters vary as a function of the device characteristics, such as pixel capacitance, phosphor efficiency and cathode uniformity [32-35].

The difference between FEDs and CRTs lies in how electrons which excite phosphors are generated and delivered to the phosphor coated anode. In CRTs, the source of electrons is the electron gun or guns for generation of either a single electron beam for monochrome CRTs or three electron beams for colour CRTs. The operation of CRT displays involves deflection of the beams in such a way that electron spot scans the screen line-by-line. In FEDs, multiple electron beams are generated from the field emission cathode and no scanning of the electron beam is required.

The most important factor is the driving voltage. For some applications where a large number of drivers are required, it is important that the driving voltage must be as low as possible so that low cost integrated circuits can be used.

The second important factor in the construction of the FED is the current density available over the whole cathode area.

There are two main FED system architectures: high voltage and low voltage [36]. The advantage of the high voltage architecture is the ability to use conventional high performance CRT phosphors. However, it requires larger cathode-to-anode distance that requires high aspect ratio spacers and also need focusing of the electron beams emitted by the cathode.

The low anode voltage system has the advantage of a simpler design with no need for focusing or high aspect ratio spacers. However, the system need low voltage phosphors, in comparison with the high voltage counterparts which require more current per area to deliver the same power to the phosphors. This might affect the lifetime of the low voltage phosphors since the phosphor luminance decays in proportion to the total electronic charge delivered to the phosphor layer. Besides, phosphor luminance decreases when power is over a wide range of voltage [37-41].

To complete the FED system, various electronic subsystems are needed to control the operation of the display. These subsystems include the video controller, panel controller, and row and column drivers [42].

A number of companies, including Candescent Technologies, Futaba, Fujitsu, FED Corporation, Motorola, Micron Display, PixTech, Raytheon and Samsung, are involved in the development of field emission displays as shown in table 2.1.

Table 2.1. Summary of performance of some of field emission display engineering/sample prototypes

Organization	Type of display	Size (diagonal)	Resolution
Pixtech	Monochrome (green)	5.2 in.	320x240
	Color	5.6 in.	320x240
Raytheon	Monochrome (green)	5.2 in.	512x512
	Color	8.5 in.	512x512
Futaba	Monochrome (green)	5 in.	320x240
Motorola	Color	5.6 in.	320x240

2.3 The fabrication processes

Various methods have been used to fabricate silicon tip arrays. They are generally classified into wet, dry, or combined etching. The principle is that silicon not protected by the mask is etched away and further back etched into the part covered by the mask, so a sharp tip is formed. Usually, an SiO_2 mask is used. The shape of tips can be a rounded whisker, sharpened pyramid, semi-spheroidal or pyramidal. For any kind of shape, the tip should be as sharp as possible, because a strong electric field is resulted at the tip and electrons can be emitted from the tip at a lower voltage.

There are several etching methods for the formation of a field emitter.

- Anisotropic wet etching uses a KOH system [43]. Etching is orientation dependent and sharply pointed pyramids are formed. The masks being used are usually SiO_2 and Si_2N_4, because they are stable and easy to form.
- The molding based technique is anisotropic wet etching of a mold. It is also called the cusp molding method. [44, 45]

- The isotropic etching method makes use of chemicals consisting of isotropic etchant (HNO_3 / HF / CH_3COOH) and isotropic oxidating agent [46-49].
- The dry etching (RIE) technique allows better control over the emitter aspect ratio. The reactants are plasma generated from the following gases [50-51] :
  1. $SF_6 + C_2ClF_5$, the mask is made out of photoresist and SiO_2
  2. $SF_6 + O_2$, the mask is made of Al or SiO_2
  3. $SF_6 + CCl_2F_2$, the mask is made of Ni
- A hybrid etching technique combines both dry and wet etching techniques.

2.3.1 The anisotropic wet etching method

Wet chemical anisotropic etching is restricted to the crystallographic orientations. The orientation of the relevant crystal planes with respect to particular directions is of great importance. The etch rate of the <111> plane is the slowest. Anisotropy is given by

$$A = 1 - \frac{R_L}{R_V}$$

where R_L and R_V are the lateral and vertical etch rates.

A process is said to be perfectly anisotropic (A=1) if the lateral etch rate is zero. On the other hand, A=0 would imply that the lateral and vertical etch rates are identical.

The method of describing anisotropy using wagon wheel pattern is shown in figure 2.6 [52]. It is used to observe the anisotropy and determine the rate of etching under a mask that is aligned along a particular crystallographic direction of a wafer of a given crystallographic orientation. The wagon wheel pattern makes anisotropic etching easily visible and minute underetching of the spokes is easily measureable in a radial direction.

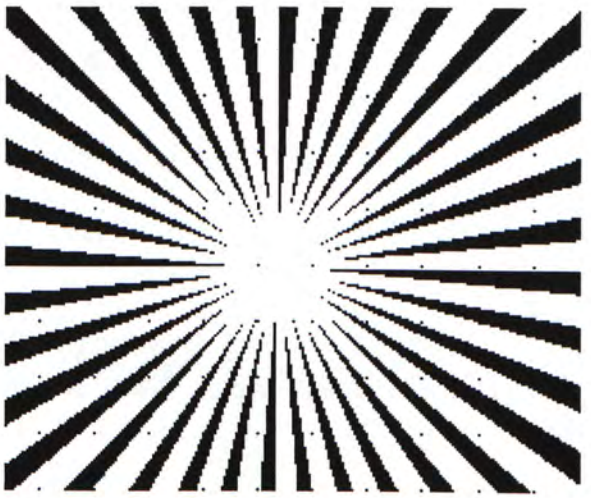

a) Mask pattern for the wagon wheel method.

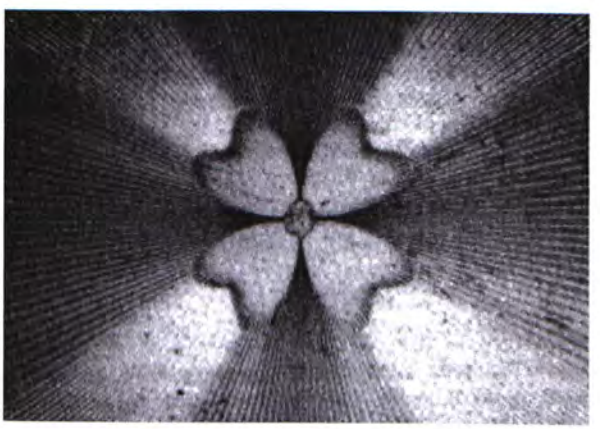

b) Photograph of the result of underetching a wagon wheel on the <100> oriented silicon wafer [52].

Figure 2.6. Illustration of a) wagon wheel pattern and b) <100> oriented silicon wafer

2.3.2 The isotropic wet etching method

Comparing with the anisotropic etching, the process of isotropic etching has some attractive features. It is a room temperature process, it is much faster and photoresist is a suitable masking material.

When an isotropic etchant is used, the etching will be uniform along radial direction, the silicon under oxide mask is etched away and a tip is eventually formed as shown in figure 2.7.

A common etchant solution to be used is a combination of Hydrofluoric acid (HF) and nitric acid (HNO_3) in acetic acid (CH_3COOH). The overall reaction is given by

$Si + HNO_3 + 6HF \rightarrow H_2SiF_6 + HNO_2 + H_2 + H_2O$

Acetic acid is used as a solvent instead of water.

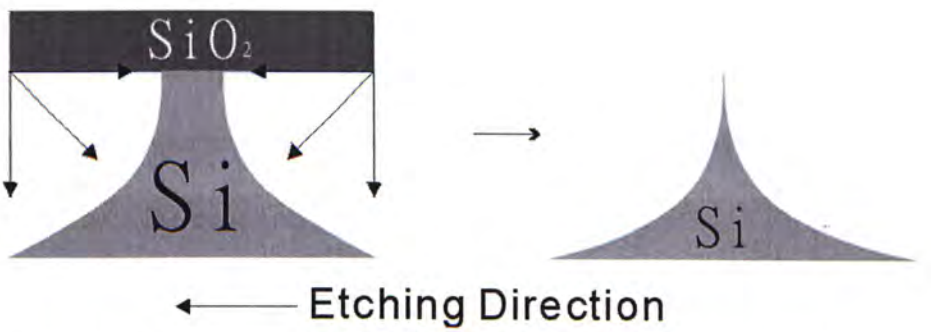

Figure 2.7. The etching direction profile by Isotropic etching solution

2.3.3 Field emission from coating materials

2.3.3.1 Coating enhancement

Silicon constitutes the primary material of fabricated FEAs. Other materials have been examined as coatings on silicon emitters. Single element metals, such as cesium, platinum, gold, nickel, potassium, lithium [53-55], metallic compounds such as refractory metal nitrides and carbides [56, 57], and various types of diamond or diamond-like-carbon (DLC) films [58-63] are examined as coatings. In this work, the field emission characteristics of porous silicon, amorphous carbon and silicon carbide are also studied.

2.3.3.2 Diamond and diamond-like films

The original interest in investigating emission properties of diamond or diamond-like-carbon (DLC) films is due to the fact that certain crystallographic orientations of diamond exhibit negative electron affinity (NEA). The bottom of the conduction band lies above the vacuum level, and, therefore, there is no potential barrier for the electron emission from the conduction band.

The electron emission current density depends not only on the barrier height, but also on the electron supply function which in turn depends on the electron concentration in the conduction band. Because of the wide band gap of diamond, the conduction band has to be populated by n-type doping to obtain significant electron emission.

Nitrogen is an n-type dopant in diamond but its energy level is significantly below the bottom of the conduction band. Consequently, the increase of concentration of electrons due to the nitrogen doping is insignificant. Exact mechanisms of the electron injection from metal contacts, and the electron transport through the diamond film still remain subjects of theoretical modelling and discussions [64-68]. While p-type doping of diamond has been demonstrated, effective n-type doping is still elusive.

A large number of investigators demonstrate that diamond and DLC coatings do exhibit a lower effective work function than Si [69-83]. The voltage for which emission is observed for all the coated FEAs is considerably lower than the voltage for the uncoated FEA. The shift in the current-voltage characteristics towards lower voltages is ascribed to the lowering of the effective work function of the emitter surface [63].

2.3.3.3 Metallic coatings

Metal carbides and nitrides are of interest because of their low reported work function, and high chemical and mechanical stability [84]. Coatings of ZrC, HfC and TaN have been examined [54, 56-57].

2.3.3.4 Porous silicon coatings

Porous silicon contains a high density of very sharp micro asperities [85-87], each of which may behave as a site for field emission [88-91]. A dramatic improvement in emission properties is observed. Porous silicon can be formed using both n-type and p-type material. Porous silicon coated FEAs exhibit a lower effective work function than uncoated FEAs. We have established that the turn-on voltage for which emission is observed for the porous silicon coated FEAs is considerably lower than that for the uncoated FEA.

2.3.3.5 Silicon carbide coatings

Silicon Carbide (SiC) properties have been widely studied and applied. The many advantages of silicon carbide, with its ability to withstand high temperatures being the most prominent, is making it a choice for new applications and an improved substitute for traditional electronic materials. The attractive properties of SiC include high electron mobility, high breakdown field strength, high thermal conductivity, and excellent chemical stability. The applications for SiC semiconductors and SiC materials range from avionic application to computers.

There is a considerable amount of effort to synthesize SiC thin layers by using ion implantion [92-98]. The electron emission characteristics of SiC prepared by carbon implantation using MEVVA ion source, have been investigated [99-100].

Dihu chen et al [99-100] had shown that the electron field emission from planar SiC/Si heterostructures at a remarkably low turn-on field is due to the improvement of the surface morphology and work function. And high emission current with a stable current density can be obtained at a lower applied field.

2.3.4 Fabrication of field emitters with gate

A silicon field emitter with a metal gate can be formed using either anisotropic or isotropic etching techniques. Figure 2.8 shows the fabrication process flow for a silicon tip with metal gate electrode. As a capping layer on the field emitter, a layer of SiO_2 is deposited. This layer forms the gate-to-base insulator. In order to define the gate electrode, a photoresist pattern is created prior to the gate metal deposition in the regions where the gate metal is not desired. Then the metal gate layer is deposited by directional e-beam evaporation, and the photoresist is removed in PR stripper to lift off the metal from the selected areas. After the metal patterning, the caps are removed via etching in buffered HF, and a hemispherical cavity in the insulator is created [101-105].

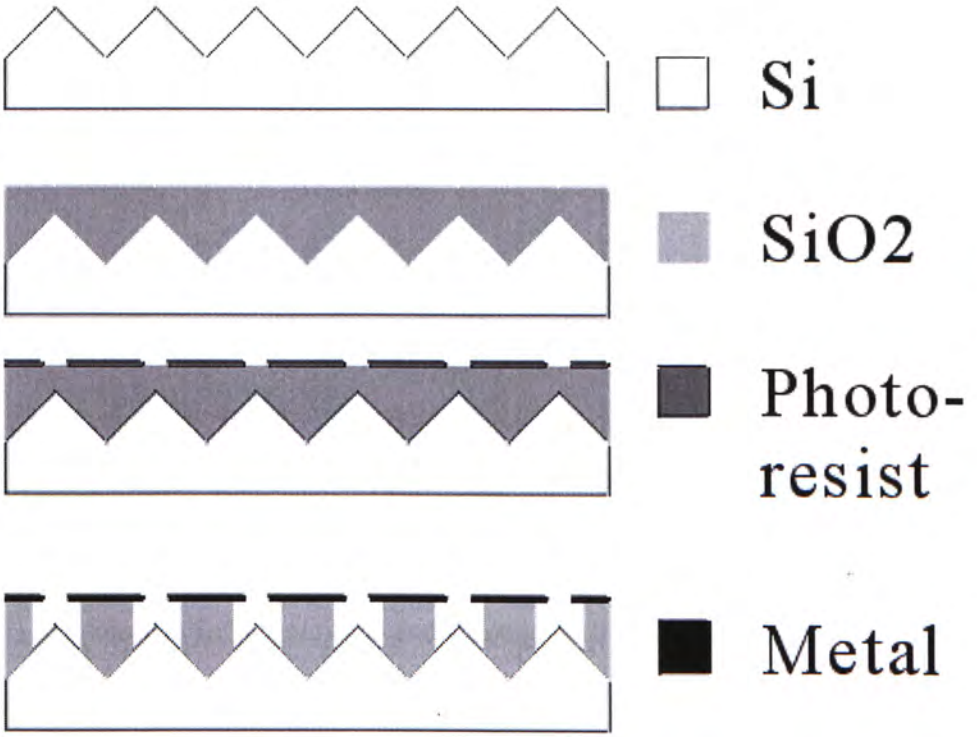

Figure 2.8. The process flow for fabrication of Silicon tip with the gate electrode

Chapter 3 Sample preparation and characterization methods

Sample preparation and characterization methods

3.1 Sample preparation

In this work, the substrates are single-side polished (100) and (111) n-type Si wafers with a resistivity of 0.01Ωcm. The wafers are cleaned by treating with 1:50 ($HF:H_2O$) solution for 15 minutes and rinsing with deionized water and are dried by blowing Nitrogen gas.

3.2 The fabrication process

3.2.1 Isotropic etching of silicon

3.2.1.1 The anodization process

Anodic etching of silicon with the aid of aqueous HF solutions is a technique that has been used for many years to thin or polish silicon wafers. HF anodic etching can also be used as a micromachining tool. In this work, the main objective is to decrease the fabrication time in conventional method.

Both porous silicon formation and electropolishing of silicon can occur in anodization method. The electropolishing of silicon depends on the HF solution concentration. In addition, the electropolishing of silicon occurs at the current densities above a critical value. Below this critical value a porous silicon film is formed. Electropolishing of silicon can be produced for both n- and p- type material

depending on whether the sample is illuminated or not, its doping concentration, the anodizing current density and HF concentration in the electrolyte.

Anodization is consistent with the following scheme of reactions.

a) Charge transfer: $Si + 2HF + 2h^{+} \rightarrow SiF_2 + 2H^{+}$

b) Disproportionation: $2SiF_2 \rightarrow Si\ (amorphous) + SiF_4$

$SiF_4 + 2HF \rightarrow H_2SiF_6$

c) Evolution of hydrogen results mainly from the reactions

$SiF_2 + 4HF \rightarrow H_2SiF_6 + H_2$

$SiF_2 + 2H_2O \rightarrow SiO_2 + 2HF + H_2$

d) The silicon dioxide may be dissolved by the reaction

$SiO_2 + 6HF \rightarrow H_2SiF_6 + 2H_2O$

3.2.1.2 Porous silicon formation

Porous silicon formation is studied because porous silicon has high density of very sharp asperities, each of which may behave as a site for field emission. A dramatic improvement in emission properties is expected.

The mechanism of formation of porous silicon takes into consideration of the disproportionation of Si^{2+} ions in solution. The formation of porous silicon may be considered as a sequence of the following steps:

$Si^{2+} + Si^{2+} \rightarrow Si^{0} + Si^{4+}$

i) Electrochemical anodic etching of the Si surface, producing mainly divalent Si^{2+} ions;

ii) Disproportionation of Si^{2+} ions near the Si electrode in accordance with reaction

$Si^{2+} + Si^{2+} \rightarrow Si^{0} + Si^{4+}$

iii) Deposition of the produced free atoms of silicon (Si^0) on crystallization centres. The role of these centres can be played by atoms of the substrate (wall of pores) or of newly formed crystallites. As is clear from reaction $Si^{2+} + Si^{2+} \rightarrow Si^0 + Si^{4+}$, only half of the dissolved Si takes part in the formation of porous silicon, whereas the remaining part transfers into solution as SiF_6^{2-} ions.

The formation of porous silicon may be considered not only as a result of surface etching of the silicon substrate, but also as a process of secondary crystallization (deposition) of silicon on this substrate.

A two step anodization method which consist of both electropolishing and porous silicon formation is used to fabricate field emitters. The uniformity of electropolishing process from point to point is very important. This is because the electropolishing of silicon is used to define the shape of the silicon field emitter. After electropolishing, porous silicon formation is used to sharpen the field emitter.

3.2.2 Anisotropic etching of silicon

Wet anisotropic etching is a process of etching of materials along preferential directions using etchant solutions.

The most frequently used etchant in wet anisotropic etching is the solution of potassium hydroxide in isopropyl alcohol (IPA) for many reasons: fast etching rate, easy to setup, strong basic character and the strong dependence of the etching rate on the crystallographic direction. In this etching method, the formation of field emitter on silicon surface greatly depends on the rate of generation of hydrogen from the following chemical reaction:

$$Si + 2H_2O + 2HO^- \rightarrow SiO_2(OH)_2^{2-} + 2H_2;$$

The etching rate depends on the concentration of IPA in KOH. This study makes use of different concentration of IPA in anistropic etching process and etching time in order to study the formation of field emitters.

In this study, the KOH concentration is kept at 5%. A constant temperature heater is used to maintain the temperature of the chemical solution at 80°C.

3.2.3 The sputtering system

Amorphous carbon (a-C) coated materials have shown a great improvement in the emission performance because of the enhancement by low work function and surface morphology. The field emission properties of a-C coating on flat silicon and porous silicon by DC magnetron sputtering are studied here.

Sputtering is a process that makes use of a glow discharge with argon gases to remove material from a target. The ejected material diffuses to and collects on the surface of the sample. In fact, it has better coverage than evaporation and induces much less radiation damage than electron beam evaporation.

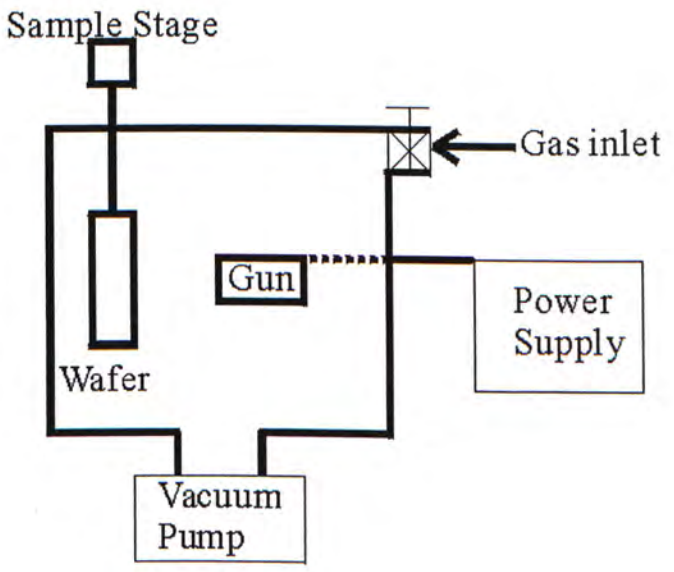

Figure 3.1. Chamber for a simple parallel plate sputtering system

In a simple sputtering system, a parallel plate plasma reactor is in a vacuum chamber as shown in figure 3.1. A gas such as argon (Ar) is used to perform the sputtering process. The gas pressure in the chamber is held at $3x10^{-3}$ torr or lower. This results in a mean free path of order of hundreds of microns.

In the process of sputtering, plasma is initiated by applying a high voltage across a gap containing the gas at a low pressure. Once plasma is formed, ions in the plasma area are accelerated towards the negatively charged cathode. When they strike the target surface, they sputter the target atoms and also release secondary electrons, which are accelerated away from the cathode. They may collide with neutral plasma species while crossing from cathode to anode. If the energy transfer is less than the ionization potential of the gaseous species, the atom can be excited to an energetic state. The atom decays from this excited state through an optical transition, providing the characteristic glow. If the energy transfer is high enough, the atom of the gaseous species will ionized and accelerated toward the cathode. The bombardment of the cathode by this ion stream gives rise to the process of sputtering of target atoms.

When an energetic ion strikes the surface of the substrate, four things can happen. Ions with very low energy may simply bounce off the surface. At energies less than 10eV, the ion may get adsorbed to the surface and giving up its energy to phonons. At energies above 10keV, the ion penetrates into the material, depositing most of its energy deep into the substrate, where it changes the physical structure. These high energies are typical for ion implantation. Between these two extremes, both energy transfer mechanisms occur. For a part of the path of the ion into the substrate, nuclear stopping at the surface is quite effective at this low energy. Most of the energy transfer occurs within several atomic layers. When this happens, atoms

and clusters of atoms will be ejected from the surface of the substrate. The atoms and atomic cluster ejected from the cathode escape with energies of 10 to 50eV. This is about 100 times higher than the energy of evaporated atoms. This additional energy provides sputtered atoms with higher surface mobility for improved step coverage relative to evaporation. At typical sputtering energies, about 95% of the ejected material is atomic. Most of the remainders are diatomic molecules.

At high energies like those used in implantation, chemical bonding processes can be largely ignored and the target can be considered as simply a collection of atoms. At very low energies, no disruption of the target occurs, and a chemical model can be readily developed. At sputtering energies, the physics of the material removal is quite complicated, involving the coupled effects of bond breaking and physical displacement.

3.2.4 The MEVVA Ion Source Implanter

In the process of ion implantation, ionized impurity atoms accelerated through by electrostatic field strike the surface of the wafer. The dose can be tightly controlled by measured the collected charge. By controlling the electrostatic field, the penetration depth of the impurity ions can also be controlled. The range and distribution of the implanted atoms depend on the ion energy, the masses of the ion and target atoms.

For conventional implanter, the current capability is usually very low. Often the metal ion beam current is at the μA level. Therefore, it is difficult in practice to perform high dose ion implantation by conventional implantation. The metal vapor vacuum arc (MEVVA) is able to provide broad metal ion beam of high beam current 8mA or more, and is especially suitable for high dose implantation. With the

MEVVA ion source, a much shorter implantation time is needed to fulfill the high dose requirement.

A schematic of the MEVVA ion source is shown in fig 3.2. The MEVVA implanter consists of three main components: the ion source, the acceleration tube, and the target station. The ion source contains the species to be implanted as the cathode.

During implantation, a trigger voltage pulse of about 5-10kV is applied to induce spark discharges between the cathode and the trigger. Then discharges occur between cathode and anode. On the cathode surface, the cathode material is vaporized and ionized, and then the plasma is formed. The plasma production is a non-stationary process and occurs as a sequence of micro-explosions on the cathode surface. This gives rise to the formation of dense plasma of the cathode material. This quasi-neutral plasma plumes away from the cathode toward the anode, allowing the arc current to flow and the phenomenon persists when an arc voltage is applied between the cathode and the anode.

A central hole located in the anode allows a portion of plasma to plume through the hole and into the field free region beyond. A system of multi-aperture extraction grids is used to extract the ion component from the plasma plume, thus forming an intense ion beam of the cathode material. The arc circuit and the first extraction grids are floated to the desired extraction voltage of about 40kV. This intermediate extractor grid is for electron suppression which is at about –2.5kV. The outermost grid is at the ground potential. Therefore, the ions from the cathode are transported to and implanted into the target.

In this work, a SiC layer on a silicon field emitter using carbon implantion with a MEVVA ion source is studied. Carbon can be used as the cathode material by

a MEVVA ion source because it is conducting and dosimetry is simplified as only the singly charged state of carbon ions exist in the plasma [106].

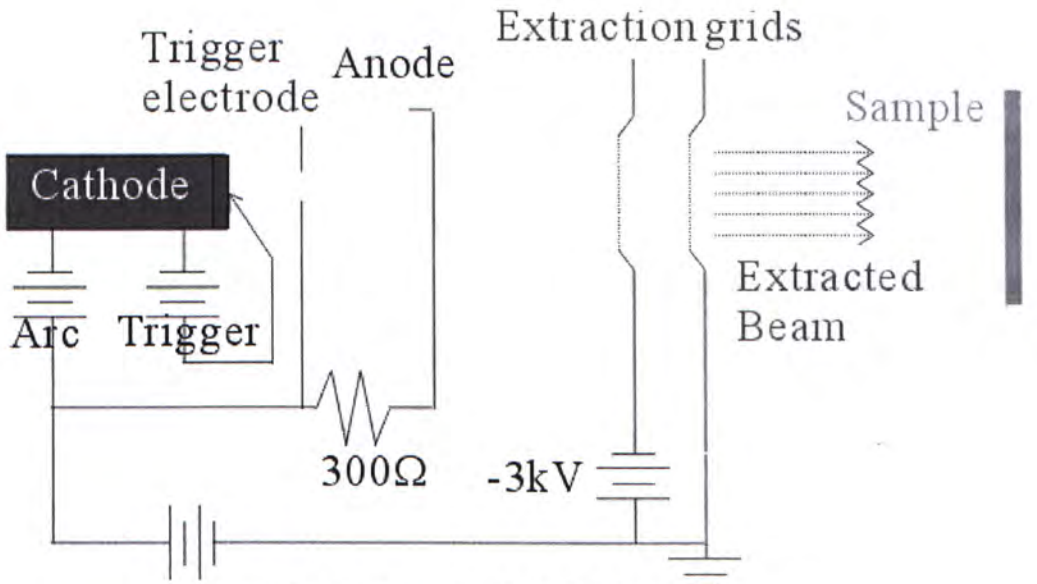

Figure 3.2. Schematic of the MEVVA ion source

3.3 Characterization methods

3.3.1 Atomic Force Microscopy (AFM)

Atomic force microscopy (AFM) was invented in 1986. In principle, AFM is based on the measurement of interaction force between the tip and sample. When the tip approaches the surface of sample within a few angstroms, the atomic interactions force between the atoms on the tip and those on the sample cause the cantilever to bend, or deflect. These atomic interactions are mainly repulsive forces in the contact region that are balanced by the total force exerted by the tip on the sample. The dependence of the magnitude of the repulsive force upon the tip-to-sample distance d is a power law. Thus several atoms on an AFM tip will interact with several atoms on the surface. The resolution of AFM is about 1nm.

A schematic of AFM is shown in Figure 3.3. A laser beam from the laser diode is reflected from the sharp tip of the cantilever into a position-sensitive photodiode detector (PSPD) when the tip is scanned over the sample. As the cantilever bends, the position of the laser beam on the detector shifts with the ability to measure a displacement as small as 10 angstroms. The ratio of the path length between the cantilever and the detector to the length of the cantilever itself produces a mechanical amplification (x100). As a result, the system can detect sub-angstrom vertical movement of the cantilever tip.

In this work, the AFM system is operated in constant contact force mode. A feedback loop operates on the scanner to maintain a constant magnitude of cantilever deflection and therefore a constant force and separation between the tip and the sample. As the scanner traces the tip across the sample, the feedback system adjusts the z position of the scanner to accommodate change on the topography. The image is generated in three dimensions. Therefore, AFM image consists of a map of z(x,y) of tip height z versus its lateral position (x, y). It can be used to study the surface morphology of the samples.

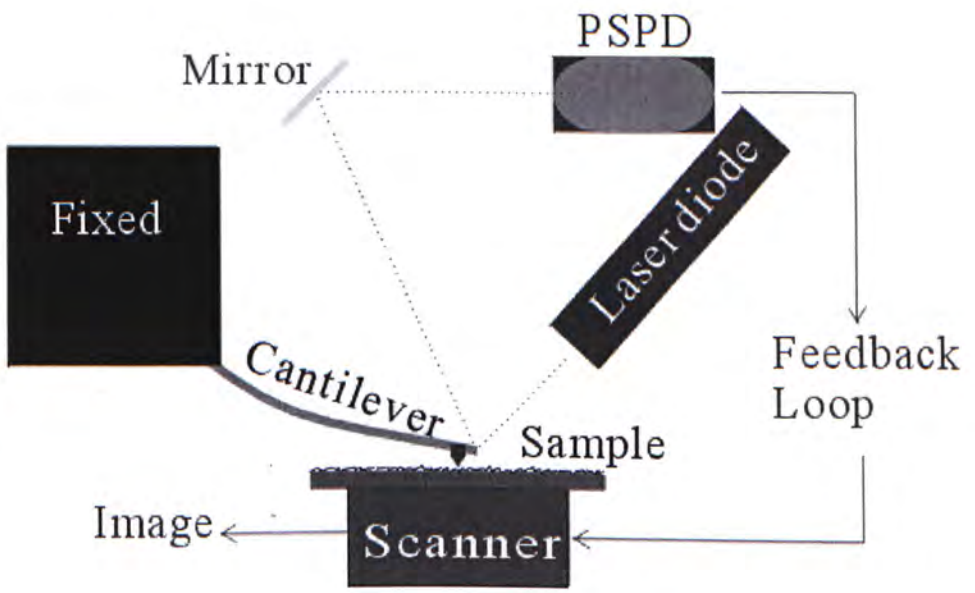

Figure 3.3. Schematic of the AFM

3.3.2 Scanning Electron Microscopy (SEM)

Scanning Electron Microscopy (SEM) is a method of visualizing the morphology of a surface with a high magnification and with a high depth-of-field. SEM uses a thermoelectron-emitting tungsten or thoriated-tungsten filament (W-source) as the electron source. During scanning process, a focused beam of electrons with energies from 5 kV to 30kV is rastered over the surface of an electrically conductive material. This causes the ejection of secondary electrons (~5eV) from the first 10-20 atomic layers of the surface. These electrons are then collected in an electron detector. The collected electron intensity is a function of the position of the beam on the surface (positions 1 to 5 in Figure 3.4) and also depends on the surface morphology, as shown in Figure 3.4. The electron intensities can be displayed on a cathode ray tube (CRT) as a visual picture and can be stored as a digital image by a computer. The use of digital imaging has many advantages, including storage and transmission of a high-resolution picture by electronic means.

Stereo-pairs of SEM images can be formed by angular rotation (10-15 degrees, typically) of the specimen about an axis through the image plane that is perpendicular to the incident electron beam. These stereo pairs can be viewed in a stereoscope to give a three-dimensional view of the surface topography. By knowing the angle of rotation and the magnification, the vertical height of surface features can be determined in the same way as is done for aerial mapping of the topography of the earth. The vertical resolution by this stereo technique is generally about $1/10^{th}$ of the lateral resolution.

An electrically conductive surface that is to be viewed by the SEM is in its natural state. If the surface is an electrical insulator, it will build up an electrical

charge and prevent high-resolution imaging. An insulating surface can be made conductive by the deposition of a very thin layer of gold or carbon on the surface.

The sample size can be a problem as the SEM sample chamber is limited in size. Therefore samples need to be cut to a size which is small enough to load into the chamber.

A conventional SEM typically provides magnifications to 50,000X. For comparison, an optical microscope is capable of a maximum magnification of about 1500X, using visual optics, or 5000-7000X, using video display. At the same magnification, the depth-of-field of the SEM is about 300 times better than that of a common optical microscope. However, the SEM is not very useful at magnifications less than about 300X; an optical microscope is a better choice to investigate surfaces at low magnifications.

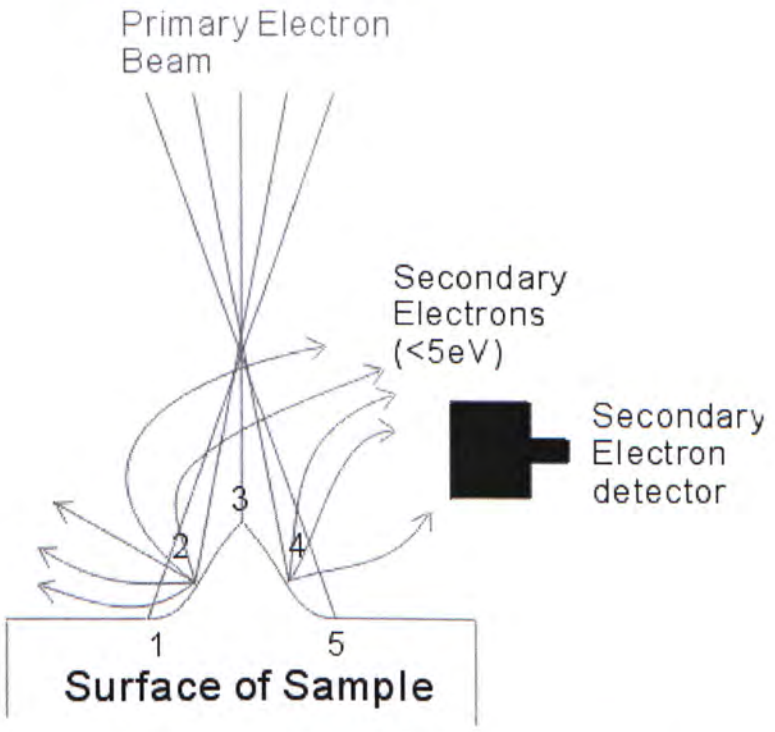

Figure 3.4. The collection of secondary electrons from surface in an SEM

3.3.3 Field emission measurement

3.3.3.1 Vacuum requirements

The vacuum condition is very important for field emission measurement. The majority of investigators developing field emitters use testing chambers with ultra-high vacuum conditions ($1x10^{-8}$ Torr or better) to a lower residual gas effects on the field emitter performance. As pressure is increased, more neutral and ionized residual gas molecules strike the emitter surface. High pressure leads to enhanced gas adsorption on the emitter surface with a corresponding work function change. The adsorbed molecules can be considered as dipoles aligned perpendicular to the surface. If the dipole has its negative charge away from the surface, the work function will be increased. The change of the work function is proportional to the value of the dipole moment and to the density of adsorbed molecules. As the work function increases, the emission current decreases.

3.3.3.2 Testing system

Fig. 3.5 and 3.6 show the details of the FEA characterization system used in this project. As shown in figure 3.5, the test devices are placed in the UHV vacuum chamber. The base pressure is at $1x10^{-8}$ Torr. The device is also connected in a grounded cathode configuration. In this system, vacuum compatible electrical feedthroughs are used so that three devices can be tested in a sequence without breaking vacuum.

The anode voltage is supplied to the device by a Hewlett Packard 4339A high resistance meter with a high voltage limit of 1kV. The variable anode potential and the anode current can be measured down to pA range.

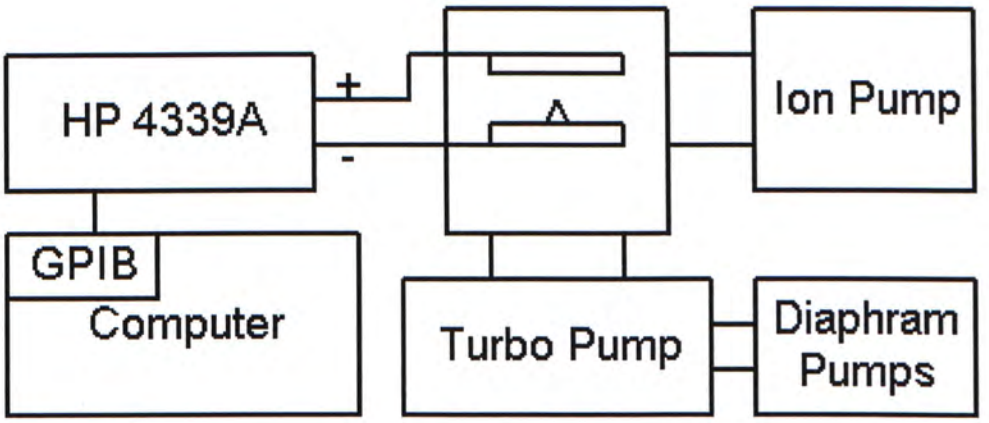

Figure 3.5. Schematic of the field emission characteristic measurement system

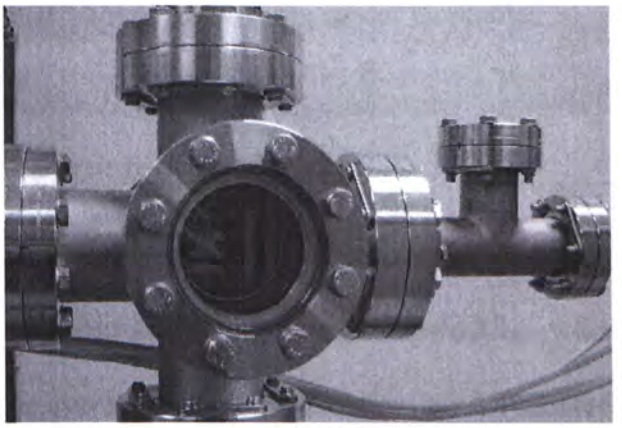

(a)

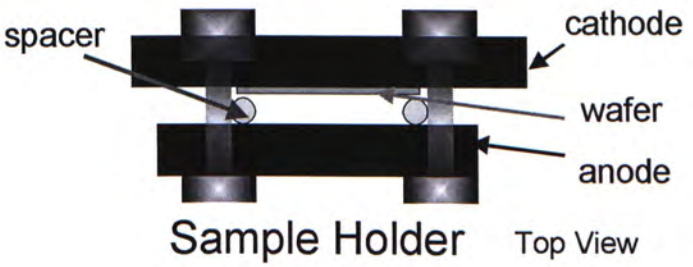

(b)

Figure 3.6. The photographic of the current-voltage measurement system
a) measurement chamber and b) the schematic structure of the sample holder

The data collection system is automated to ensure that the performance tests are carried out consistently, with accurate and complete collection of all relevant data. The system records measured anode current, anode voltage automatically by using a computer through the GBIB interface.

Emission current versus voltage characteristics is measured by a diode configuration structure with a copper plate as the anode. The sample under test is separated from the anode by a glass spacer with a circular opening of various diameters. The typical thickness of the glass plate spacers used is 20 μm measured by a precision thickness gauge with an accuracy of ±1μm as shown in figure 3.6b. The normal current density is defined as the ratio of the total emitted current to the area of the circular opening of the glass spacer and the nominal field is defined as the ratio of the applied voltage to the glass spacer thickness.

3.3.3.3 Fluctuation of field emission

Typically, the stability can be described graphically by the fluctuation of the emission current. The fluctuation is defined by $(I-I_{ave})/I_{ave}$ where I is the emission current and I_{ave} is the average emission current during the measurement.

Fluctuation in field emission current is due to changes in the surface configuration, surface level caused by gas discharge during emission and the gradual damage of field emitter by ion bombardment from the background gas in the vacuum chamber.

The fluctuation of field emission current also arises from current fluctuations and random fluctuations. Current fluctuations are due to the discrete nature of the electron (shot noise) and random fluctuations in the emission are from the active atomic sites on the cathode surface (flicker noise).

In thermionic emission, current fluctuation noise can be reduced by two or three orders of magnitude if the current flow is space charge limited with a potential minimum in front of, and a retarding field at the cathode. However field emission, which is the preferred electron source in vacuum microelectronics, requires an

intense accelerating field at the cathode which does not allow for any mechanism for reduction in current fluctuation noise.

In general the current fluctuation noise at a given current for all applications will be substantially higher with single field emission tips and arrays of tips than with conventional thermionic cathodes. This is both because more noise is generated, and the suppression of noise by space charge is no longer a simple option. With an emission cathode the electric field at the tip must be very high. A space charge minimum can be formed between the gate electrode and the anode, but this necessitates a fraction of the beam current to be collected by the gate electrode.

Chapter 4 Fabrication of Silicon Tips and their field emission characteristics

4.1 The anodization etching process

In conventional wet etch processes, the etching process produces gases. There is difficulty in removing all of these etch products and the flow of the etchant varies from point to point. Therefore, the uniformity and reproducibility of the fabrication of the field emitter is difficult to control in conventional methods.

A new fast fabrication method consisting of two step anodization of silicon with different HF solutions is used here to form high aspect ratio silicon Field Emitter Arrays on n-type silicon with resistivity of 0.01Ωcm. A Silicon dioxide mask is used to define the field emitter array. It will be shown that the field emission characteristics of field emitter fabricated by this method is better than the field emitter fabricated by conventional methods. Field emitter arrays with good uniformity and reproducibility have been obtained.

4.1.1 INTRODUCTION

A conventional silicon field emitter array (FEA) is fabricated by isotropic wet etching (nitric acid) or anisotropic wet etching (potassium hydroxide). The usage of wet etching has several problems: (1) the etch rate is too slow and (2) the uniformity of the silicon tip size is not good because the etching rate depends on the etchant flow rate onto the wafer.

Electrochemical etching by using hydrofluoric acid (HF) is widely used for the formation of porous silicon. This has been studied since the 1950s [107] and much attention has been paid to the formation mechanisms [108]. It has been used in the fabrication of thick buried silicon dioxide layer for silicon-on-insulator devices [109-110]. Recently, porous silicon has been applied to the fabrication of microelectromechanical systems (MEMS) and silicon field emitters [111-113]. The porous silicon can be removed easily with nitric acid solution at room temperature. Using this technology to fabricate field emitter arrays, we can overcome the problem of variable chemical etching rate of silicon along different crystallographic directions.

In conventional wet etch processes, the film to be etched is not directly soluble in the etchant solution. It is usually necessary to change the material to be etched from a solid to a liquid or a gas. If the etching process produces a gas, this gas can form bubbles that can prevent the transport of fresh etchant to the surface. This is an extremely serious problem since the formation of the bubbles cannot be predicted. This problem is most pronounced near the pattern edges. Agitation in the wet chemical bath will reduce the ability of the bubbles to adhere to the wafer to some extent. Even in the absence of bubbles, small geometry features may etch more slowly.

In this work, in order to overcome the problems of wet solution etching, a new fabrication method using anodization is used. This method can produce well-controlled, uniform and symmetric silicon field emitters. Anodization is used to form a thick porous silicon layer which is removed by chemical etching. The microstructures of the porous silicon formed can be controlled by various

anodization parameters such as etchant concentration, anodization time, current density, substrate resistivity and the dopant in the substrate.

4.1.2 EXPERIMENTAL DETAILS

The sample is etched in two different concentrations of etching solution at a constant current density of 90mA/cm^2. The schematic of the electrochemical etching cell used for the silicon tip formation is shown in Figure 4.1.1. A platinum wire is used for the counter electrode. Positive voltage is applied between the sample and the counter electrode. A constant current is supplied by a KEITHLEY 2400 SMU which is controlled by a computer and the current-voltage versus time during the anodization processes is recorded.

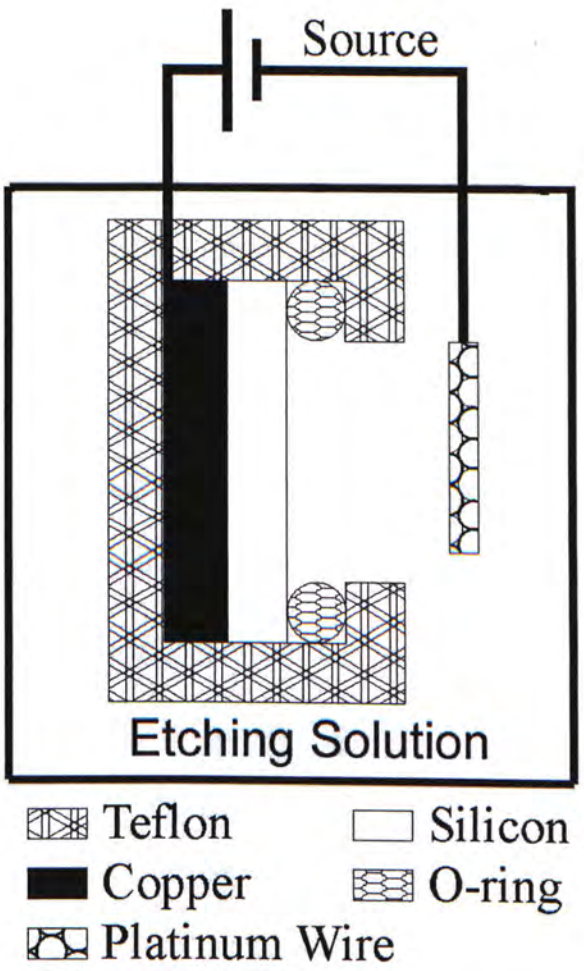

Figure 4.1.1 Anodization set-up

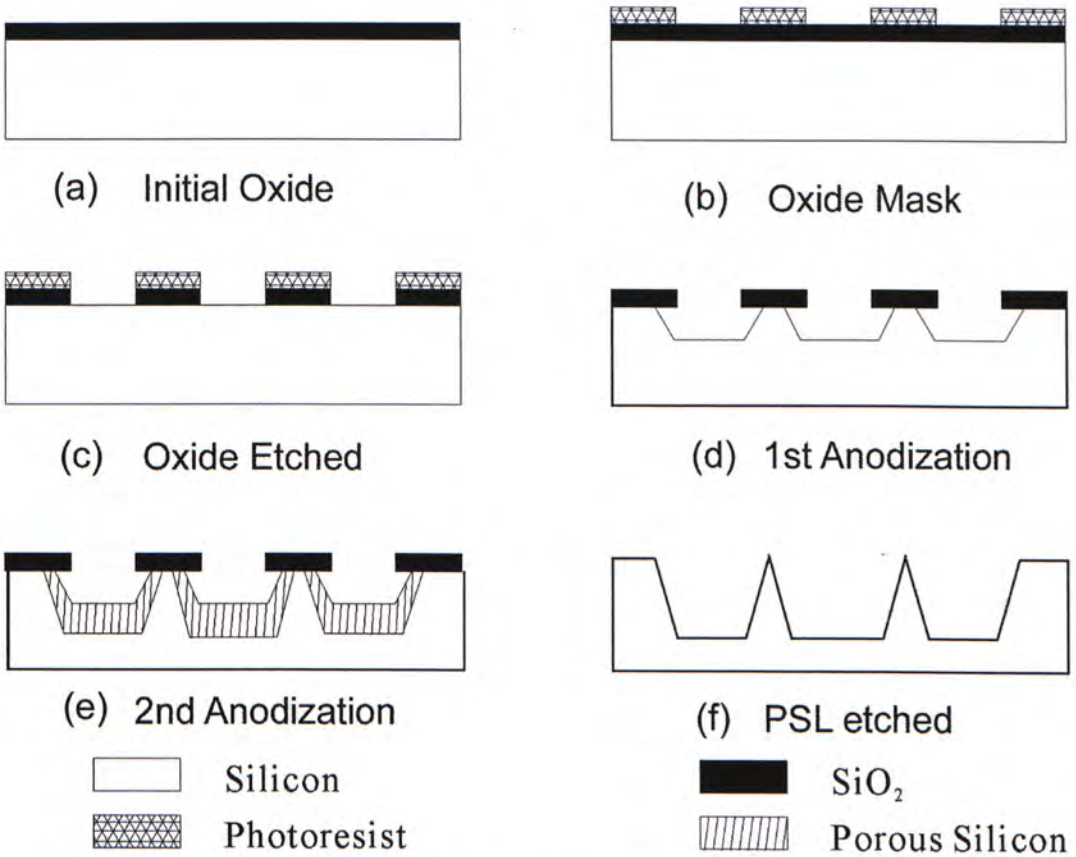

Figure 4.1.2 Fabrication process of silicon FEA using two step anodization method.

The process flow for the electrochemical etching is shown in Figure 4.1.2. Starting material is n-type Si (100) substrate with 0.01Ωcm resistivity. It is covered with a thermally grown, 1μm, thick silicon dioxide. The silicon dioxide is photolithographically patterned to form 20μm diameter circular discs with a spacing of 20μm which is used as a mask for the following anodization etching process. Figure 4.1.3 is the circular discs pattern mask.

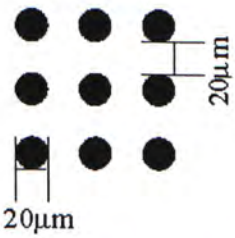

Figure 4.1.3 Circular discs pattern mask

Firstly, electropolishing of the silicon surface is performed by anodizing the substrate in a dilute HF:H_2O (4:75) solution with a current density of 90mA/cm^2 for 1 minute in the dark.

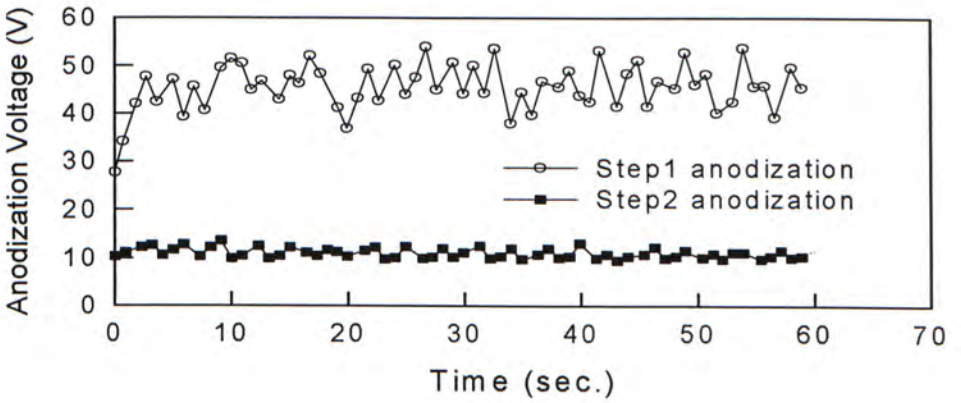

Figure 4.1.4 Voltage as a function of anodization time with current density of 90mA/cm^2

Secondly, porous silicon is formed by anodization in a HF:H_2O:C_2H_5OH = 20:37:16 solution with current density of 90mA/cm^2 for 1 minute in dark. Under these conditions, the anodization voltage with time is stable in these two steps which is shown in Figure 4.1.4.

Finally, the porous silicon layer formed by anodization is removed chemically by a HF:CH_3COOH:HNO_3=2:3:95 solution for 20 seconds.

Table 4.1.1 Experimental Detail of two step anodization method

Material	Step	Experimental condition	Reaction time
Silicon (100) n-type 0.01Ωcm	1	Current density of 90mA/cm^2 HF:H_2O = 4:75	1 min
	2	Current density of 90mA/cm^2 HF:H_2O:C_2H_5OH= 20:37:16	1 min
	3	Wet etching HF:CH_3COOH:HNO_3=2:3:95	20sec

4.1.3 RESULTS AND DISCUSSION

4.1.3.1 N type (100) sample

Electrochemical etching of silicon in a hydrofluoric acid solution has attracted much interest due to the formation of porous silicon which can easily removed by HNO_3.

The silicon wafer electrode is covered either by a porous silicon layer or is electrochemically polished depending on the applied potential for a given HF concentration in the solution.

In the first anodization step, the electropolishing of silicon occurs under anodization. At this current density, fluoride ions and HF molecules directly remove silicon atoms and this reaction is responsible for the electropolishing [114]. In this step, the concentration of HF is suitable for electropolishing of n-type silicon in dark with a very good uniformity. The etching rate is about 5μm per minute. After the first anodization, silicon tip shape is formed and the thermally grown silicon dioxide is also there to protect the top of the silicon tip.

In the second anodization step, the porous silicon is formed by anodization. After this, the porous silicon is removed by using a HNO_3:HF:CH_3COOH=2:3:95 solution. Then the silicon tip is fabricated.

The formation of porous silicon can occur only at certain current densities and in a solution of a specific HF concentration. This is because both porous silicon formation and electropolishing of silicon can occur. The electropolishing of silicon depends on the concentration of the HF solution. It only occurs at current densities above a critical value. Below this value, a porous silicon film is formed. However, the exact regimes of current density and HF concentration in which porous silicon formation and/or polishing occurs have not been determined. In addition, there has

been no explanation of the transition from porous silicon formation to electropolishing. Porous silicon can be produced for both n- and p- type material depending on whether or not the sample is illuminated, its doping concentration, the anodizating current density and HF concentration in the electrolyte.

Although, the dissolution reaction occurs readily for p-type silicon and illumination is required for n-type Si in the solution with a concentration of $HF:H_2O$ is 1:1 or 1:2. In fact, at a voltage higher than the critical voltage, porous silicon will grow even if the sample is not illuminated.

In second step anodization, the etching solution concentration is suitable for the formation of porous silicon that can be easily removed by nitric acid. And the porous silicon thickness increases with anodization time and the porous silicon layer is very uniform in thickness. Ethanol is necessary to reduce the surface tension of the etchant to avoid adhesion of developed gas bubbles during anodization, especially under the perforated mask.

The advantage of the anodization process is that FEA can be fabricated onto all kind of Si substrates with different orientations. Using the wagon wheel mask which is shown in figure 4.1.5, the etching rate along different crystallographic directions can be determined. When etching method is isotropic, etching rate should be the same in all directions (Fig. 4.1.6).

An SEM photomicrograph of a test pattern formed by anisotropic KOH etching is shown in figure 4.1.7. The etching is not uniform as shown in the figure. Unlike etching in KOH or EDP [115], isotropic etching pattern profile is uniform as shown in figure 4.1.8. The formation of the porous silicon is isotropic which is independent of the crystalline orientation. Therefore, anodization method is an isotropic etching method which produces isotropic etching as shown in Figure 4.1.8. The silicon undercut formed under the Wagon wheel Mask is isotropic so that the etching rate of all orientations is same.

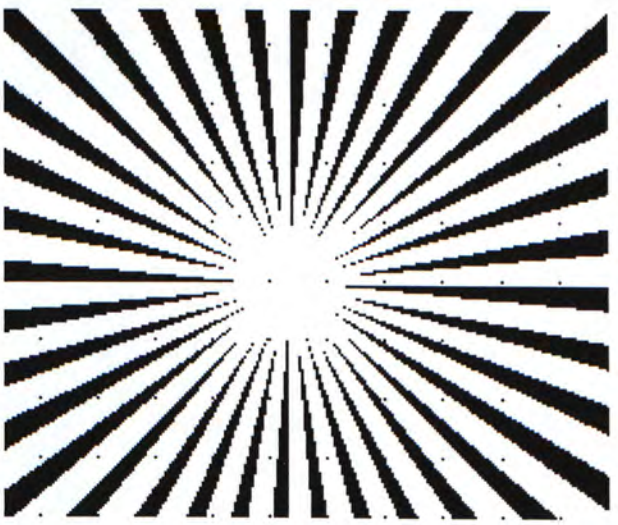

Figure 4.1.5 The Wagon wheel mask

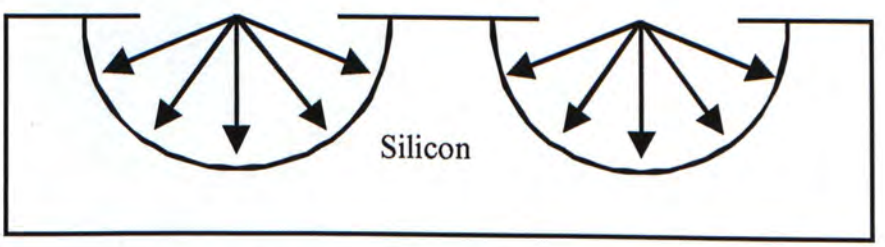

Figure 4.1.6 Isotropic Etching direction

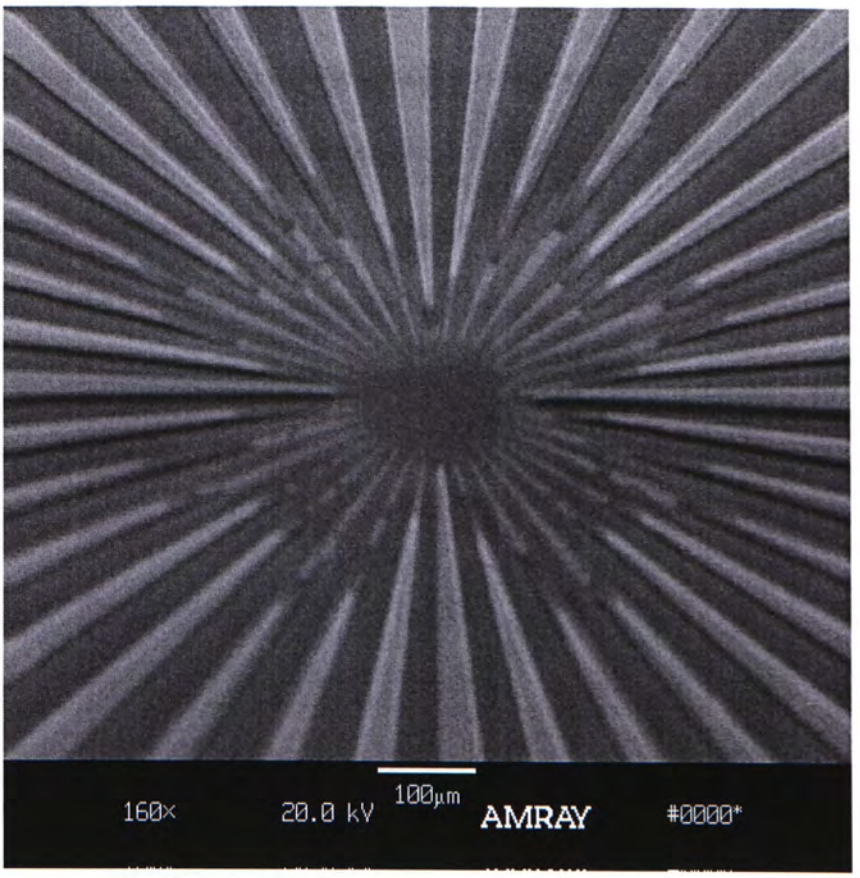

Figure 4.1.7 An-isotropic etching test pattern formed by using KOH method with a Si oxide mask.

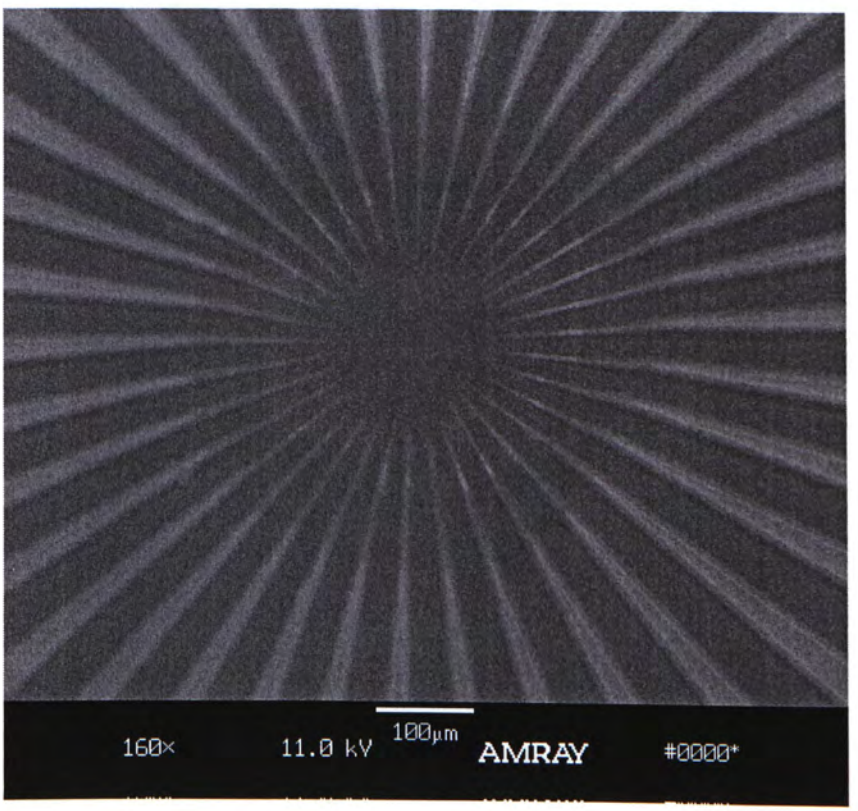

Figure 4.1.8 Isotropic etching test pattern formed by using anodization method with a Si oxide mask.

With a circular oxide mask, the tips of FEA formed are conic. A typical scanning electron microscope (SEM) photomicrograph of circular silicon-tip arrays fabricated by using the two step anodization method with a base diameter of about 10μm is shown in Figure 4.1.9 and Figure 4.1.10.

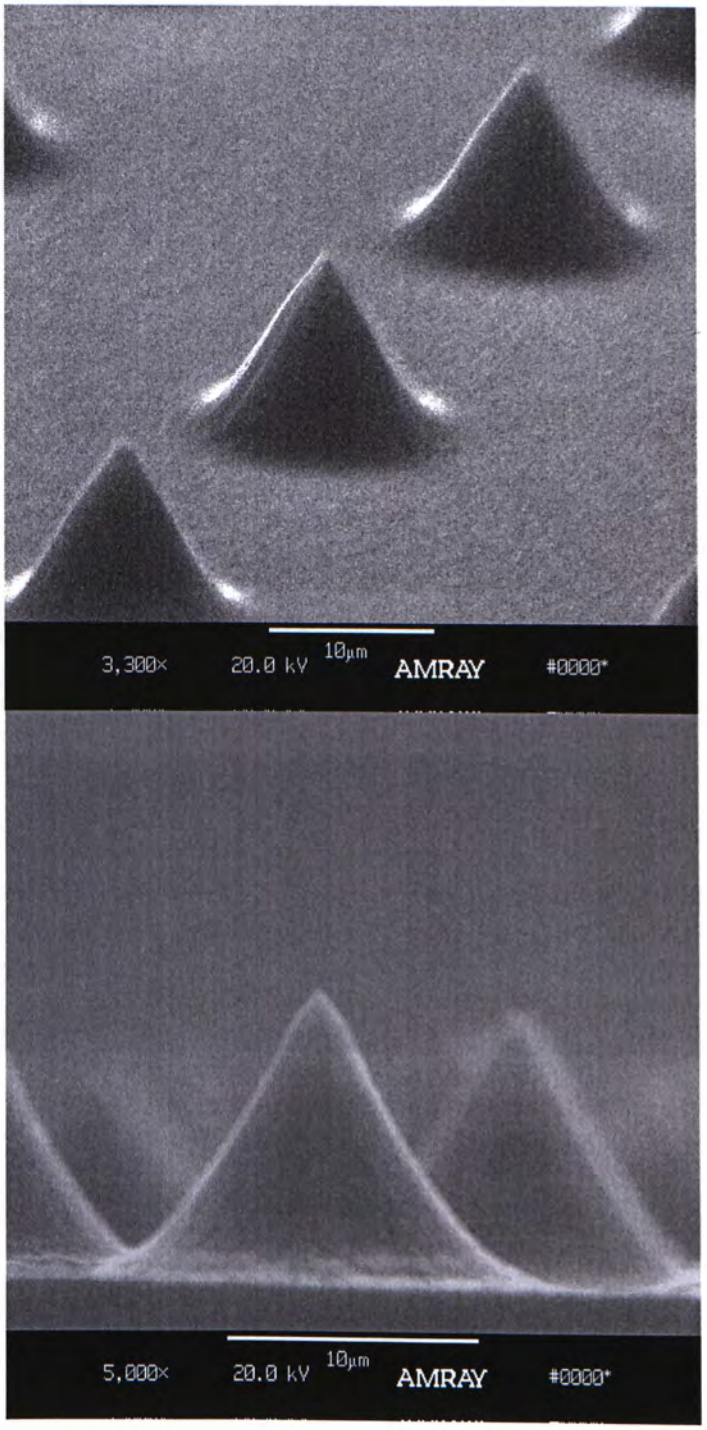

Figure 4.1.9 Typical SEM photomicrograph of conic silicon-tip array fabricated by using a two step anodization method. The base diameter of the tips is about 10μm.

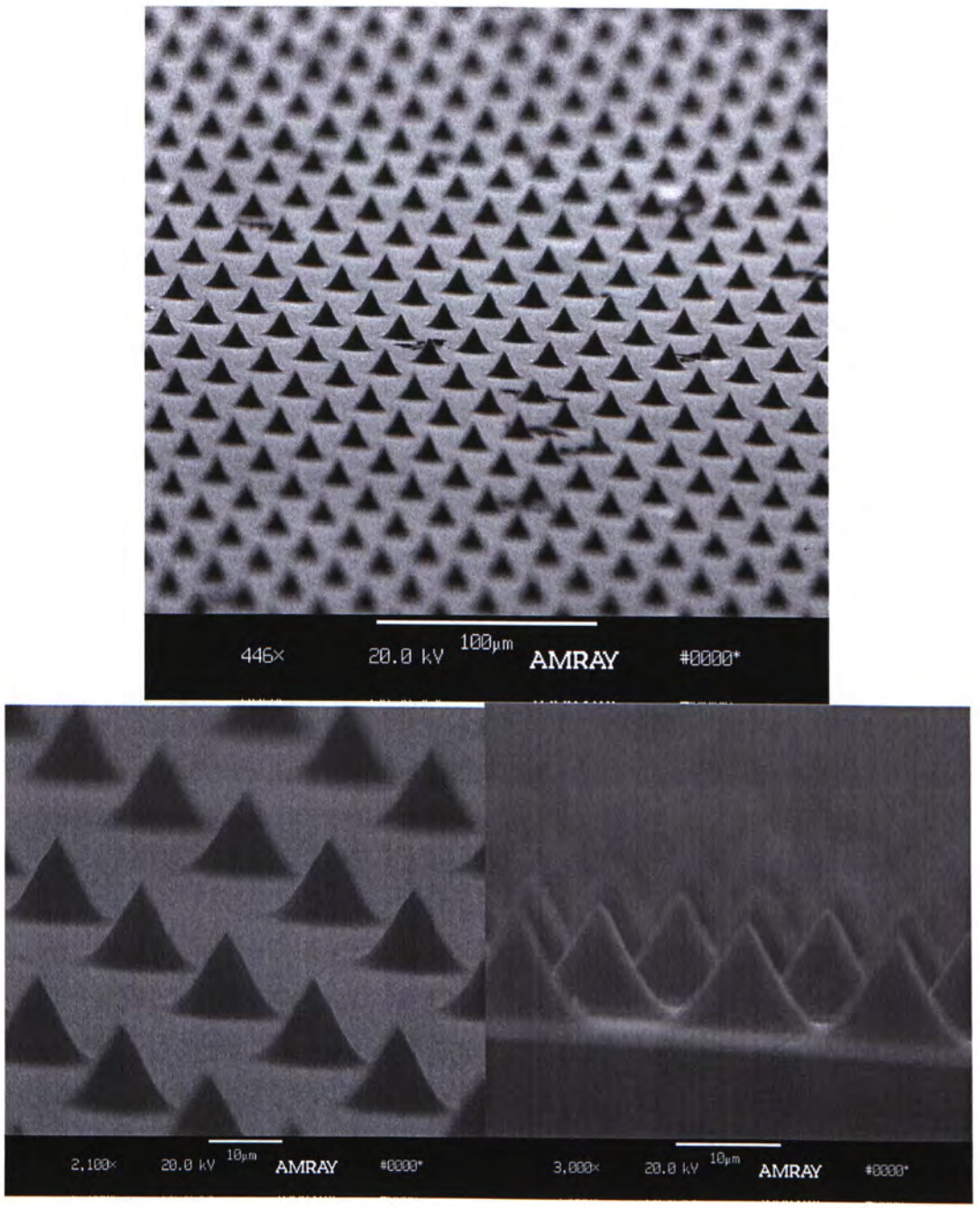

Figure 4.1.10 Typical SEM photomicrograph of conic silicon-tip array fabricated by using a two step anodization method.

The SEM figures show that size of the tips are uniform in size and FEAs with a uniform area density of tips are fabricated.

In the field emission characteristics, electrical testing is performed in a high vacuum chamber at a pressure of $1x10^{-8}$ Torr. Emission current versus voltage characteristic is measured by a diode configuration. The emitter/collector spacing is 20µm using a glass spacer. The typical thickness of the glass plate spacers used is

20 μm measured by a precision thickness gauge with an accuracy of ±1μm. The measurement is carried out for a voltage range from 0 to 1000V.

Figure 4.1.11 shows the I-V characteristic and the Fowler-Nordheim (FN) plot for conic FEAs fabricated by conventional and anodization method. The linearity of the FN plot shows that the anode current is due to electron field emission. The turn-on voltage of the anodization method field emitters is approximately 27V/μm at an emission current density of $1\mu A/cm^2$. This is better in comparison with the silicon tips fabricated by using an isotropic etching solution of nitric acid with a turn-on field of about 35V/μm.

The inverse of the slope in the FN plot is $\beta/\phi^{3/2}$ where β is the field enhancement factor and ϕ is the work function of the emission surface in volts [116]. The value of $\beta/\phi^{3/2}$ are determined to be 17 and 20 for the conventional and anodized conic FEA samples respectively as shown in figure 4.1.11.

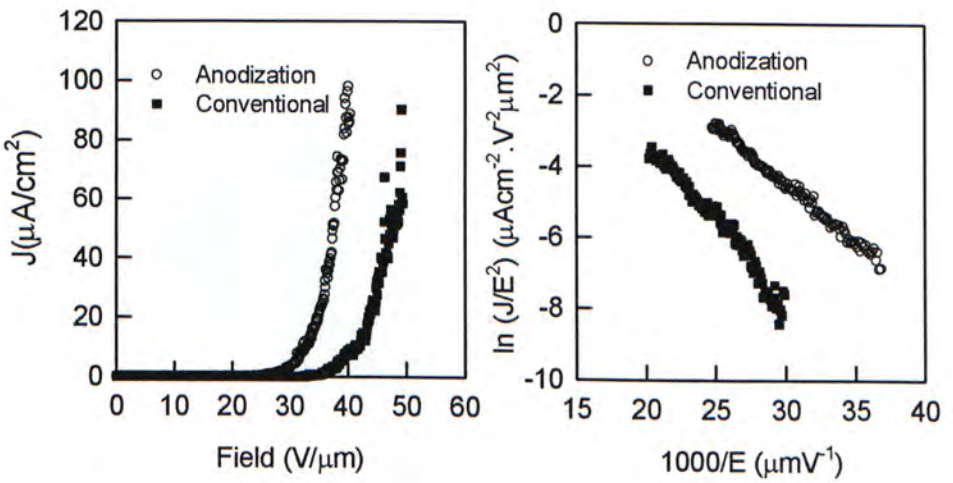

(a) (b)

Figure 4.1.11 (a) Current-voltage characteristic for FEA fabricated using the two step anodization method and using a conventional HNO_3 etching method. (b) data plotted in Fowler-Nordheim coordinates.

As the silicon substrates used are the same in both cases, they should have the same work function. Therefore the field enhance factor is improved by the modification of surface morphology by the anodization process [117]. Figures 4.1.12, 4.1.13 and 4.1.14 show the atomic force microscope (AFM) micrographs of the Si surface after various treatments. The roughness of the two step processed surface is much higher than that fabricated by nitric acid solution. Micro asperities seen after removal of the porous silicon must act as micro cathodes on the apex of the Si tips. The sample surface after nitric acid etching is relatively flat. For those surfaces prepared by anodization, small and dense protrusions are observed. These protrusions can improve the efficiency of electron field emission from the surface.

From the anodization process, tips are also fabricated using a square mask, chess mask and negative circular mask on n-type silicon (100) with 0.01Ωcm resistivity.

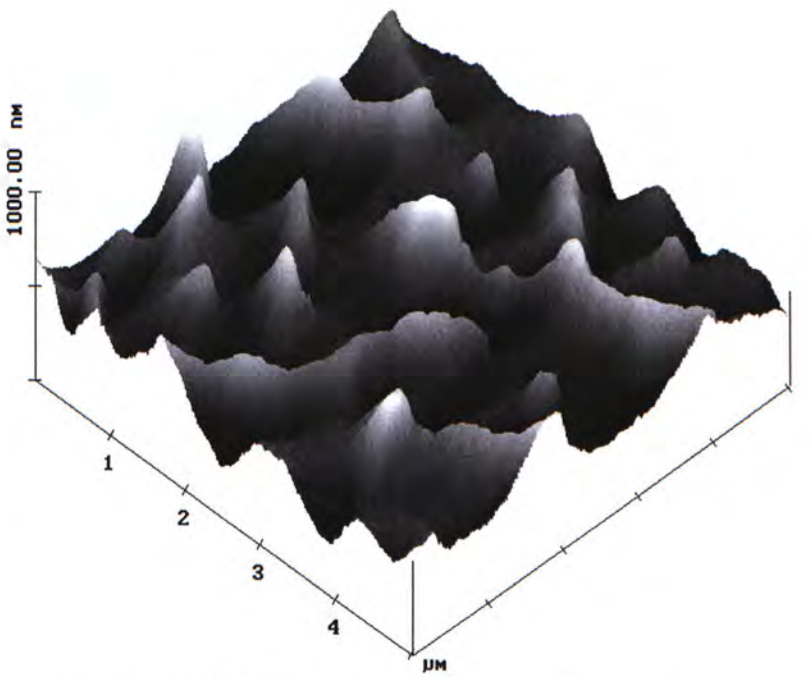

Figure 4.1.12 AFM micrographs after first anodization
Roughness (Rms) = 72.775nm

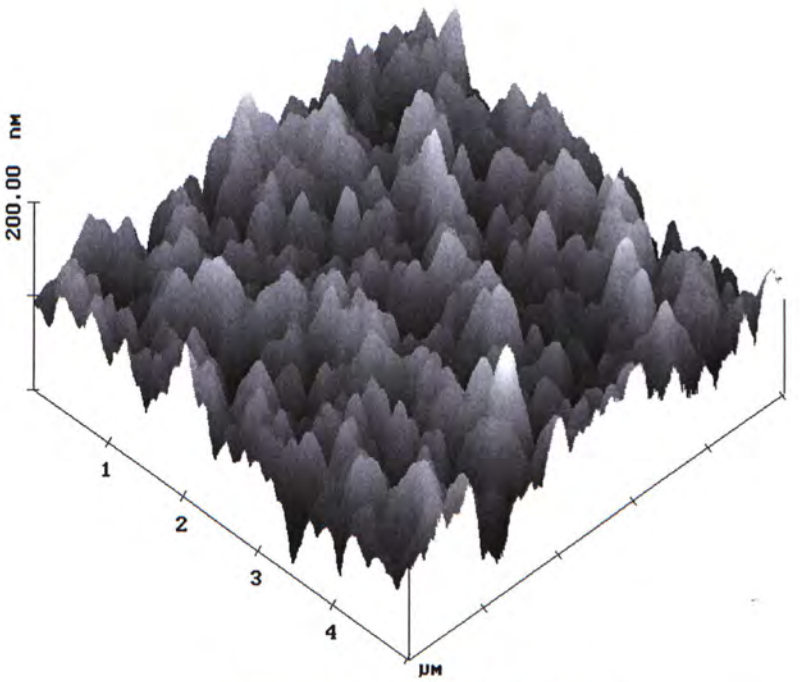

Roughness (Rms) = 28.512nm

Figure 4.1.13 AFM micrographs after porous silicon removal

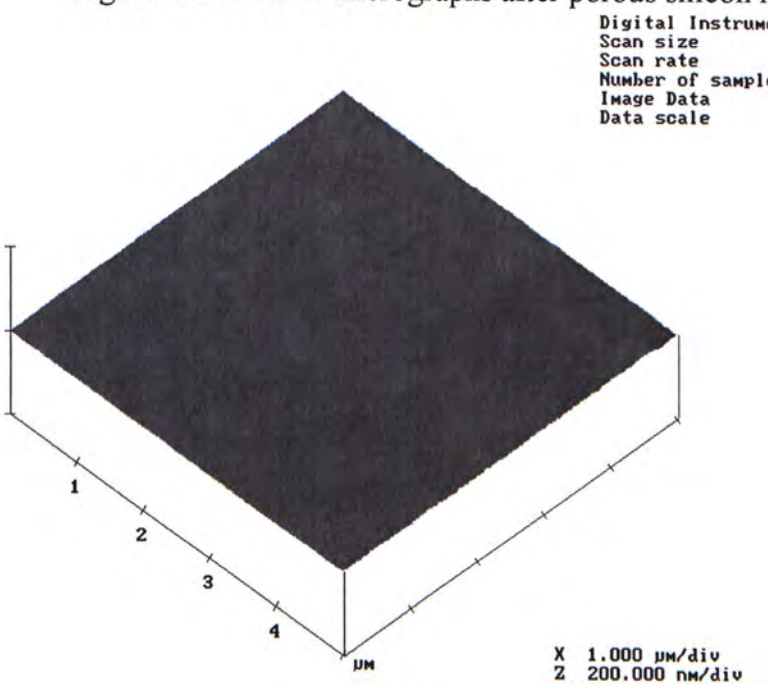

Roughness (Rms) = 1.367nm

Figure 4.1.14 AFM micrographs of sample prepared by using nitric acid etching method

The experimental details of the fabrication process is shown in table 4.1.2. The first and second anodization times are different because the etching profile of square mask pattern is different from that of the circular mask pattern. In this case, a different anodization time is used to optimize the sharpness and uniformity of the

field emitter tips. For the square and chess mask pattern, the anodization time is the same as the additional area to be etched in chess mask pattern is smaller. But for the negative circular mask pattern, a larger anodization current density is used because more area of silicon needs to be etched.

The FEAs fabricated using square, chess and negative circular masks are shown in the SEM micrographs , Figure 4.1.15, Figure 4.1.16, Figure 4.1.17 respectively.

Table 4.1.2. Experimental Detail of different mask pattern on silicon (100)

Substrate	Mask Pattern		First anodization	Second anodization	SEM
	Square 20μm x 20μm with space 20μm	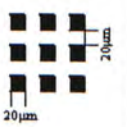	70mA/cm^2 for 1 mins	70mA/cm^2 for 2 mins	Figure 4.1.15
N type (100) 0.01Ωcm	Chess 20μm x 20μm with space 20μm		70mA/cm^2 for 1 mins	70mA/cm^2 for 2 mins	Figure 4.1.16
	Negative circular 20μm with space 20μm		90mA/cm^2 for 1 mins	90mA/cm^2 for 2 mins	Figure 4.1.17

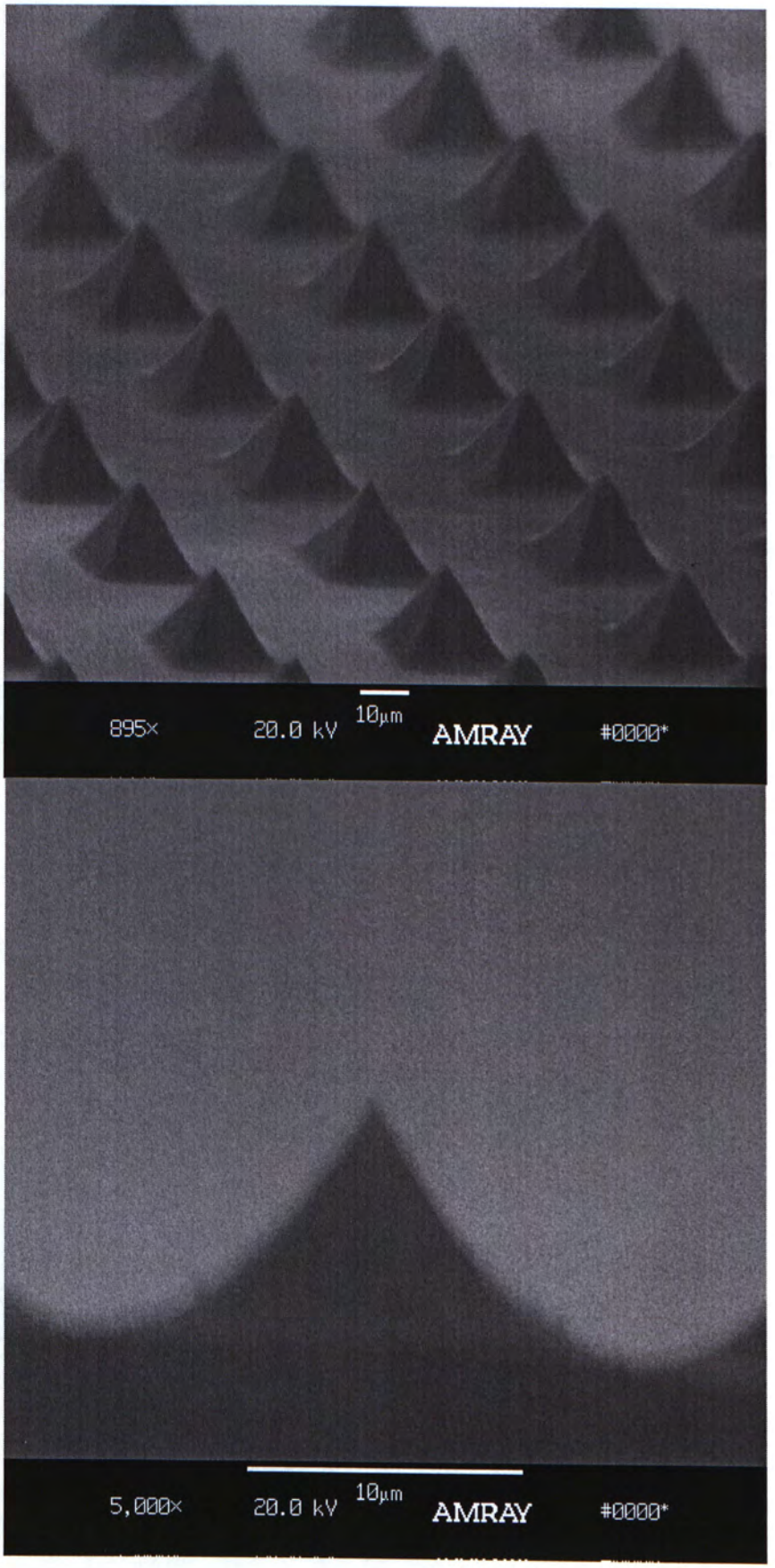

Figure 4.1.15 Typical SEM photomicrograph of silicon-tip array fabricated by using a two step anodization method with the square mask.

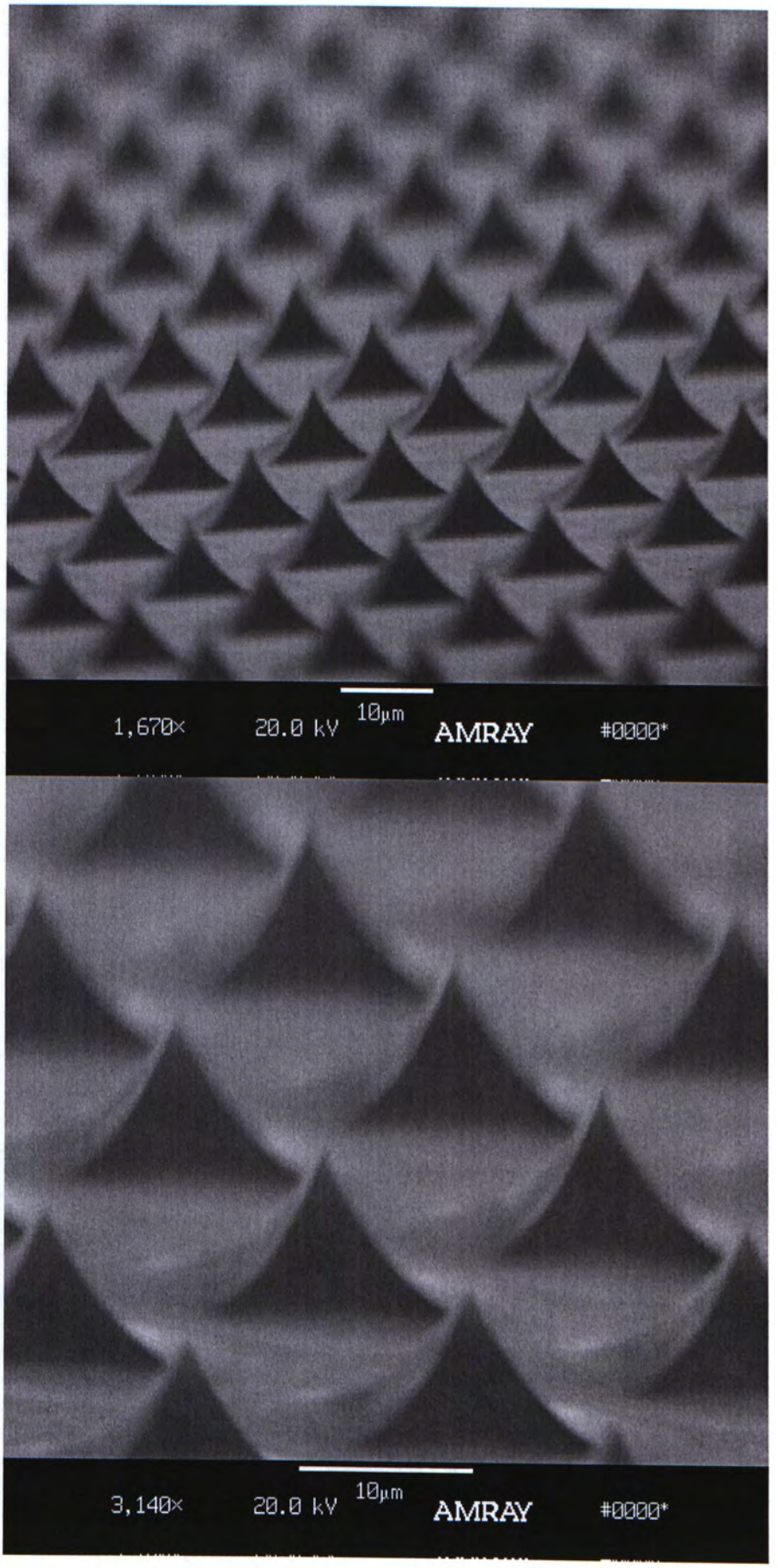

Figure 4.1.16 Typical SEM photomicrograph of silicon-tip array fabricated by using a two step anodization method with the chess mask.

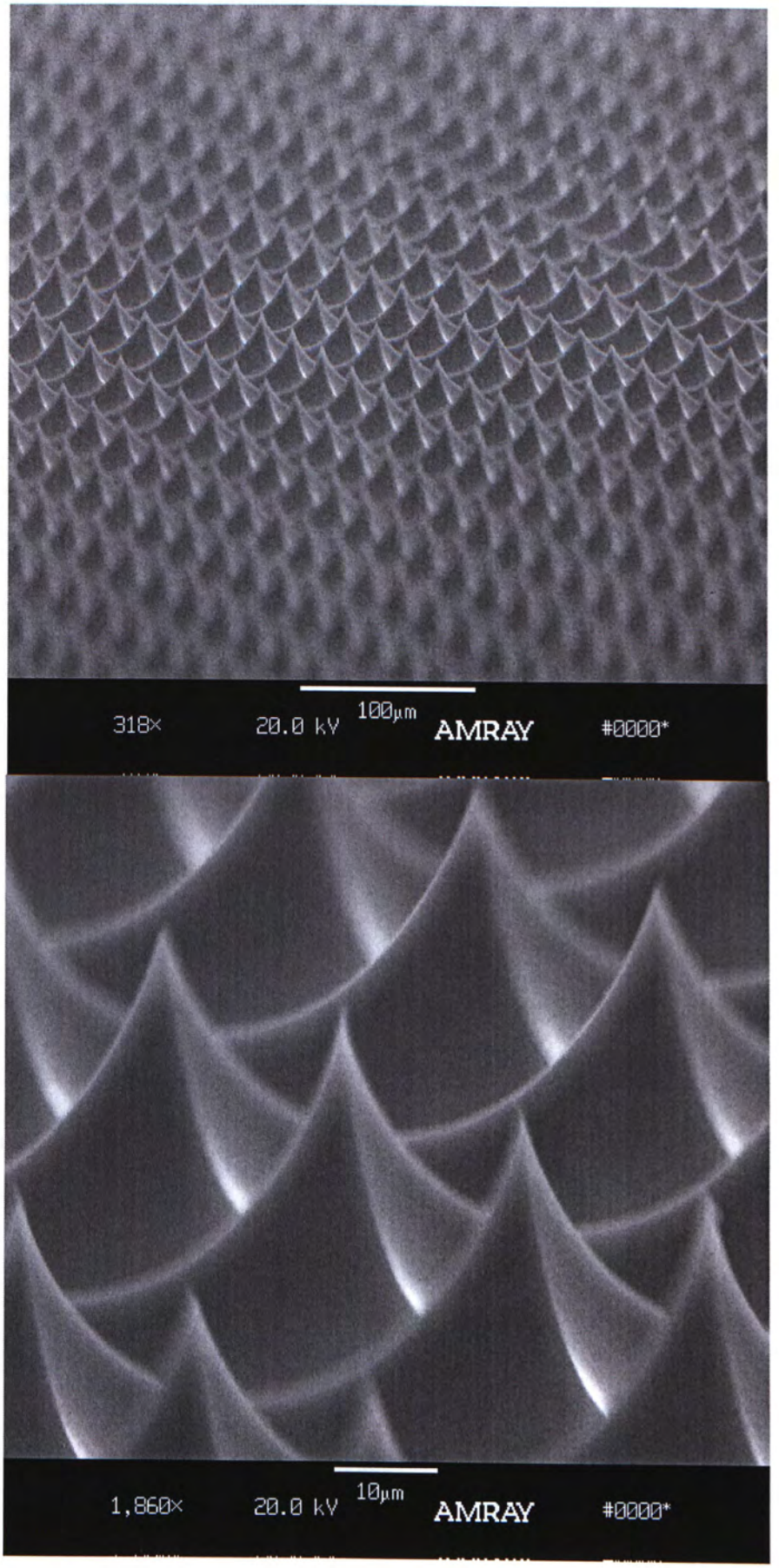

Figure 4.1.17 Typical SEM photomicrograph of silicon-tip array fabricated by using a two step anodization method with the negative circular mask.

Figure 4.1.18 shows I-V characteristic and the Fowler-Nordheim (FN) plot for FEAs fabricated by a conventional and the anodization method with different shapes of masks. The linearity of the FN plots as shown in figure 4.18b, shows that the anode current is due to electron field emission.

The turn-on voltage of the fabrication field emitters with circular, square, chess and negative circular are approximately 27V/μm, 28V/μm, 26V/μm and 33V/μm respectively when the emission current density reaches 1μA/cm^2. From figure 4.1.18b, the value of $\beta/\phi^{3/2}$ are determined to be 20, 25, 18, 16 and 17 for the anodized FEA samples with circular, square, chess, negative circular and conventional method respectively. The value of $\beta/\phi^{3/2}$ of samples with square are better than those prepared with other masking patterns because of the shape of the emitter.

For the turn-on voltage of the field emitter with circular, square and chess masks is almost the same. This may be due to the same base and height size (10μm). The turn-on voltage of field emitters fabricated with the negative circular mask is higher than for the other mask patterns. The base and height size is about 30μm in this case.

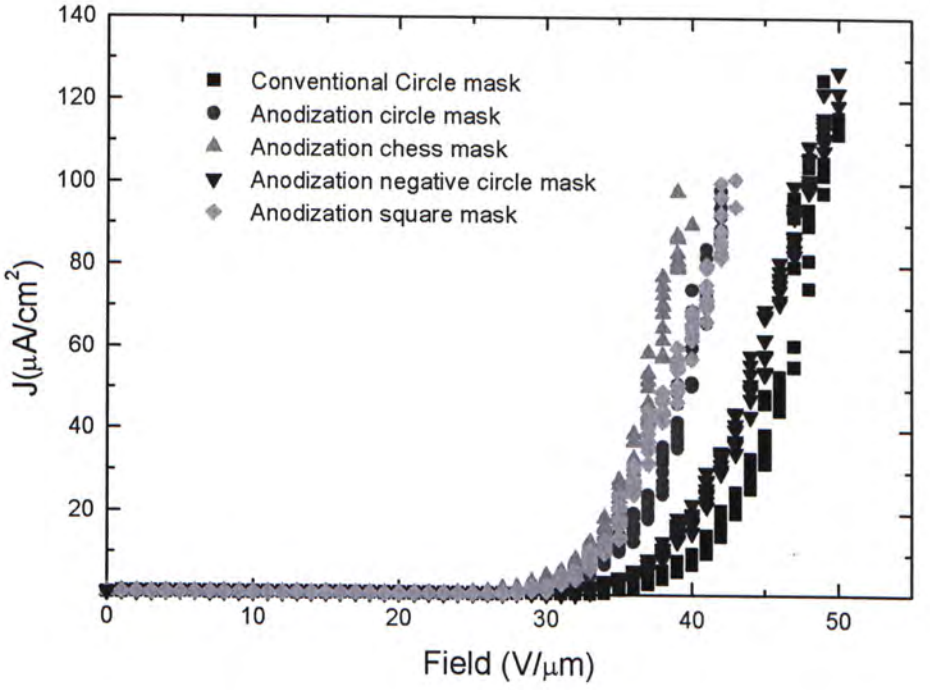

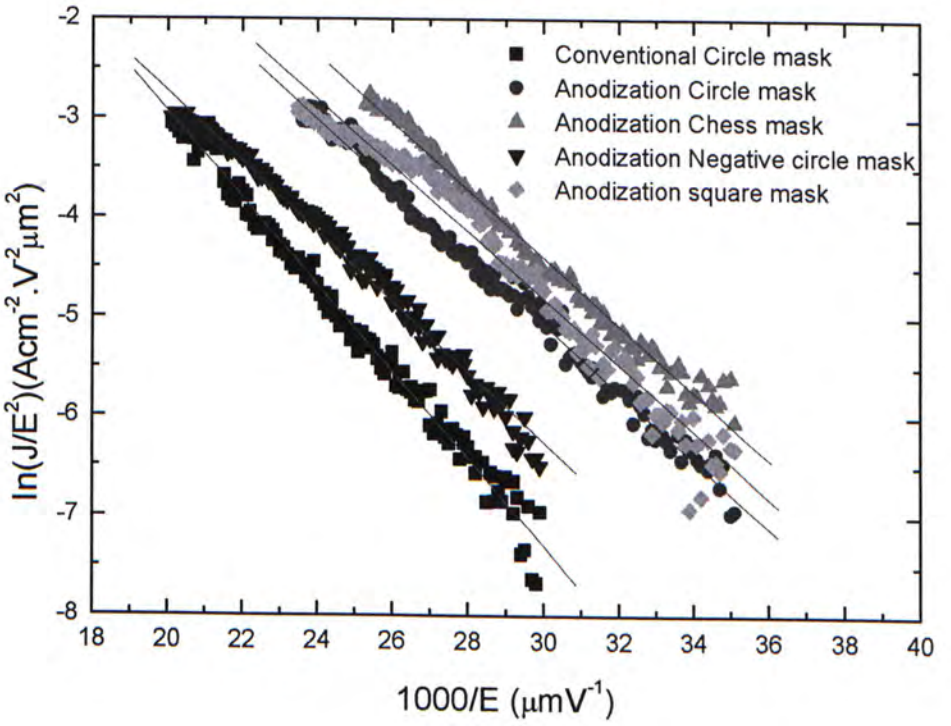

Figure 4.1.18 (a) Current-voltage characteristic for FEA fabricated using the two step anodization method and using a conventional HNO_3 etching method. (b) Data plotted in Fowler-Nordheim coordinates.

4.1.3.2 N type (111) sample

By the anodization process, (111) n-type silicon can also be used for silicon field emitter fabrication. The experimental detail is shown in table 4.1.3. SEM micrographs of field emitters fabricated with circular and negative circular masks on N-type Si(111) are in Figure 4.1.19 and Figure 4.1.20 respectively. For (111) silicon, the fabricated silicon FEA has a tip sharpness better than those fabricated on Si (100). In fact, the anodization current density for (111) orientation silicon is also larger than (100) orientation silicon. This may be due to the difference in etching rates of Si along (100) and (111) directrions. Etching rate along (111) direction will be slower due to lower surface energy.

Table 4.1.3 Experimental Detail of different mask pattern on silicon (111)

Substrate	Mask		First anodization	Second anodization	SEM
N type (111) 0.01Ωcm	Circular 20μm with space 20μm	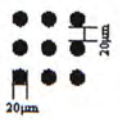	90mA/cm^2 for 1 mins	90mA/cm^2 for 1 mins	Figure 4.1.19
	Negative circular 20μm with space 20μm	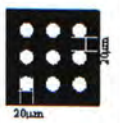	90mA/cm^2 for 1 mins	90mA/cm^2 for 2 mins	Figure 4.1.20

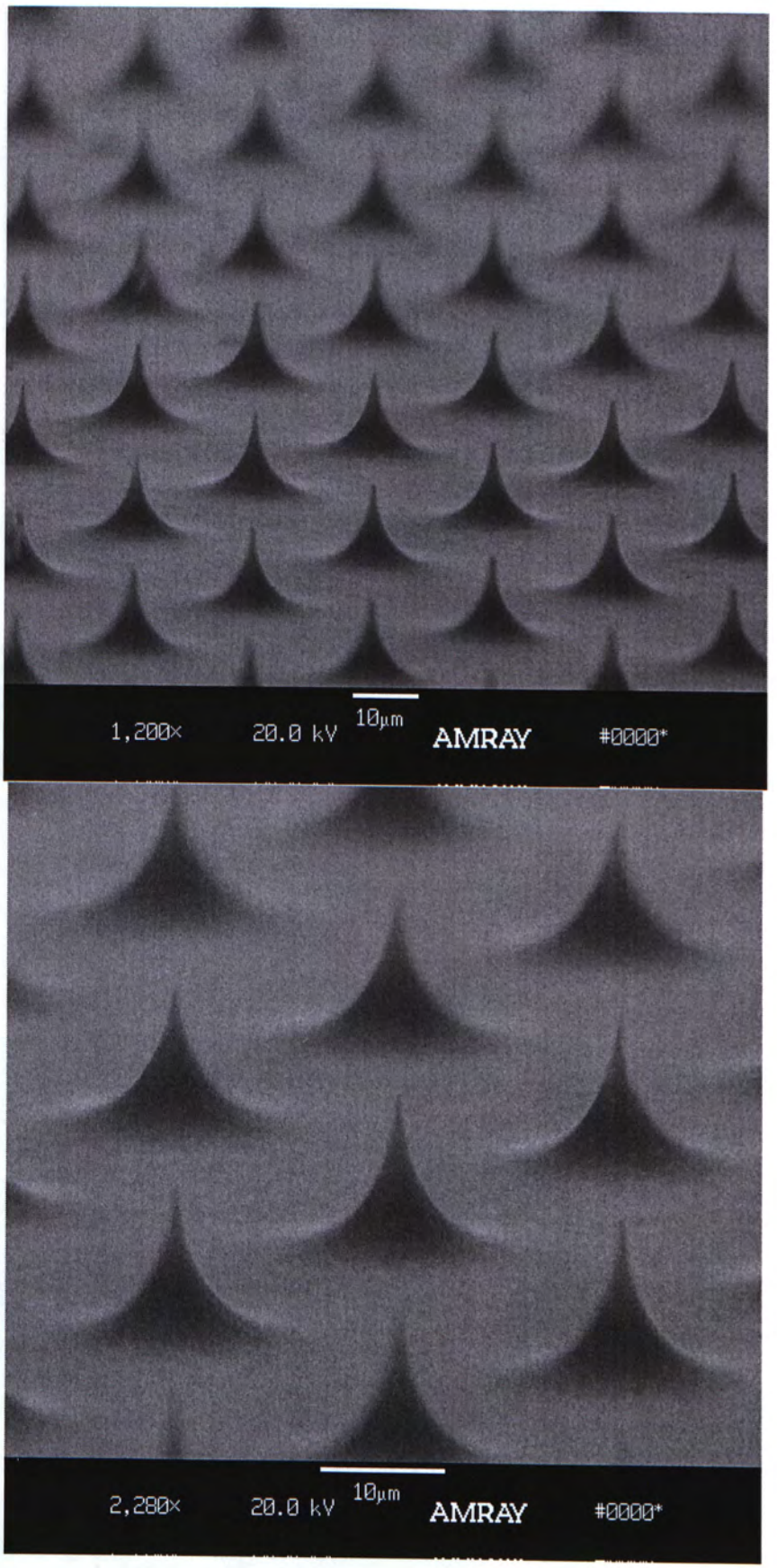

Figure 4.1.19 Typical SEM photomicrograph of silicon-tip array fabricated on substrate n-type Si(111) by using a two step anodization method with the circular mask.

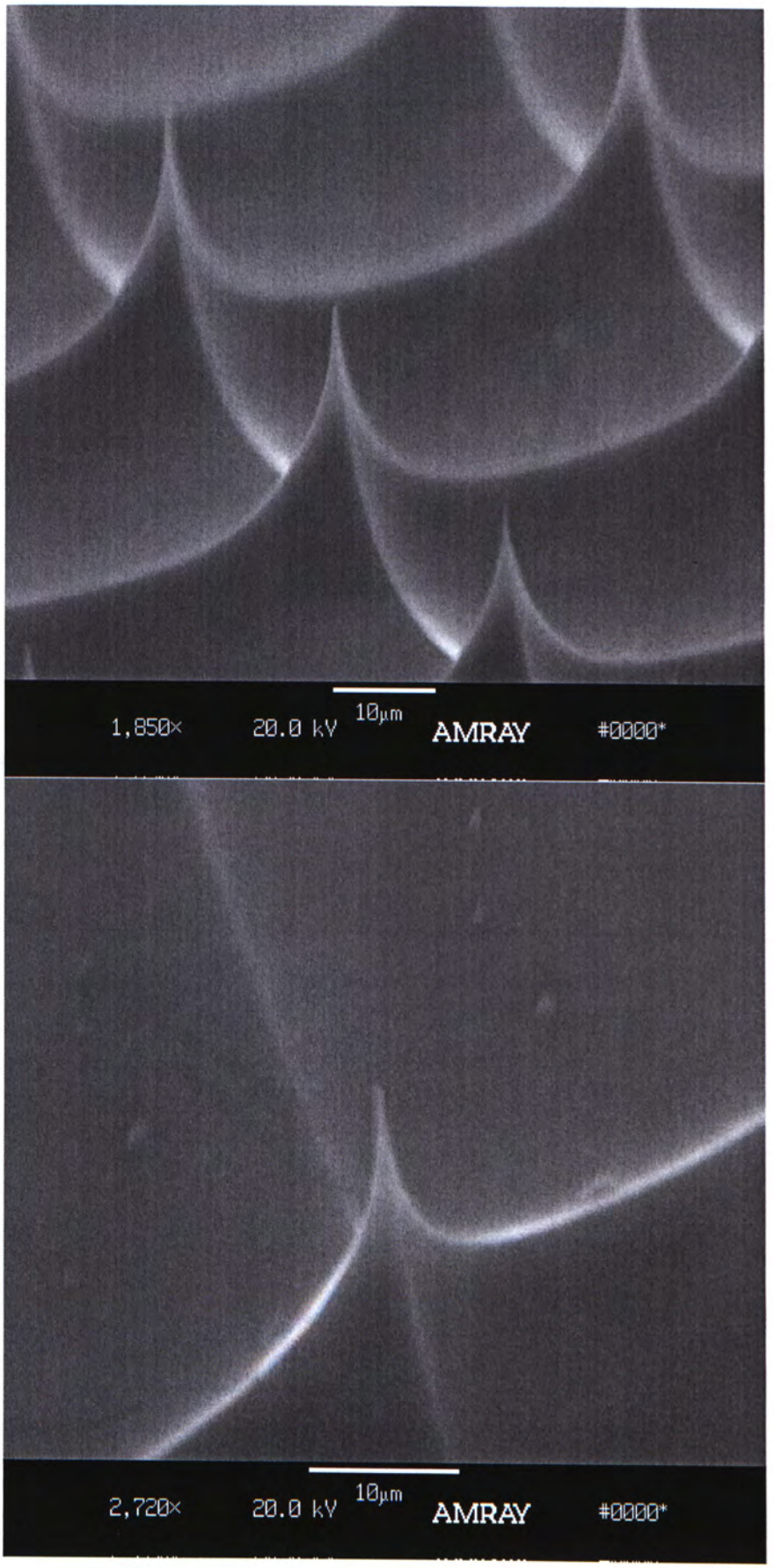

Figure 4.1.20 Typical SEM photomicrograph of silicon-tip array fabricated on substrate 111 by using a two step anodization method with the negative circular mask.

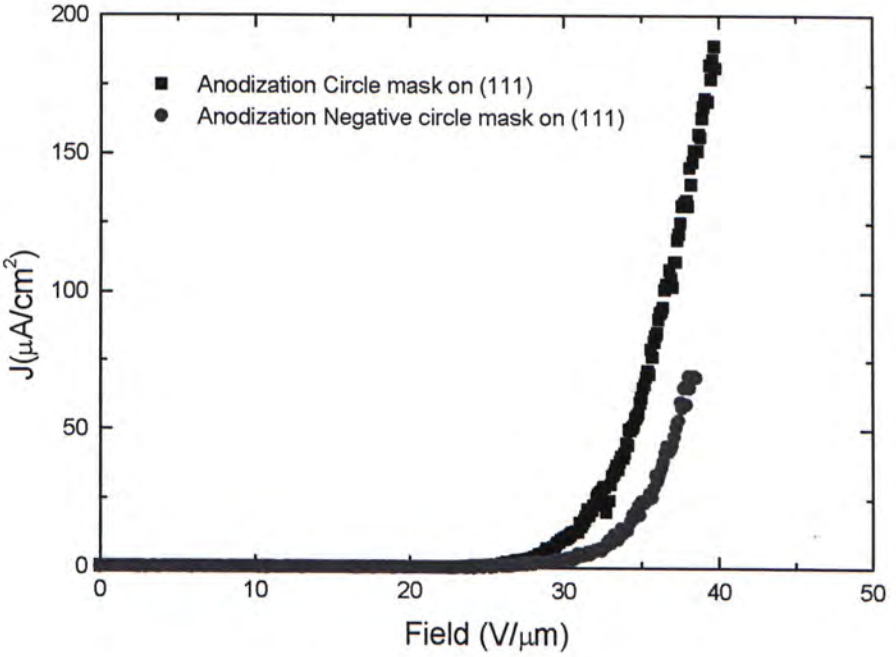

Figure 4.1.21 Current-voltage characteristic for FEA fabricated using the two step anodization method on (111) n-type silicon.

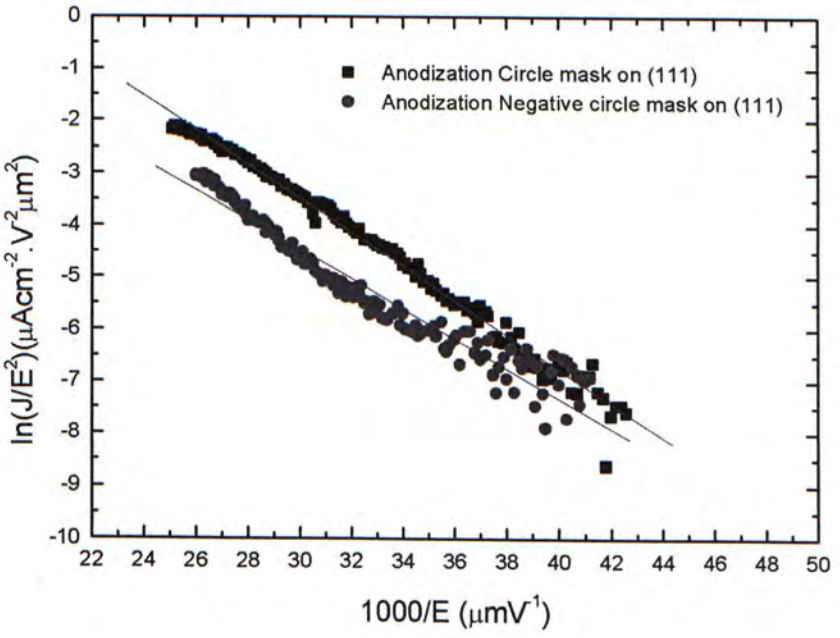

Figure 4.1.22 Data plotted in Fowler-Nordheim coordinates.

Figure 4.1.21 and 4.1.22 shows the I-V characteristics and the Fowler-Nordheim (FN) plot for FEAs fabricated on (111) silicon field emitter with circular and negative circular shaped masks.

The turn-on voltage of the fabrication field emitters with circular and negative circular is approximately 26 V/μm and 27V/μm respectively when the emission current density reaches 1μA/cm^2 as shown in figure 4.1.21. The value of $\beta/\phi^{3/2}$ are determined to be 23, 20 for the anodized FEA samples on (111) n-type silicon with circular and negative circular method respectively.

For the FEA fabricated on Si (111) n-type, the turn-on voltage and the value of $\beta/\phi^{3/2}$ is also better than those fabricated on (100) n-type silicon. This is because of the sharpness of the emitter formed on (111) silicon is greatly improved from two step anodization method as shown in figure 4.1.19 and 4.1.20.

4.1.3.3 Fluctuations of the emission current

The fluctuations of the emission current from the silicon field emitters fabricated with different masks was measured. The fluctuation is defined by $(I-I_{ave})/I_{ave}$ where I is the emission current and I_{ave} is the average emission current during the measurement. The r.m.s. value of the current fluctuations is also calculated.

The emission current from the conventional method shows a larger fluctuation than that of the anodization field emitter with circular mask as shown in figure 4.1.23a. The two step anodization method cause a geometrical change in the tip apex. The field emitter from the anodization method is more stable than that of the field emitter by conventional method. This is because of the increase in the number of emission sites which has the same effect as the ensemble averaging in tip arrays from anodization.

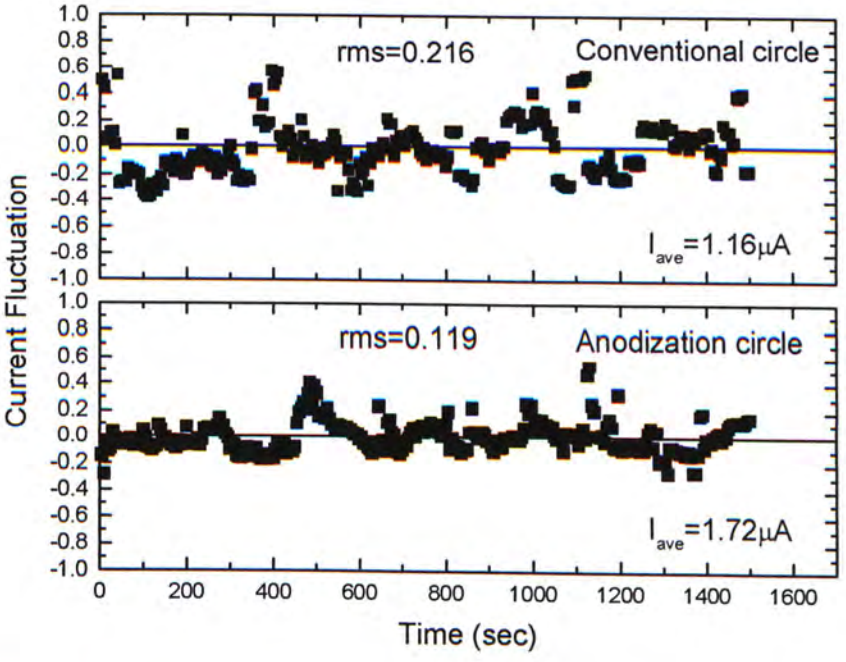

Figure 4.1.23 Fluctuation of emission current of (a) conventional circular mask and (b) anodization circular mask

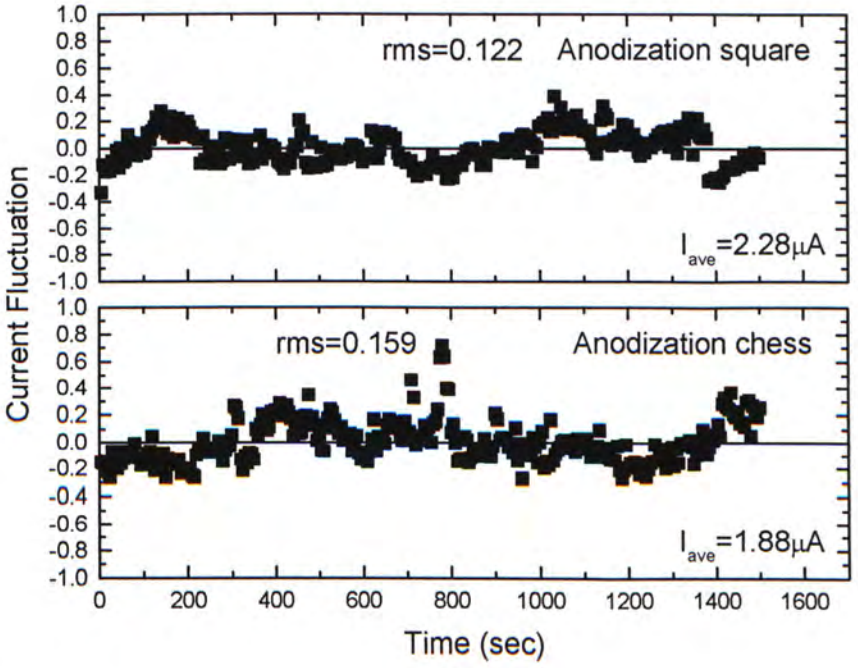

Figure 4.1.24 Fluctuation of emission current of (a) anodization square mask and (b) chess mask

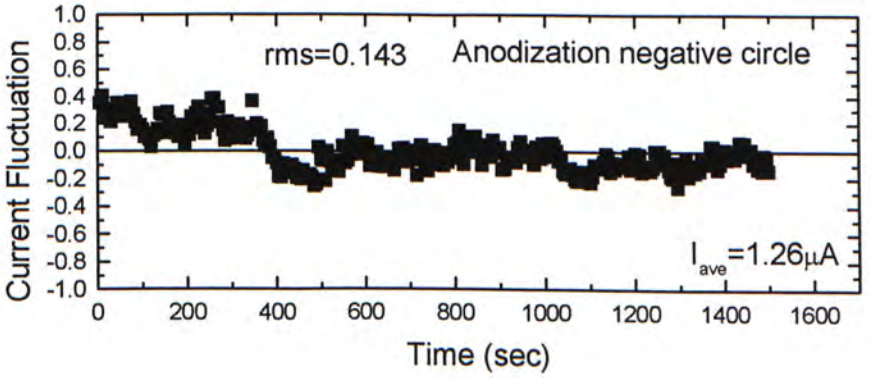

Figure 4.1.25 Fluctuation of emission current of anodization negative circular mask

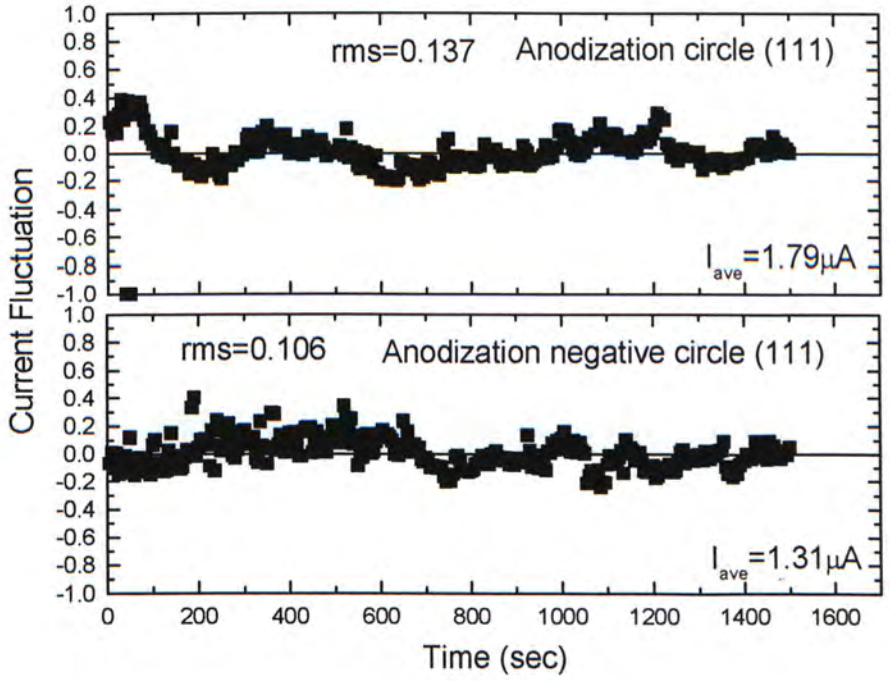

Figure 4.1.26 Fluctuation of emission current of (a) anodization circular mask on (111) and (b) negative circular mask on (111)

From figure 4.1.24, the emission current from the field emitter fabricated using the chess shape mask shows a larger fluctuation than that fabricated with the square mask. This fluctuation of the emission current may be due to the space charge between two neighboring tips.

From figure 4.1.23 and figure 4.1.25, the fluctuation of the emission current from the field emitters fabricated by anodization with circular mask is lower than that of the field emitter fabricated with negative circular mask. This is due to the larger number of emission sites in the former case.

In (111) orientation, the emission current from the field emitter fabricated with the negative circular mask shows a smaller fluctuation than that fabricated with circular mask as shown in figure 4.1.26. This may be due to better sharpness in the field emitter fabricated with negative circular mask.

A summary of the field emission characteristics of FEA fabricated by different mask pattern and silicon substrates with different orientations is in table 4.1.4. It shows that the overall turn-on field from the two step anodization method is between 26 and 33 V/μm. The overall current density of the field emitter and the value of $\beta/\phi^{3/2}$ is also improved when compared with conventional wet etching.

Table 4.1.4. Summary of field emission characteristic of different mask pattern field emitter

Material	Technique	Experimental condition	Current density ($\mu A/cm^2$)	Turn-on Field (V/μm)	$\beta/\phi^{3/2}$	Stability rms value of fluctuation
Silicon (100) n-type 0.01Ωcm	Wet isotropic etching	Circular mask	130	35	15	0.216
Silicon (100) n-type 0.01Ωcm	Two Step Anodization	Circular mask	100	27	19	0.119
		Square mask	100	28	19	0.122
		Chess mask	130	26	18	0.159
		Negative circular mask	100	33	19	0.143
Silicon (111) n-type 0.01Ωcm	Two Step Anodization	Circular mask	180	26	19	0.137
		Negative circular mask	70	27	22	0.106

4.1.3.4 The effect of the concentration of HF solution on First Step Anodization

In the electropolishing processes, the concentration of the HF solution is very important. This is because the uniformity depends greatly on the concentration of the HF solution and the current densities being applied. If this is not optimized, the etching rate and the shape of the field emitter will vary from point to point. For example, the size of the tip is not uniform at the center and edges of the sample if an

HF:H_2O=1:100 solution is used. FEA with uniform size distribution of tips are fabricated with the HF:H_2O =4:75 solution.

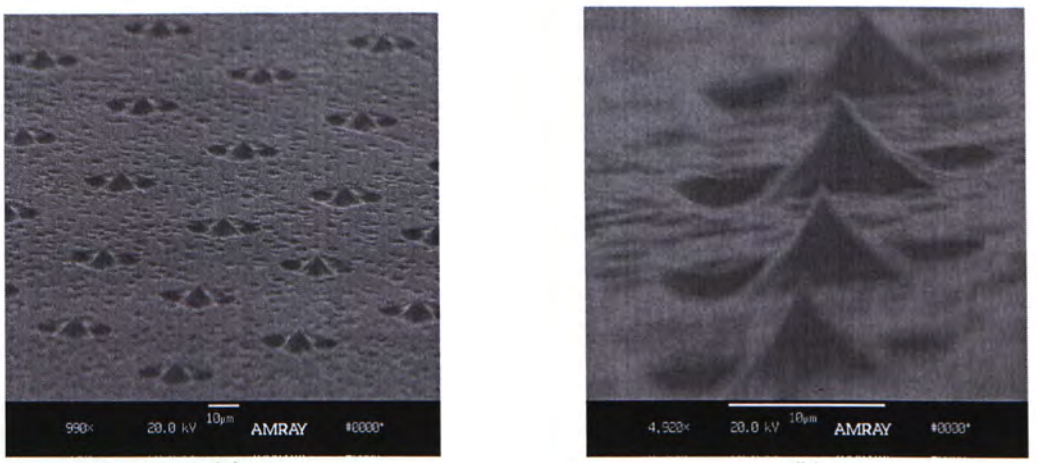

(a) (b)

Figure 4.1.27 Typical SEM photomicrograph of silicon-tip array fabricated by using HF:H_2O (1:100) solution with a current density of 90mA/cm^2 for 1 minute in the dark (a) Center of sample (b) Edge of sample.

4.1.3.5 The effect of the concentration of HF solution on the Second Step Anodization-Porous silicon formation

During the formation of porous silicon, the uniformity and the thickness of porous silicon greatly depend on the concentration of HF and current densities applied. If the processing conditions are not optimized, the uniformity, the thickness of porous silicon and the shape of the field emitter vary from point to point along the sample. Typical examples is shown in Figure 4.1.28.

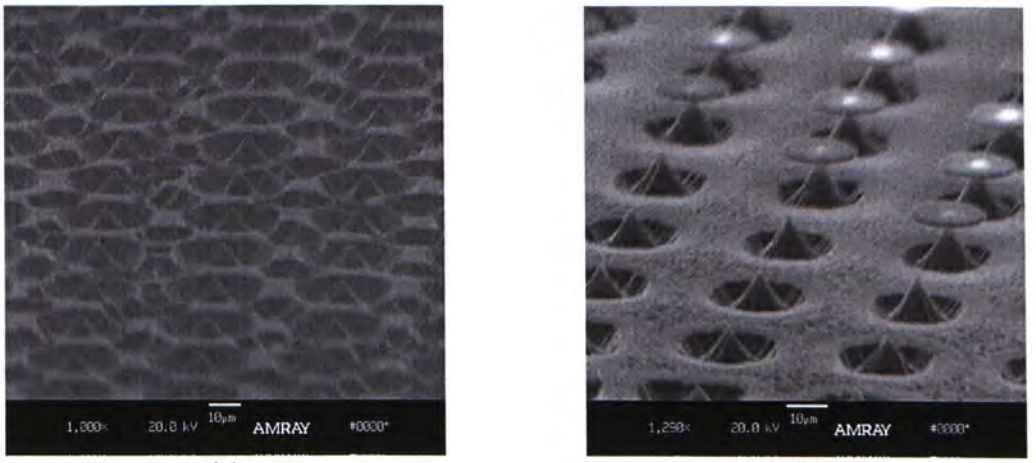

(a) (b)

Figure 4.1.28 Typical SEM photomicrograph of silicon-tip array fabricated by HF:H_2O:C_2H_5OH = 1:1:1 solution with current density of 90mA/cm^2 for 1 minute in dark (a) Center of sample (b) Edge of sample.

4.1.3.6 Gated silicon field emitter

As the two step anodization method is a very simple and fast etching method for fabrication of field emitter arrays, we also studied improvement of the fabrication process for gated emitters.

A schematic diagram of the fabrication process of gated FEA using the two step anodization method with only one photolithography step is shown in figure 4.1.29.

In this fabrication process, the two step anodization method is used to decrease the fabrication time. In addition, only one step of photolithography is needed which can minimize the complexity of the gated field emitter fabrication processes.

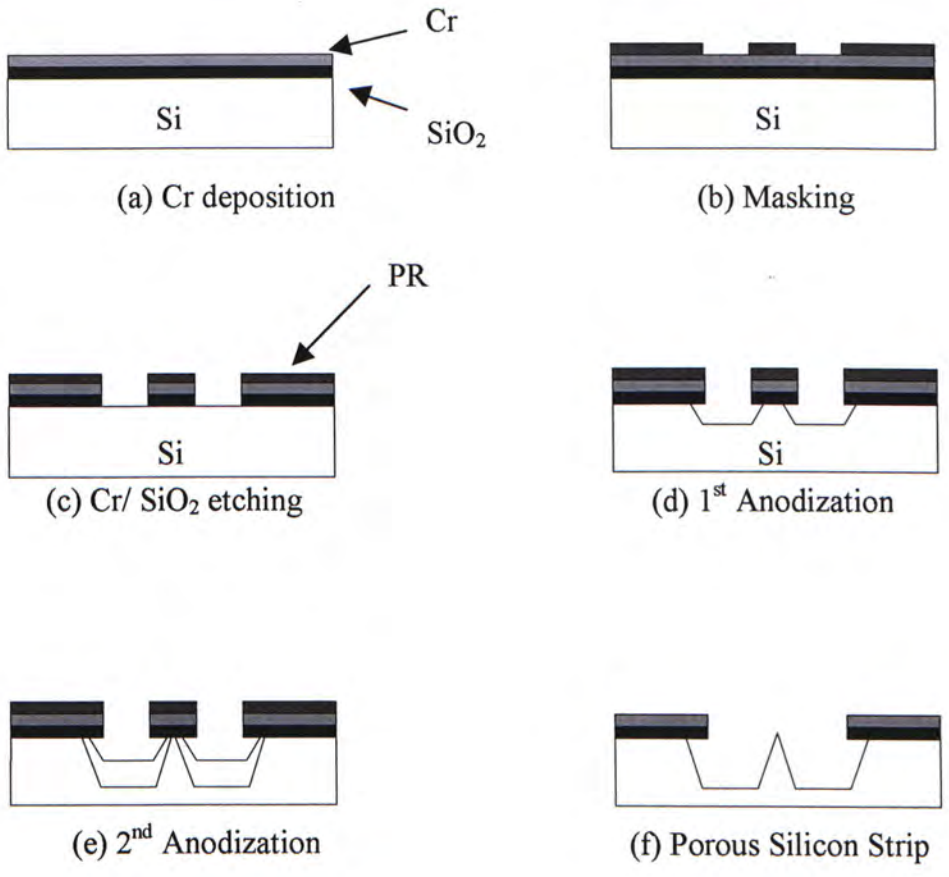

Figure. 4.1.29. Fabrication process of gated FEA using two step anodization methods with only one photolithography step.

In this method, chromium (Cr) is first deposited on a 0.01Ωcm <100> silicon wafer with 1μm thermal oxide by using evaporation as shown in figure 4.1.29a. Positive Photoresist AZ-1450J is used to define the gated mask onto the Cr surface. After the coating of photoresist, Cr and SiO_2 are wet etched as shown in figure 4.1.29b and 4.1.29c. And then the two step anodization method is used to fabricate the gated FEA with SiO_2 as the insulator.

In the first anodization step, the concentration of solution is $HF:H_2O$ (4:75). Current densities of $70mA/cm^2$ is used for 1 minute. After the first anodization step, the shape of silicon field emitter is defined. The Cr/SiO_2 cap still remains on the top of the tip. Then the second anodization step is performed by using the solution of $HF:H_2O:C_2H_5OH$ (20:37:16) with a current density of $70mA/cm^2$ for 1 mins. Finally, the porous silicon layer is removed by $HF:CH_3COOH:HNO_3$ (2:3:95) solution while the etching is terminated, it is followed by the PR strip. The mask pattern is shown in figure 4.1.30.

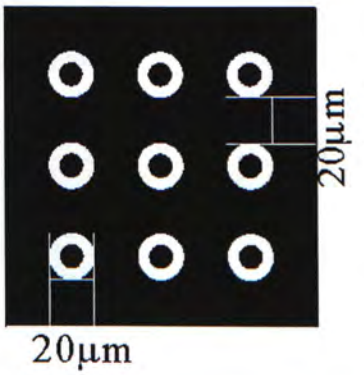

Figure 4.1.30 The mask pattern of gated silicon field emitter

Figures 4.1.31 and 4.1.32 show typical SEM photomicrographs of the gated FEA with circular mask and square mask respectively. However, the Cr gate layer can be easily shorted to silicon tip in this wet etching method. Therefore, field emission measurement cannot be performed.

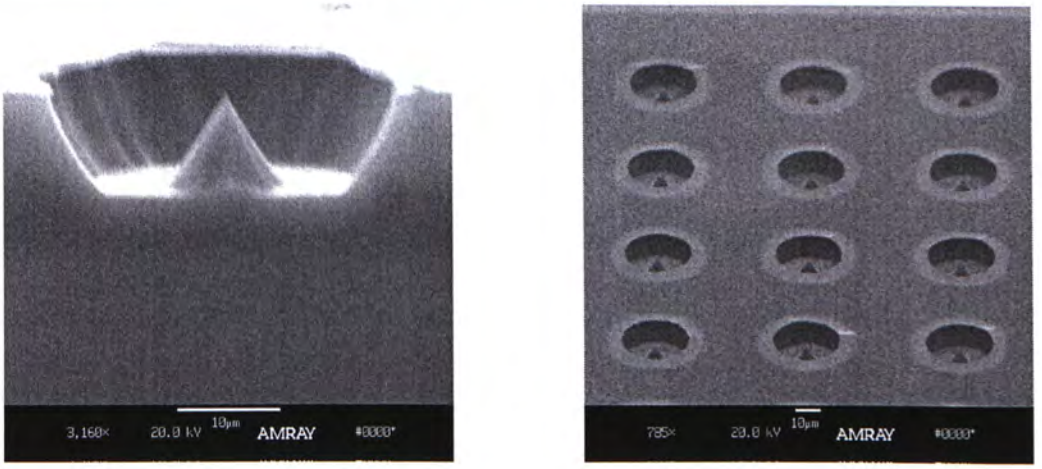

Figure 4.1.31 Typical SEM photomicrograph of gated FEA with circular mask.

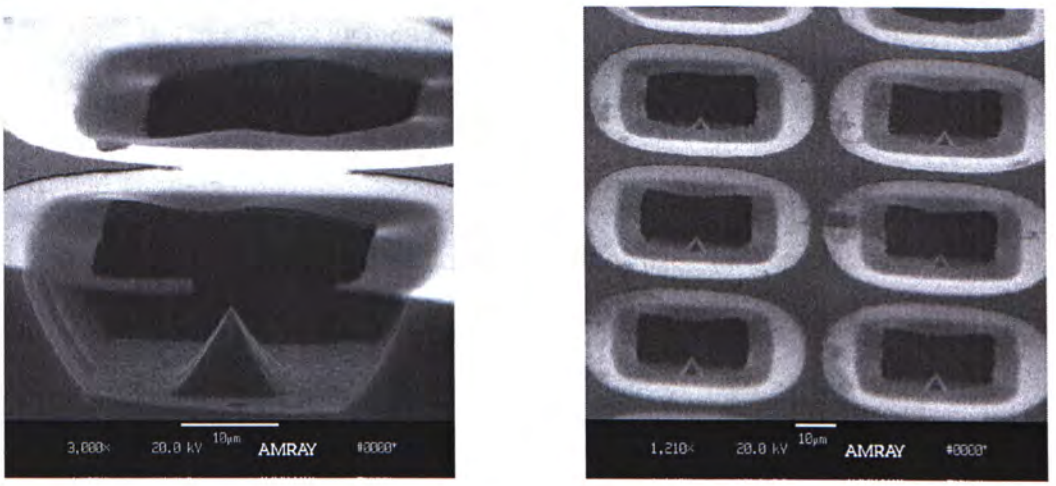

Figure 4.1.32 Typical SEM photomicrograph of gated FEA with square mask.

4.1.4 CONCLUSIONS

A two step anodization of silicon with different HF solutions is performed to fabricate high aspect ratio silicon Field Emitter Arrays on n-type silicon with different shapes. The field emission characteristics of the field emitters from this method are better than those fabricated by isotropic HNO_3 etching solution. By this method, different shaped emitter arrays with good uniformity and reproducibility have been fabricated. The overall improvement in field emission properties is attributed to the increase in surface roughness by the anodization process.

4.2 Anisotropic texturing process

In the previous section, the field emitters fabricated by the anodization etching method have been studied to improve the field emission characteristics in comparison with those fabricated by conventional wet isotropic etching. However, the overall current density and the value of $\beta/\phi^{3/2}$ of the fabricated field emitters are only slightly improved in comparison with emitters fabricated by conventional wet etching. There can be further improvement in current density if the size of the emitter apex is reduced further and the density of emitters is increased. We will shows in this section that anistropic texturing improves the size and density of silicon field emitters.

In the texturing method, anisotropic etching solutions are used to cause the formation of randomly distributed silicon field emitters on an Si(100) surface without any masking pattern. The field emission characteristics are studied.

4.2.1 Introduction

In the texturing process, anisotropic etching solutions of potassium hydroxide (KOH) and Isopropyl alcohol (IPA) are used to form the randomly distributed silicon field emitters on the Si(100) surface without any masking pattern [118-122].

Pyramid formation on the surface of the (100) mono-crystalline silicon wafers by using anisotropic texturing solutions is an important and effective means of reducing the reflectivity from the front-side surface of silicon solar cells [118]. In this study, the pyramids so formed are used to fabricate a field emitter.

The formation of the randomly distributed pyramids is thought to be caused by the hydrogen bubbles evolving during the etching reaction [123]. These bubbles

stick onto the silicon surface and perturb the etching process leading to the formation of <111> facets.

Relatively mild KOH solutions with low concentrations (less than 5%) of IPA are used to generate the textured surface with microscopic pyramids on the <100> silicon surface. The etching rate is found to be 0.1-0.5 μm/min.

The hydrogen bubbles, their density and the rate of the etching reaction define the geometry and density of the silicon field emitters with a pyramid base size of about 1μm.

The concentration of KOH in IPA, etching time and temperature are optimised in order to achieve regularly shaped and repeatable high density of silicon field emitters on the Si (100) surface. The mechanism of texturing process is shown in Figure 4.2.1.

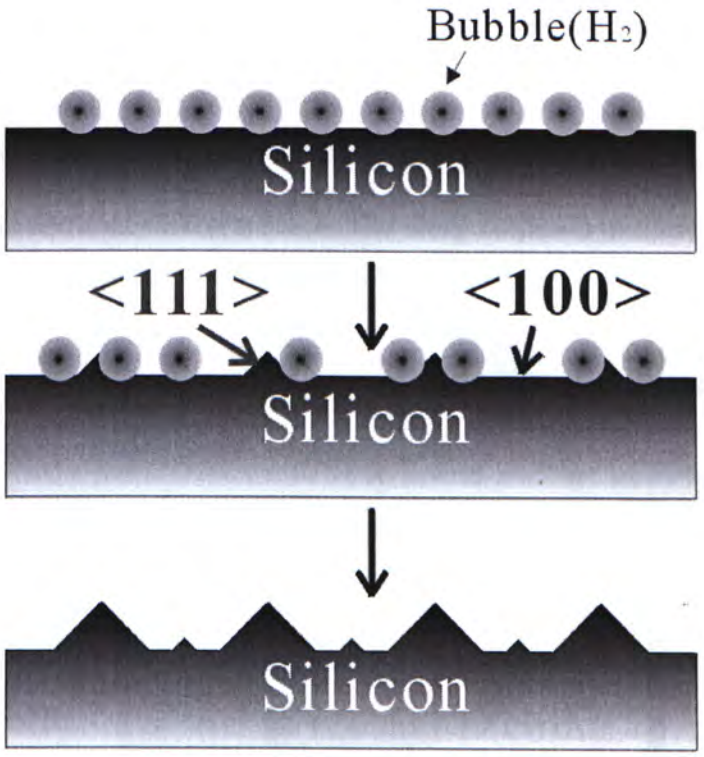

Figure 4.2.1 The mechanism of texturing process

4.2.2 Experimental details

In this work, the two evaluated factors are the IPA concentration and the etching time. The boiling point of IPA is 82.5°C. So, the IPA should never be added to the solution if the temperature is at or above this temperature. For safety reasons, it is prudent to add IPA into the water prior to adding the KOH.

The silicon wafer is held in a Teflon wafer basket and is immersed in the etching solution. The wafer basket is kept at a height of about 3cm above a magnetic stirrer. The rotational speed of the stirrer can be varied.

A motor is used to vibrate the Teflon wafer basket in order to avoid too many bubbles becoming attached to the silicon wafer. This is because too many hydrogen bubbles attached onto the silicon wafer will affect the geometry and density of the textured silicon surface. The setup is shown in figure 4.2.2.

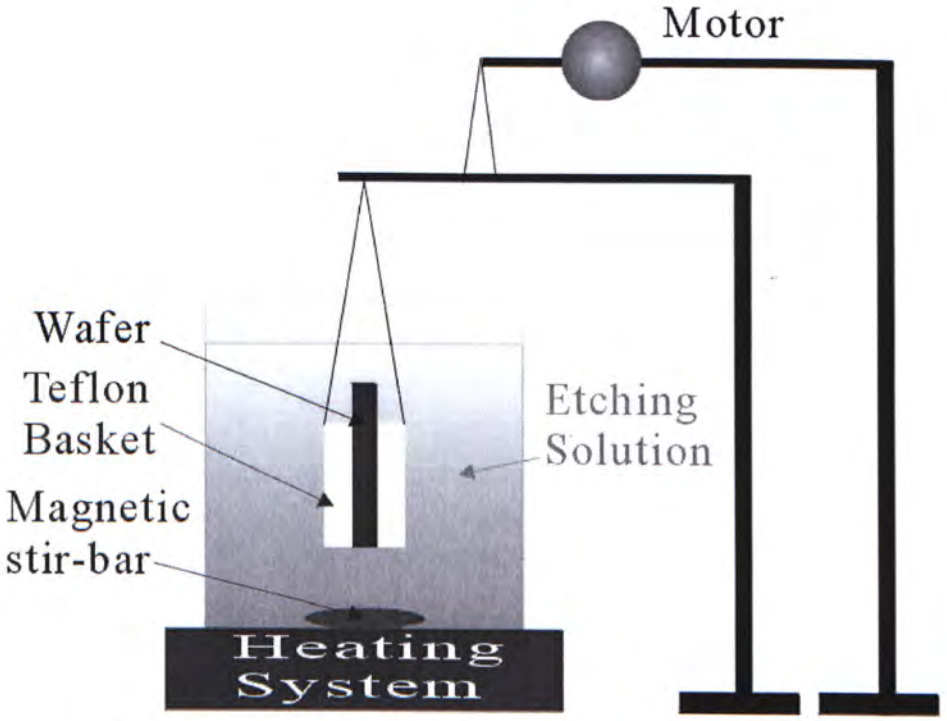

Figure 4.2.2 Experimental Setup for texturing process

The silicon wafer is first etched in a buffered-HF solution. After the buffered HF etching, the wafer is stored in isopropyl alcohol (IPA) to prevent surface oxidation. The wafer is then immersed in the etching solution for the required period of time, then removed and rinsed in deionized water. A constant temperature heating system is used to maintain the temperature of the chemical solution at 80°C. The etching solution is prepared with deionized water, graded KOH and IPA solution.

Table 4.2.1 Experimental detail of field emitter with different concentration of IPA and etching time

Material	Experimental condition	IPA(%)	Etching time (min)
Silicon (100) n-type 0.01Ωcm	Temperature at 80°C, KOH concentration 5%	3%	5 min, 10 min, 20 min
		6%	5 min, 10 min, 20 min
		10%	10 min

4.2.3 Results and Discussions

In this experiment, the temperature of the solutions is kept constant at 80°C and the KOH concentration is kept at 5%. The reaction time and IPA concentration are varied.

Figure 4.2.3 shows optical micrographs of the Si (100) surface treated with etching solution with IPA concentration varying from 1% to 6% for 10 minutes. The size and the density of the silicon field emitters are found to vary. The etching solution with 3% concentration of IPA is found to give smaller size and higher density of field emitters.

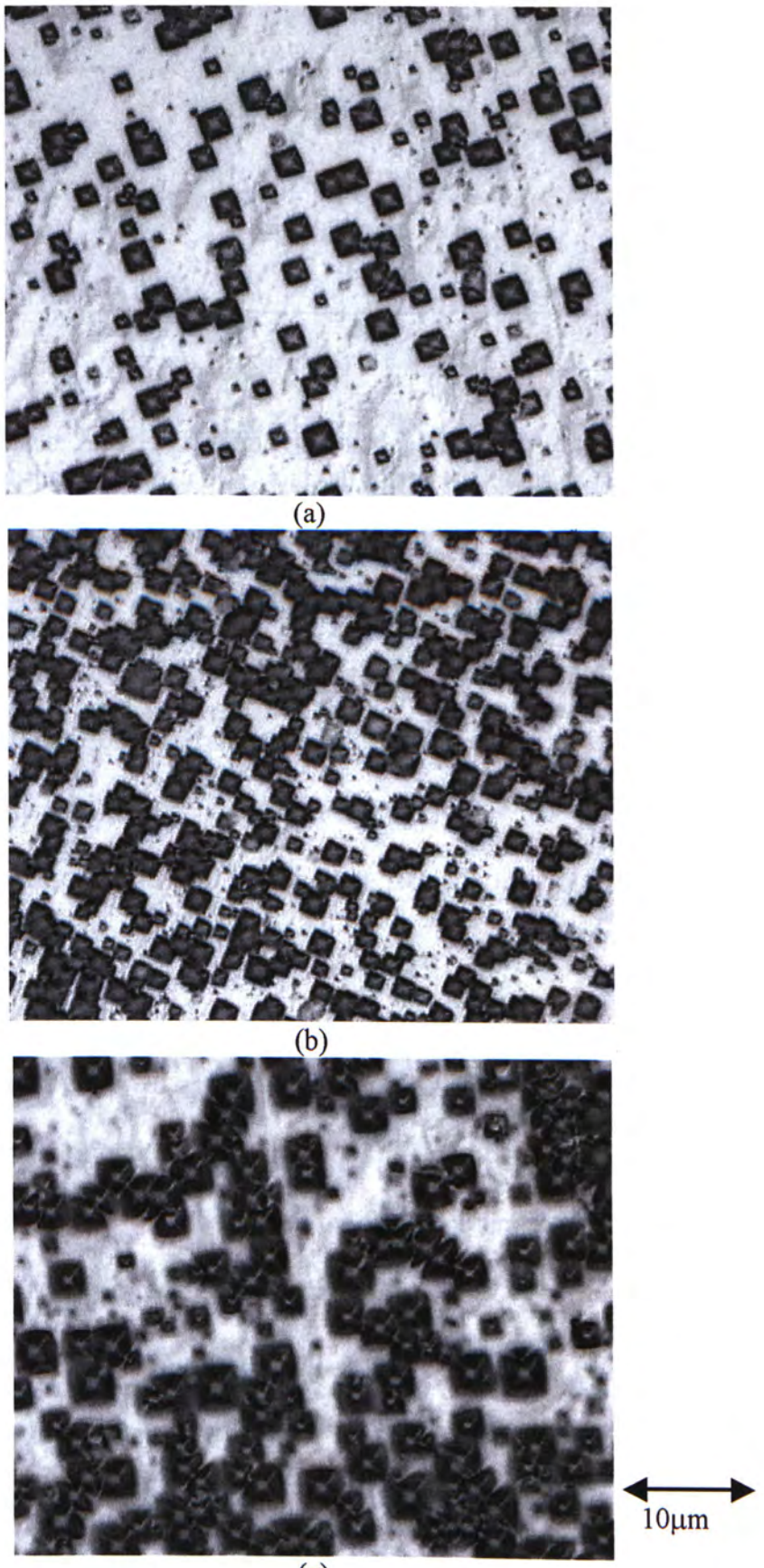

Figure 4.2.3 Microscopy photograph of texturing process from 5% KOH solution, etching time is 10min at 80°C with different IPA concentration (a) 1%, (b) 3% and (c) 6%

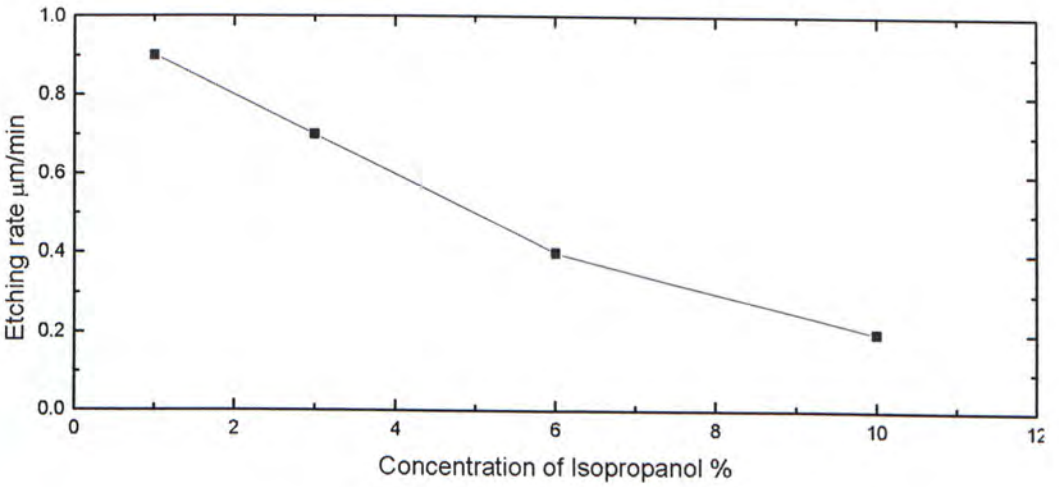

Figure 4.2.4 The etch rate of silicon as a function of the IPA concentration at the etchant temperature of 80°C and the concentration of KOH is 5%

The etching rate of silicon as a function of the IPA concentration is shown as figure 4.2.4. The IPA concentration should be kept at a relatively low level in order to obtain the optimum etching rates. But with IPA below 1%, it is found that no silicon field emitters are formed.

Etching time is also found to affect the size and density of the silicon field emitters. In Figure 4.2.5, optical micrographs of the samples etched with 3% IPA for 10 and 20 minutes are shown. The size of the field emitters are nearly the same but there is higher density of field emitters for longer etching.

In Figure 4.2.6, optical micrographs of the samples etched with 6% IPA for 10 and 20 minutes are shown. The size of the field emitters is found to decrease and there is a higher density upon longer etching.

The size of emitters fabricated with a 6% IPA solution (Fig. 4.2.6) is larger than those fabricated with a 3% IPA solution (Fig. 4.2.5) while etching time is 20 minutes. In all cases, 100% texturing can be obtained. Under 100% texturing, the density of silicon field emitters prepared in 3% IPA solution is higher than for the 6% IPA solution.

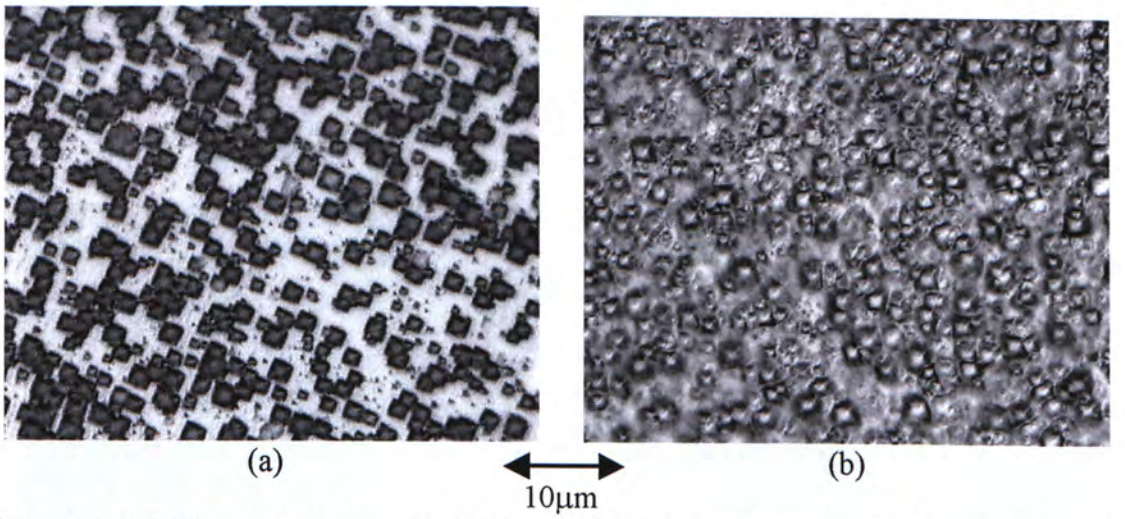

Figure 4.2.5 Microscopy photograph of texturing process from 5% KOH solution with 3% IPA solution at 80°C for different etching time (a) 10min and (b) 20min

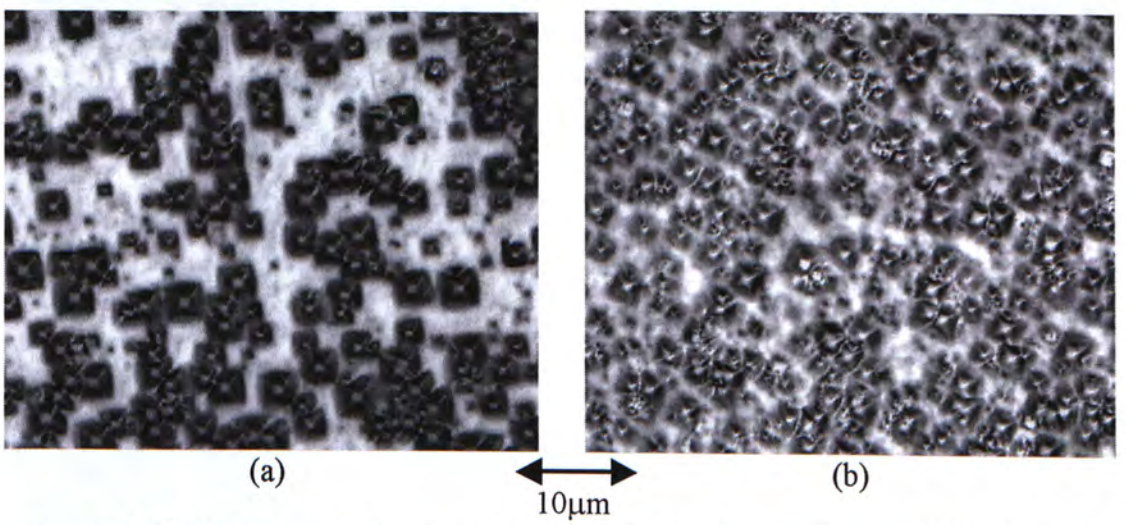

Figure 4.2.6 Microscopy photograph of texturing process from 5% KOH solution with 6% IPA solution at 80°C for different etching time (a) 10min and (b) 20min

SEM micrographs with higher magnification of samples treated with different of IPA concentrations are shown in Figure 4.2.7, Figure 4.2.8 and Figure 4.2.9. The size and density of the field emitters are consistent with the results from the optical micrographs.

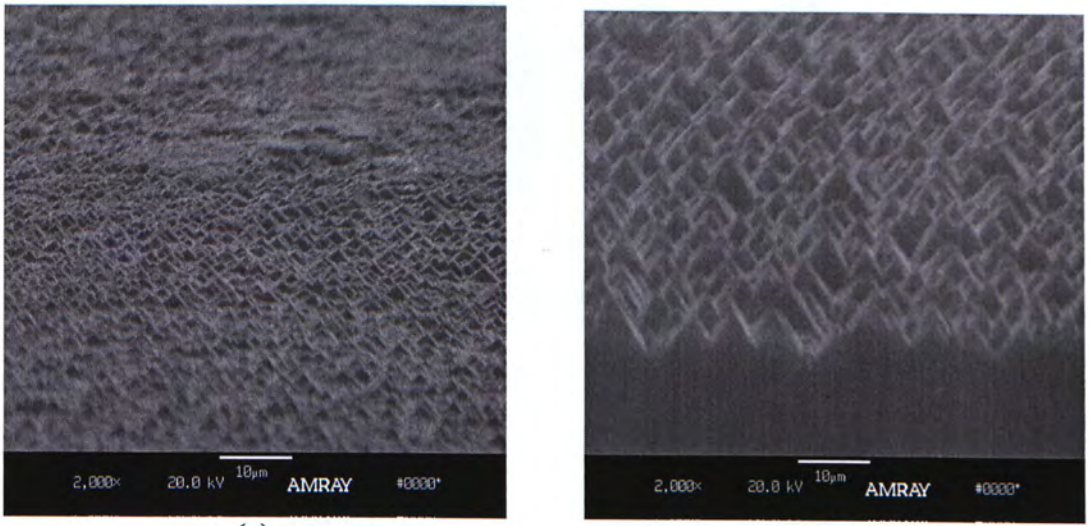

(a) (b)

Figure 4.2.7 2000X SEM micrograph of texturing process for etching 20min in 5% KOH solution at 80°C with (a) 3% IPA and (b) 6% IPA

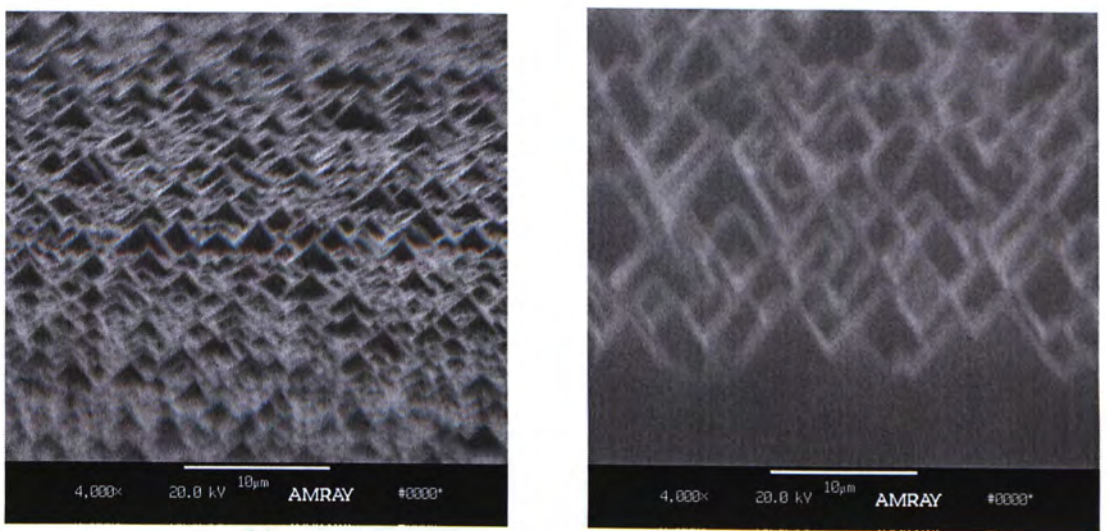

(a) (b)

Figure 4.2.8 4000X SEM micrograph of texturing process for etching 20min in 5% KOH solution at 80°C with (a) 3% IPA and (b) 6% IPA

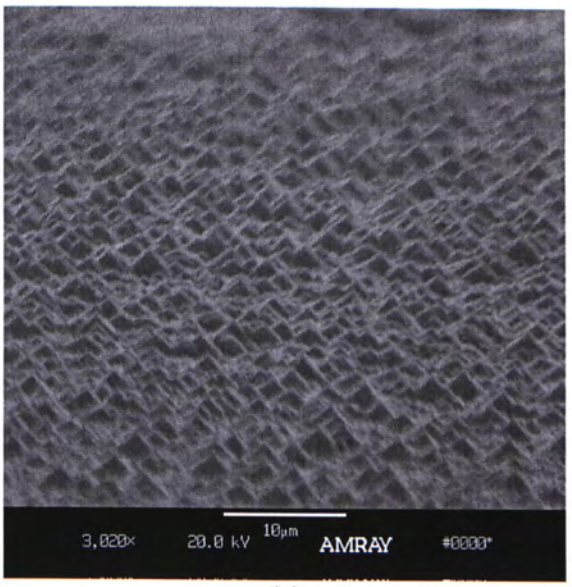

(a)

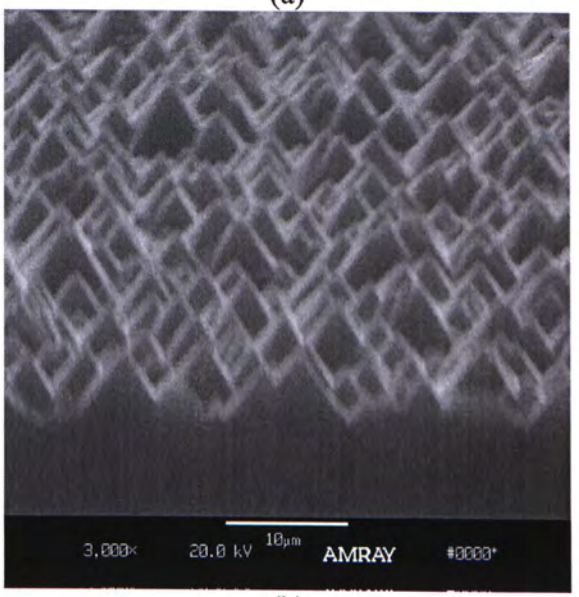

(b)

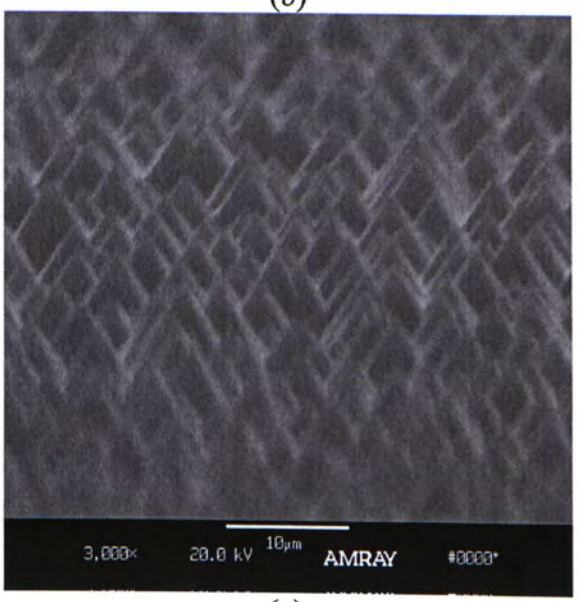

(c)

Figure 4.2.9 3000X SEM micrograph of texturing process for etching 20min in 5% KOH solution at 80°C with (a) 3% IPA, (b) 6 % IPA and (c) 10% IPA

The field emission characteristics of silicon field emitters fabricated by using 3%, 6% and 10% IPA with 5% KOH solution at 80°C for 10 min were measured and the results are shown in figure 4.2.10 and figure 4.2.11.

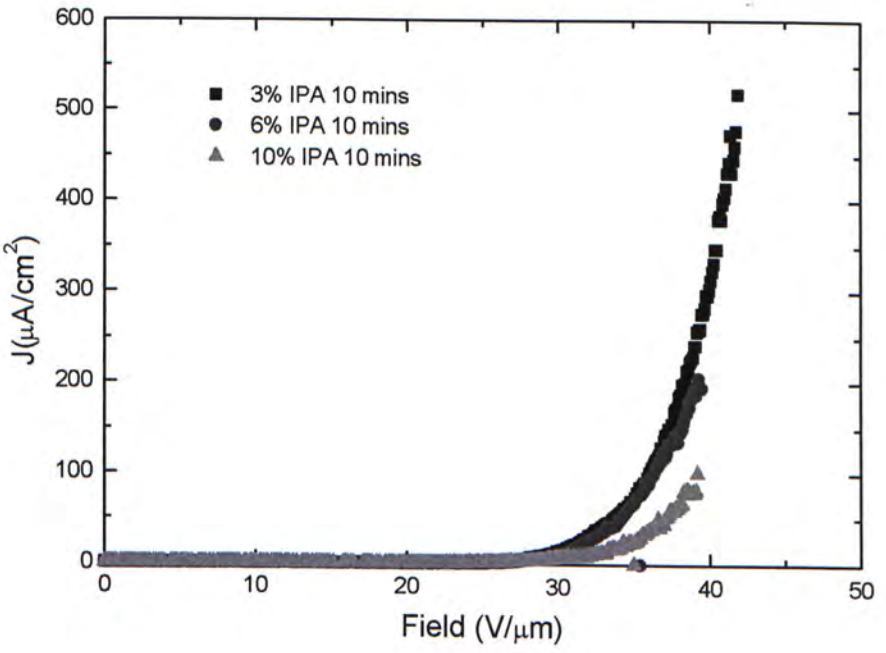

Figure 4.2.10 Field emission properties of field emitters prepared by IPA concentration of 3%, 6% and 10% with 5% KOH solution at 80°C for 10 min.

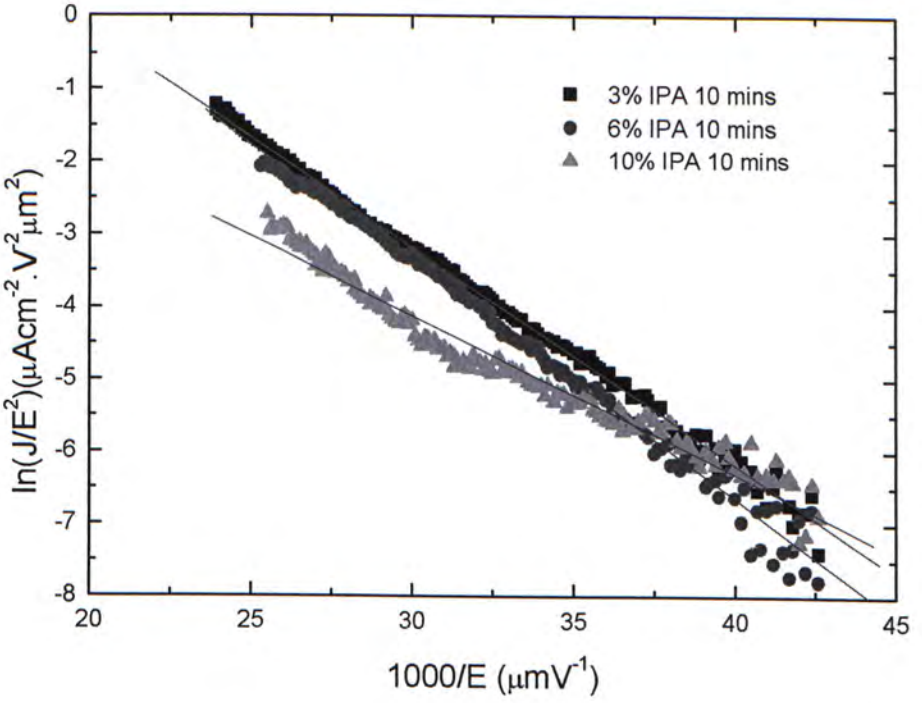

Figure 4.2.11 F-N properties of field emitters prepared by IPA concentration of 3%, 6% and 10% with 5% KOH solution at 80°C for 10 min.

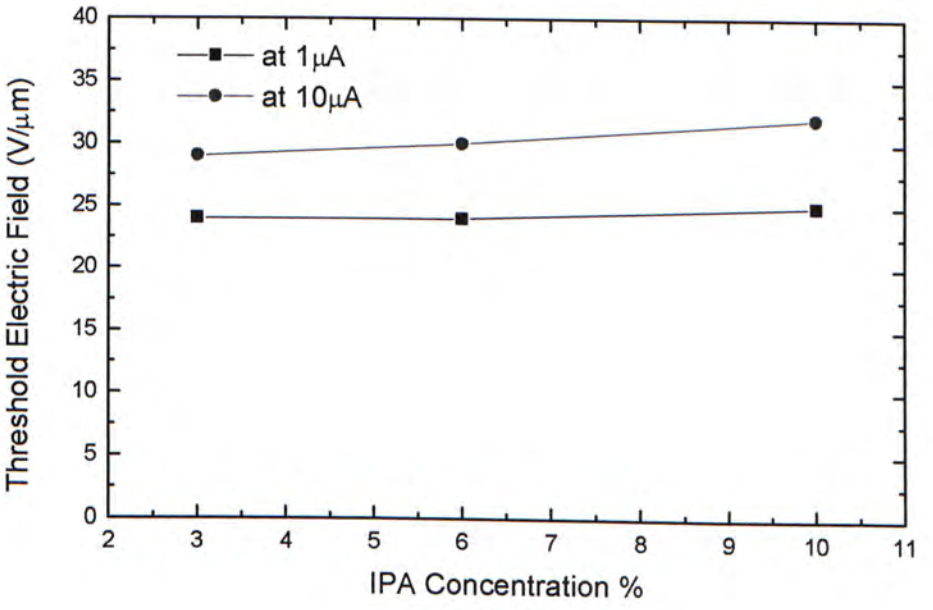

Figure 4.2.12 The threshold electric field (the applied electric field for emission current of 1μA and 10μA) as a function of the IPA concentration

With an etching time of 10 minutes, the turn-on field of silicon emitter prepared by using solution with 3%, 6% and 10% IPA is 24 V/μm, 24 V/μm and 25 V/μm, respectively. The emission turn-on field is defined as the field producing $1\mu A/cm^2$ of emission current.

It is appears that the lower percentage of IPA concentration gives rise to the low turn-on field. This is caused by the creation of randomly distributed silicon field emitters.

When the IPA concentration is increased from 3% to 10% with etching time of 10 minutes, the turn-on field of the emitters increases from 24V/μm to 25V/μm. The value of $\beta/\phi^{3/2}$ of emitter is determined to be 23, 20 and 20 for the samples with 3%, 6% and 10% of IPA respectively from figure 4.2.11.

Figure 4.2.12 shows that threshold electric field with emission current at 1μA and 10μA slightly increases when the concentrations of IPA increases. This may be due to the decrease in the density of silicon field emitter when the concentration of IPA increases. Also, the size of the silicon field emitters is increased when the concentrations of IPA increase from 3% to 10%.

Silicon field emitters prepared in 3% IPA solution for 10 minutes have emission current densities of $100\mu A/cm^2$ at 35V/μm.

Figure 4.2.13, shows the field emission properties of samples prepared in a 3% IPA with 5% KOH solution at 80°C for different etching time of 5min, 10min and 20min. The turn-on field is 38V/μm, 24V/μm and 25V/μm respectively. From figure 4.2.14, the corresponding value of $\beta/\phi^{3/2}$ of emitter is determined to be 12, 23 and 24 respectively.

In figure 4.2.15, the field emission properties of samples treated with etching solution containing IPA concentration of 6% for different etching times of 5min,

10min and 20min are shown. The turn-on field is 27V/μm, 26V/μm and 24V/μm respectively and from figure 4.2.16, the value of $\beta/\phi^{3/2}$ is determined to be 18, 20 and 26 respectively.

The turn-on voltages for the etching times of 10 min and 20 min are lower than for 5 min. Also, the value of $\beta/\phi^{3/2}$ and the emission current density increases with the increase in the etching time. This may be due to the increase in the number density of field emitters.

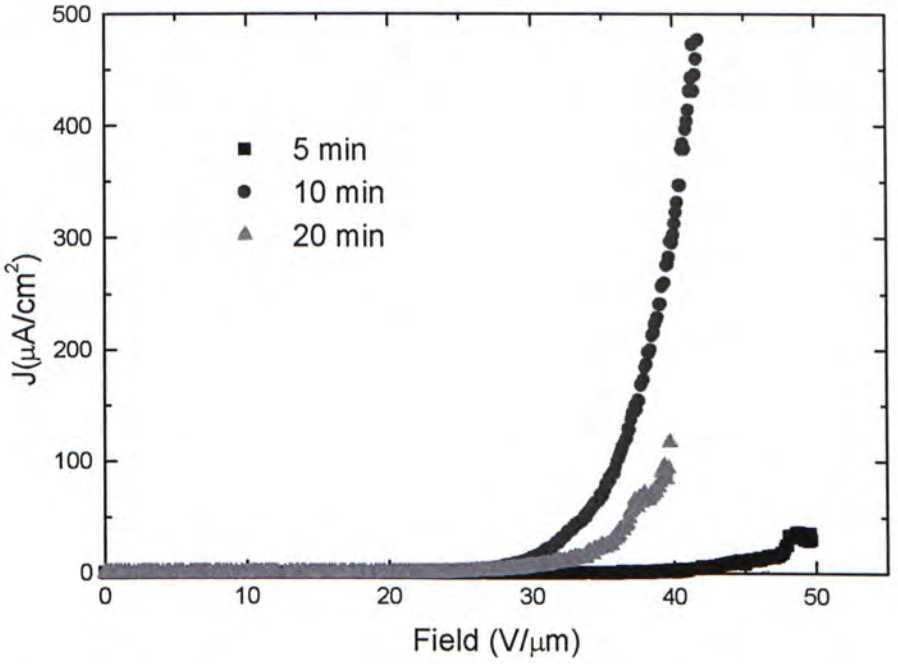

Figure 4.2.13 Field emission properties of sample treated with concentration of 3% IPA with 5% KOH solution at 80°C for different etching time of 5min, 10min and 20min.

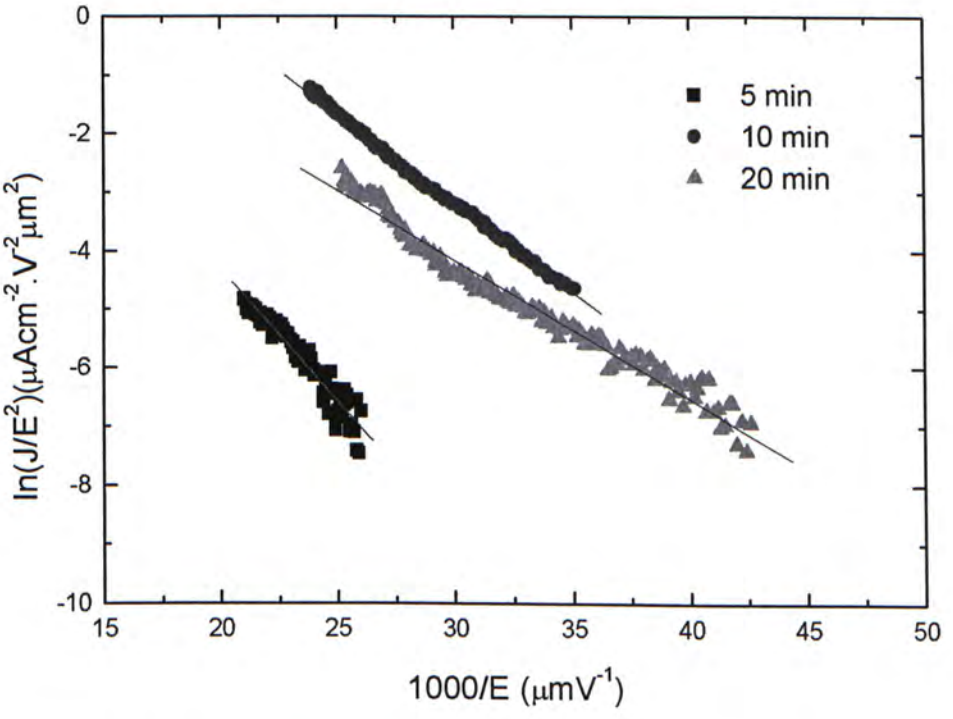

Figure 4.2.14 F-N properties of sample treated with concentration of 3% IPA with 5% KOH solution at 80°C for different etching time of 5min, 10min and 20min.

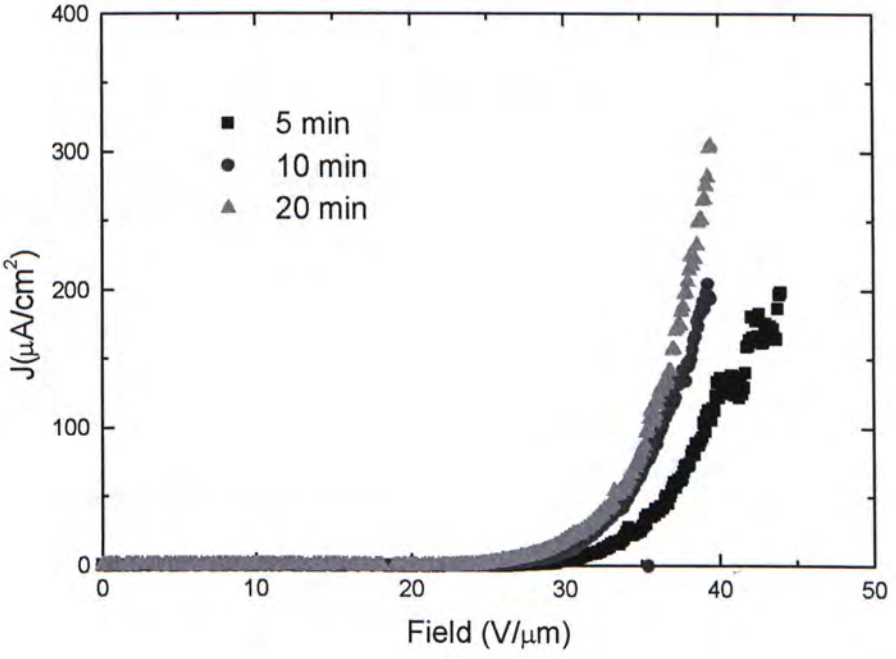

Figure 4.2.15 Field emission properties of sample treated with concentration of 6% IPA with 5% KOH solution at 80°C for different etching time of 5min, 10min and 20min.

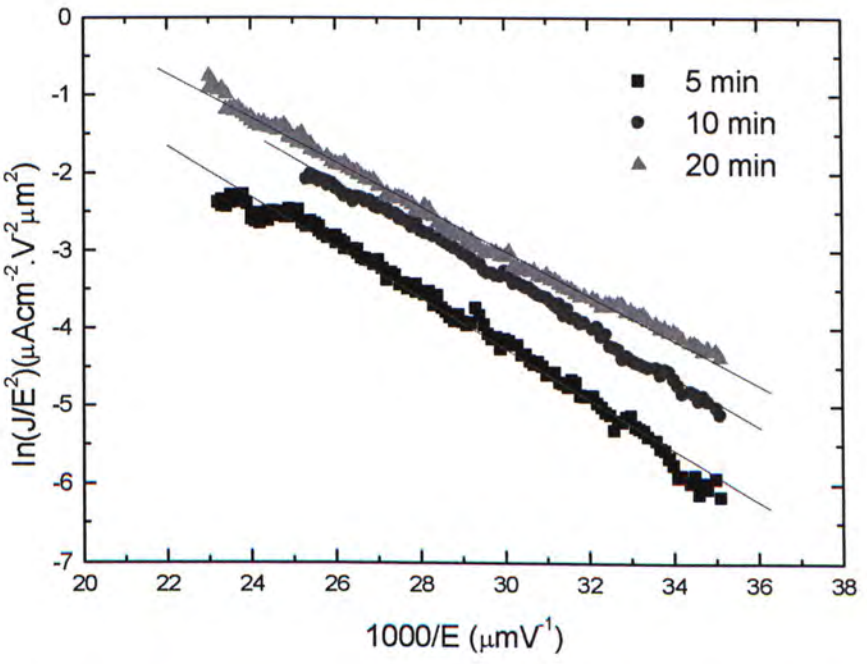

Figure 4.2.16 F-N properties of sample treated with concentration of 6% IPA with 5% KOH solution at 80°C for different etching time of 5min, 10min and 20min.

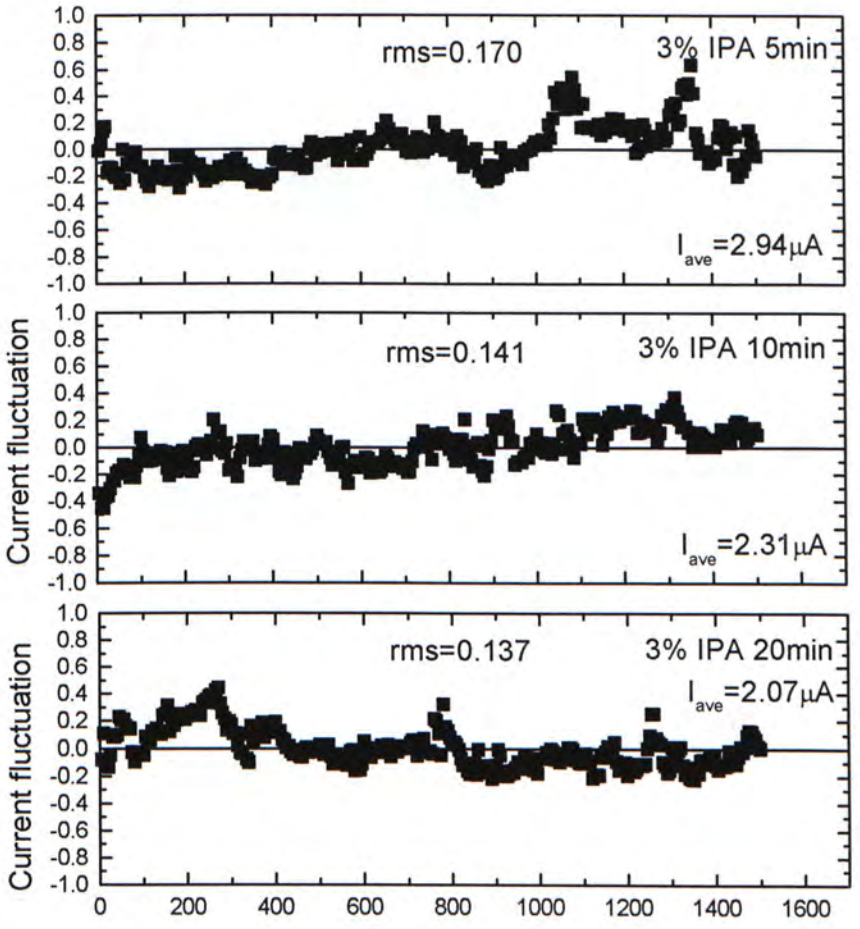

Figure 4.2.17 Fluctuation of emission current of FEA prepared by 3% IPA, 5% KOH and etching time is (a) 5min, (b) 10min and (c) 20min

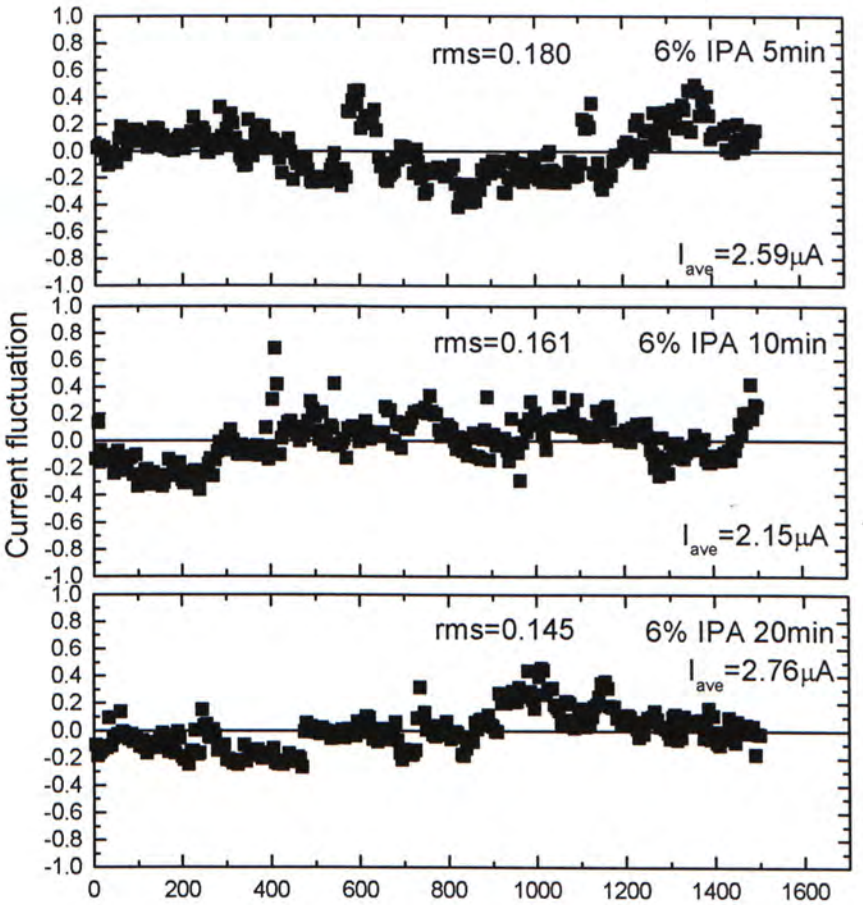

Figure 4.2.18 Fluctuation of emission current of FEA from 6% IPA, 5% KOH and etching time is 5min, 10min and 20min

For both 3% and 6% of IPA, figures 4.2.17and 4.2.18 show that the fluctuation of field emission current is improved when the etching time is increased. The effect on the fluctuation of field emission current may be due to the density of field emitters. If the density of the field emitters is higher, a more stable field emission current can be obtained. Therefore, increasing the etching time can improve the stability of field emission current.

In addition, the concentration of IPA can also affect the fluctuation of emission current. The higher the concentration of IPA, the larger the size of field

emitters. The fluctuation of emission current is also increased when the size of the field emitters is increased. Table 4.2.2 shows the summary of field emission characteristic of field emitters prepared with different concentration of IPA and etching time.

Table 4.2.2 Summary of field emission characteristic of field emitter with different concentration of IPA and etching time.

Material	Technique	Experimental condition	Current density ($\mu A/cm^2$)	Turn-on Field (V/μm)	$\beta/\phi^{3/2}$	Stability rms
Silicon (100) n-type 0.01Ωcm	Wet KOH etching	3% IPA, etching time 5 min	50	38	14	0.170
		3% IPA, etching time 10 min	500	24	21	0.141
		3% IPA, etching time 20 min	100	25	27	0.137
		6% IPA, etching time 5 min	200	27	20	0.180
		6% IPA, etching time 10 min	200	26	20	0.161
		6% IPA, etching time 20 min	300	24	22	0.145

4.2.4 Conclusion

Fabrication of very high density randomly distributed silicon field emitters using KOH and IPA solutions without any masking pattern have been successfully achieved. No oxidation and masking processes are required. This process to be a very effective way fabrication very small silicon emitters with typical aperture diameter of less than 5μm. Emission current is greatly dependent on the aspect ratio and surface roughness. In this texturing process, KOH and IPA solutions provide an effective means of increasing the aspect ratio and the surface roughness of the silicon wafer. The fabricated silicon field emitter arrays has lower turn-on voltage and higher field emission current density than conventional Si tip arrays.

4.3 Formation of a Porous Silicon layer on silicon

In this section, the field emission of porous silicon (PS) layers on Si substrates is studied. PS has high density of very sharp asperities, each of which can be behave as a site for field emission.

4.3.1 Introduction

One of the critical factors in a field emission device is the apex of the cathode from which electrons being emitted. For low voltage applications, the apex radius must be very small so that the field enhancement factor for field emission is large. Porous silicon contains a high density of very sharp asperities, each of which may behave as a site for field emission. A dramatic improvement in emission properties has been observed [124]. The performance of silicon field emitter tips has been improved by the formation of a porous silicon layer on the surface [124-128].

TEM analysis of the emitter tips of a PS layer has confirmed that it is covered with a high density of asperities [125]. In addition, porous silicon layers formed on gated silicon devices [129, 131] have shown very similar improvement as the ungated emitters. The field emission properties from PS layer has been ascribed to be the field enhancement effect associated with the geometrical shape of the fibrils [130].

A PS layer is prepared by the electrochemical etching technique in which a silicon substrate is anodized in HF etchant with a Pt electrode. The electrochemical anodization of silicon under specific conditions results in the formation of a layer of porous material characterized by a high density of ultrasharp silicon fibrils [132-134]. It is believed that these fibrils serve to significantly enhance the macroscopically applied electric field and thus allowing low voltage emission [135, 136].

The PS film thickness and porosity are directly proportional to the current density applied and anodization time [137]. In this section, field emission properties of porous silicon formed with different anodization times is studied.

4.3.2 Experimental Details

Porous silicon is prepared on n-type (100) silicon wafer with a sheet resistivity of 0.01Ωcm by anodization in the dark. The electrolyte used is $HF:H_2O:C_2H_5OH$ = 20:37:16. Before anodization, the Si wafer is rinsed in acetone and dipped in the HF solution ($HF:H_2O$=1:50) for a few minutes to remove the SiO_2.

A constant current source is used for the anodization process. The use of ethanol along with HF for anodization readily eliminates the sticking of hydrogen bubbles on the Si anode surface by increasing the wetting of the surface. Hence, the samples obtained are more homogeneous, both laterally and in thickness. The anodization process is carried out in the dark environment and at room temperature of about 20°C.

A thin surface layer of porous silicon is used for field emission. With anodization current density of $10mA/cm^2$, a study of the field emission properties of PS formed by treating with different anodization times of 15sec, 30sec, 1 min, 3min and 5min is performed.

Table 4.3.1 Experimental detail of porous silicon with different anodization time		
Material	Experimental condition	Etching time
Silicon (100) n-type 0.01Ωcm	$HF:H_2O:C_2H_5OH$= 20:37:16 10mA/cm^2 anodization current density	15 sec, 30 sec, 1 min, 3 min, 5 min

The samples are dried immediately after anodization in order to prevent flaking and further deterioration of the physical integrity of the PS layer.

4.3.3 Results and discussions

By observation by naked eye, the prepared PS layer has a uniform dark colour and the colour is uniform along the sample from the center to the edge. This indicates that the anodization etching process yields a uniform PS layer.

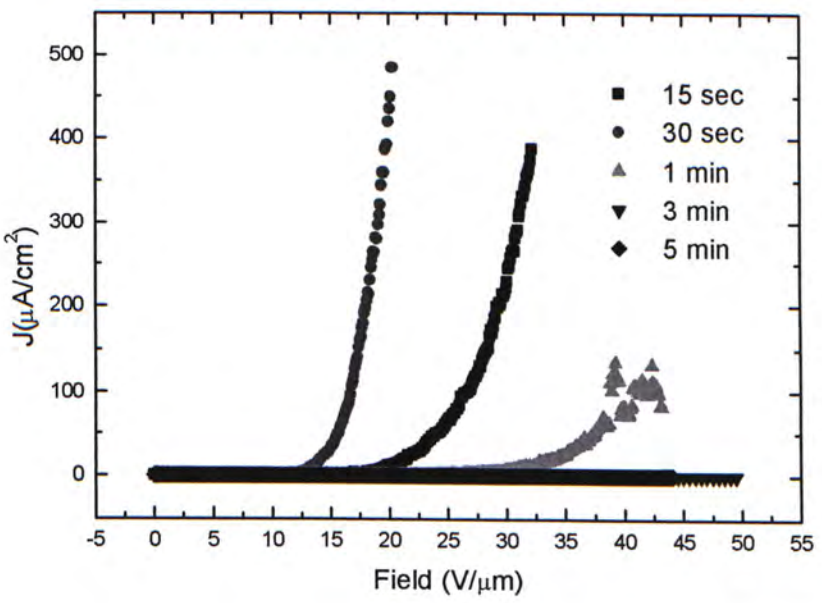

Figure 4.3.1 Field emission characteristic for porous silicon field emitter on (100) n-type silicon prepared at different anodization time 15 sec, 30 sec, 1min, 3min and 5min with a current density of 10mA/cm^2.

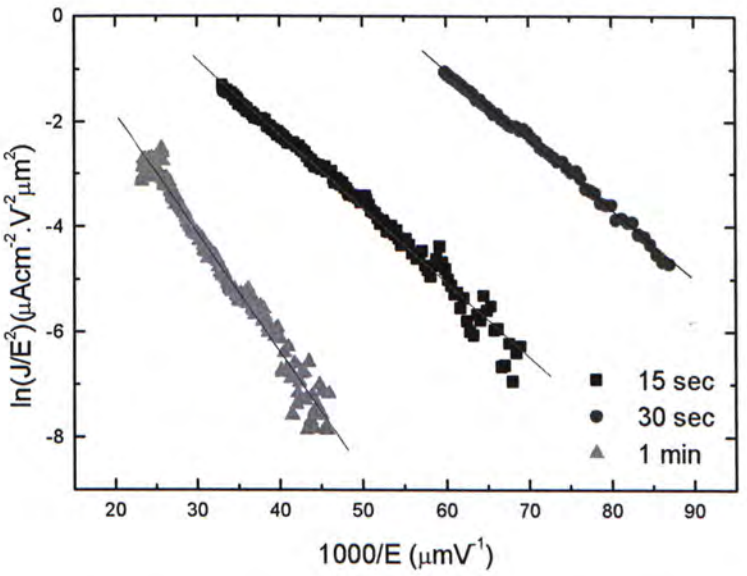

Figure 4.3.2 Fowler-Nordheim characteristic for porous silicon field emitter on (100) n-type silicon prepared at different anodization time 15 sec, 30 sec, 1min, 3min and 5min with a current density of 10mA/cm^2.

Porous silicon has a different thickness and surface morphology when it is prepared by varying the anodization time in the same etchant and applied current densities. The thickness and surface roughness of the PS layer increases with the anodization time. In order to estimate the influence of anodization time on the field emission properties of the porous silicon, the anodization time of PS varied from 15 seconds to 5 minutes.

From figure 4.3.1, for anodization times of 15 seconds, 30 seconds and 1 minute, the turn-on field of porous silicon is 16 V/μm, 12 V/μm and 25 V/μm respectively at the emission current density of 1μA/cm^2.

With the anodization time of 30 second, the sample has yielded a current density of 160μA/cm^2 while operated at 18V/μm as shown in figure 4.3.1. When the anodization time is 15 second, operated at 29V/μm, a current density of 150μA/cm^2 is obtained. And a high operation voltage of about 40V/μm is needed to have current densities of 100μA/cm^2 for the sample anodized for 1 minute.

The reason for the enhancement of the field emission current is due to the nanometer-sized tips.

When the anodization time increases to 3min and 5min, the field emission properties cannot be measured below 50V/μm. The high turn-on voltage of these sample may be due to the increased thickness of PS layer. The thickness of porous silicon layer will affect the resistance of the film and obstruct the electron flow from the substrate to the surface and to vacuum.

The value of $\beta/\phi^{3/2}$ of porous silicon from figure 4.3.2 are determined to be 49, 51 and 30 for samples prepared with anodization time of 15 seconds, 30 seconds and 1 minute, respectively. F-N plots revealed that the value of β could be increased by porous silicon fibrils.

It is apparent that thin PS contributes to a low turn-on field as shown in 4.3.1. And the low turn-on field is due to the high density of ultra-sharp silicon fibrils on PS [125, 130]. When anodization time of PS is too short or too long, the turn-on field is high. When anodization time of PS is 30 second, the field emission efficiency is optimised.

Figure 4.3.3 shows the fluctuation of field emission current. When the anodization time is 30 second, the fluctuation of field emission current is more stable when compared with samples with anodization times of 15 second and 1 minute.

The fluctuation of field emission current may be due to differences in the density and thickness of the PS layer. If a higher density of PS fibrils is formed, a more stable field emission current is obtained. The thickness of PS layer also influences the fluctuation of field emission current. This may be due to the high resistivity of the PS layer and the resulting current limiting mechanism. The fluctuation of field emission current of PS probably arises from the burn out of individual fibrils as the voltage is increased.

The current fluctuation is often attributed to the non-uniform contributions of individual emitters of the PS layer. In order to achieve stable emission, individual emitters should contribute equally over the whole area. In this case, the anodization process has to be controlled well to ensure the uniformity of the porous silicon formed.

Good emission characteristics of porous silicon is associated with the formation of a surface morphology of densely distributed small protrusions whilst minimising the thickness of the PS layer.

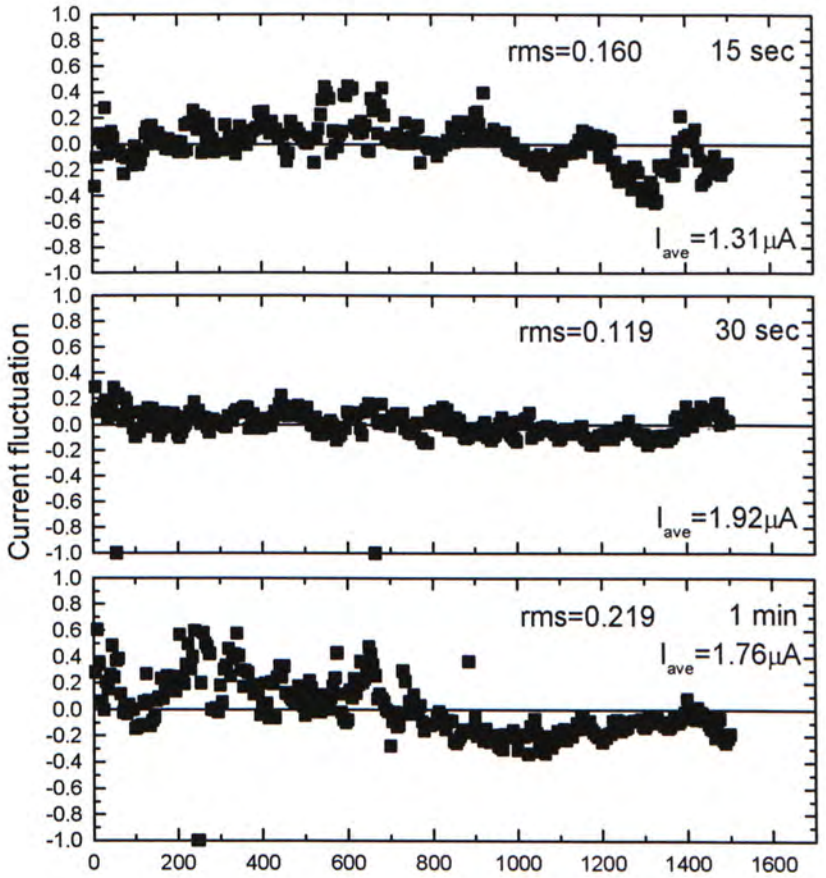

Figure 4.3.3 Fluctuation of emission current of PS layer for anodization time of 15 sec, 30 sec and 1 min

Table 4.3.2. Summary of field emission characteristic of porous silicon with different anodization time

Material	Technique	Experimental condition	Current density ($\mu A/cm^2$)	Turn-on Field (V/μm)	$\beta/\phi^{3/2}$	Stability rms
Silicon (100) n-type 0.01Ωcm	Porous silicon layer Anodization current Density is $10mA/cm^2$	Anodization time is 15 sec	400	16	45	0.160
		Anodization time is 30 sec	500	12	28	0.119
		Anodization time is 1 min	100	25	45	0.219

4.3.4 Conclusion

PS layers with high porosity and small thickness are investigated as field emitters. The PS layers exhibit impressive electron field emission properties. Most noticeably is the large electric field enhancement associated with the ultra-sharp PS fibrils. It is believed that these fibrils significantly enhance the applied electric field and thus allowing low voltage emission. The thickness of PS layer is also associated with the field emission enhancement factor.

In this section, the measured large field emission current is due to the high density of field emission sites. The simple fabrication process makes PS an attractive alternative to other well-investigated cathode technologies. The fabrication technology proposed is simple and can be used in FED application.

Chapter Summary

In this chapter, three fabrication methods are described for improvement the field emission properties by improving the field enhancement factor.

First is the two-step anodization method. The anodization of silicon with different concentration of HF solution is performed by a two step anodization method. High aspect ratio silicon field emitter arrays are fabricated. Different shapes of silicon field emitter with good uniformity and reproducibility can be fabricated on both <111> and <100> silicon. The overall current density and turn-on voltage of field emitter is about 100μA/cm^2 and 26-33 V/μm respectively.

Second is the anisotropic texturing process. Randomly distributed silicon field emitters are formed on the (100) crystallographic plane without using any masking pattern. Base size and height of the field emitters is very small of about 1μm^2 and 1μm respectively. The overall current density of the field emitters is about 100-500μA/cm^2. The overall turn-on voltage is about 24-38 V/μm. The value of $\beta/\phi^{3/2}$ of field emitter is also increased.

Third is the formation of porous silicon layer. PS has high density of very sharp asperities, each of which can behave as a site for field emission. A dramatic improvement in the emission properties of PS is observed. The turn-on voltage of PS layers is greatly improved to about 12-25 V/μm. The overall current density of field emitters is about 100-500μA/cm^2. The value of $\beta/\phi^{3/2}$ of porous silicon is also greatly improved due to the high density of sharp asperities.

Chapter 5 Improvement in the Field emission characteristics of the silicon tips upon coating with low work function materials.

5.1 Amorphous carbon coating

As described in the previous chapter, the stability of field emission of porous silicon is not very good. This may be due to change different in resistance of the PS layer caused by the continuous burning out of PS fibres during the emission process. In this section, amorphous carbon (a-C) coatings on silicon and porous silicon are investigated. These are found to improve the stability, turn-on voltage and the value of $\beta/\phi^{3/2}$ of the PS layer.

5.1.1 Introduction

By advanced semiconductor microfabrication technology, silicon has become a popular selection for field emitter cathode material in fabricating vacuum microelectronic devices. However, Si has limited properties for the usage as a field emitter cathode material. Silicon generally shows unstable emission behavior, presumably due to native oxide, chemical reactions with residual gases and adsorbed impurities. Recently, there have been many investigations to improve field emission properties by using a protective coating.

In order to stabilize and enhance emission behavior, surface treatment such as etching the native oxide layer and coating with an a-C is desirable. An a-C film coating on flat silicon or PS layer by using a DC sputtering system at low substrate temperature is described here.

5.1.2 Experimental details

The starting material is n-type (100) silicon with a resistivity of 0.01Ωcm. The PS layer is formed by anodization as described in previous chapter.

With an anodization current density of 10mA/cm^2 for different anodization times of 0 sec, 15sec, 30sec, 1min and 3min. different thicknesses of PS layer are fabricated and an a-C film is deposited on the PS layers by DC magnetron sputtering.

Before loading the porous silicon into the sputtering chamber, the samples are cleaned in D.I. water, and then dried. The sputtering system is pumped down to a base pressure of 3x 10^{-6} torr and the carbon sputtering is performed under the conditions as shown in Table 5.1.1:

Table 5.1.1 Experimental detail of a-C on flat silicon sample with different sputtering time

Material	Experimental condition	Sputtering Time	Anodization Time
Silicon (100) n-type 0.01Ωcm	Substrate heating: 120°C Target : Carbon 99.999% Distance between target and substrate: 3cm *Prior to deposition:* Base pressure: 3x10^{-6} torr *During deposition:* Argon pressure: 3x10^{-3} torr Target power: 28-30 watts	30 min	0 sec, 15 sec, 30 sec, 1 min, 3 min
		60 min	0 sec

An a-C film is deposited onto a PS layer by DC magnetron sputtering of a high purity 99.999% graphite target. The film is deposited at a constant DC current density of $0.05A/cm^2$. During sputtering, the indicated bias voltage is between 530 and 580 volts. The overall power used is about 28-30 watts. The sputtering pressure is 3×10^{-3} torr. The deposition rate is about 1 to 2nm/min. After removal from the chamber, the samples are again washed in D.I. water to remove any surface contaminants.

Field emission of electrons involves tunnelling through the surface barrier. This requires high applied electric fields. If the barrier to emission can be sufficiently lowered, the emission can occur from a flat surface.

In this work, a-C films with different thicknesses is prepared with various sputtering times under the same condition. The thickness increases with increasing deposition time. In order to estimate the influence of thickness of a-C film on the field emission properties, two different times of deposition 30 and 60 minutes are used.

The morphology of an a-C film coated on to porous silicon is investigated by atomic force microscopy (AFM).

5.1.3 Result and discussion

Figure 5.1.1 shows the I-V curves for various thicknesses of a-C coatings on planar silicon substrates. The turn-on voltage for 30 and 60 minute deposition is $12V/\mu m$ and $15V/\mu m$ respectively when the emission current is $1\mu A/cm^2$. From figure 5.1.2, the value of $\beta/\phi^{3/2}$ is determined to be 37 and 32 respectively.

From figure 5.1.1, the emission current is increased because of the a-C coating on planar silicon. A thicker film appears to have a deleterious effect on the

emission behavior. This is possibly due to an increase in series resistance of the film, which effectively reduces the electron field strength at the vacuum gap.

If the film thickness is too large, the a-C film would not be fully depleted, and therefore, the energy loss of the hot electrons relative to the conduction band would be increased and thus would be prevented it from escaping from the surface.

If the film thickness is too thin, electrons that are emitted from the heterojunction either thermally or by tunnelling will not gain enough energy relative to the conduction band for them to be able to surmount the emission barrier to vacuum. A variation of the threshold field as a function of thickness is observed. As the film thickness increases, the field emission efficiency of the structure is reduced.

In general, if a larger sp^3 fraction exists in the a-C film, the film has a wider band gap. Wide band gap diamond-like carbon (DLC) film has a low electron affinity and even might have negative electron affinity (NEA) [140-141]. D. Won Han et al [142] reported that the sp^2 bonded structure in the a-C film acts as the electron conduction path, and that easier electron transport induced the field emission. Other reports show similar results, which implies that the threshold voltage decreases with the increase of sp^2 fraction in the a-C film [143-144].

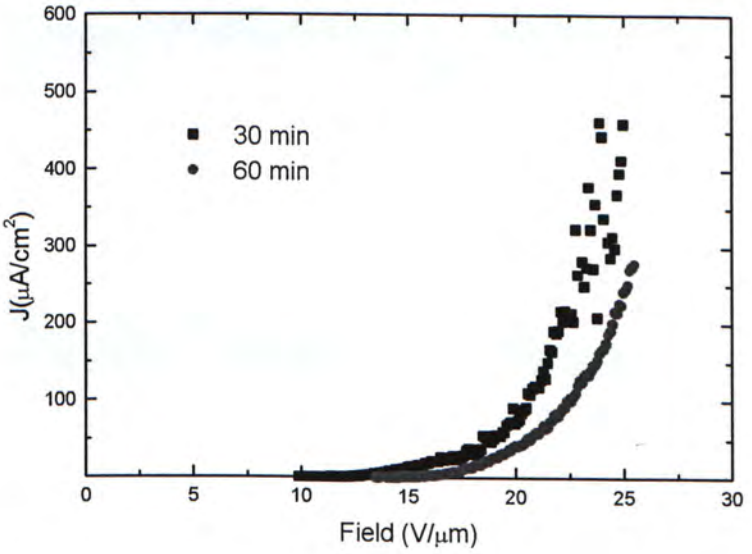

Figure 5.1.1 Field emission characteristics for a-C deposited by sputtering on (100) n-type silicon for 30 and 60 minutes.

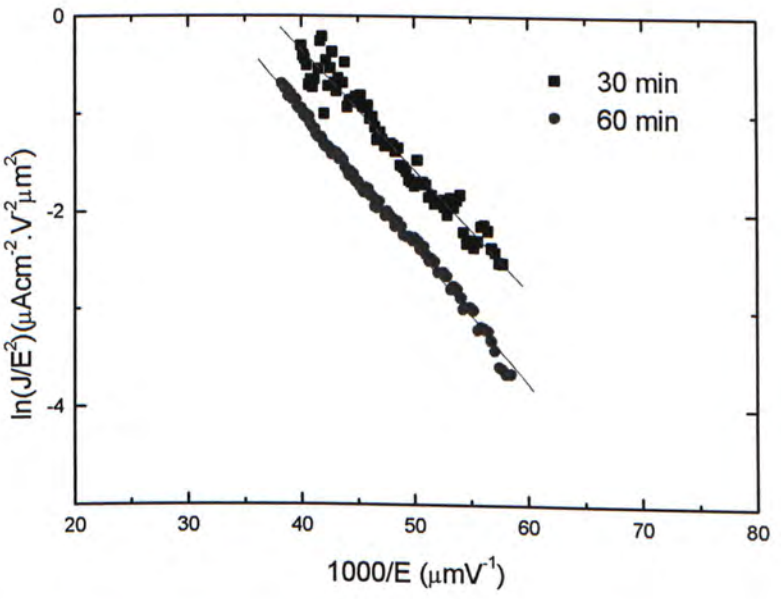

Figure 5.1.2 F-N characteristic for a-C deposited by sputtering on (100) n-type silicon for 30 and 60 minutes.

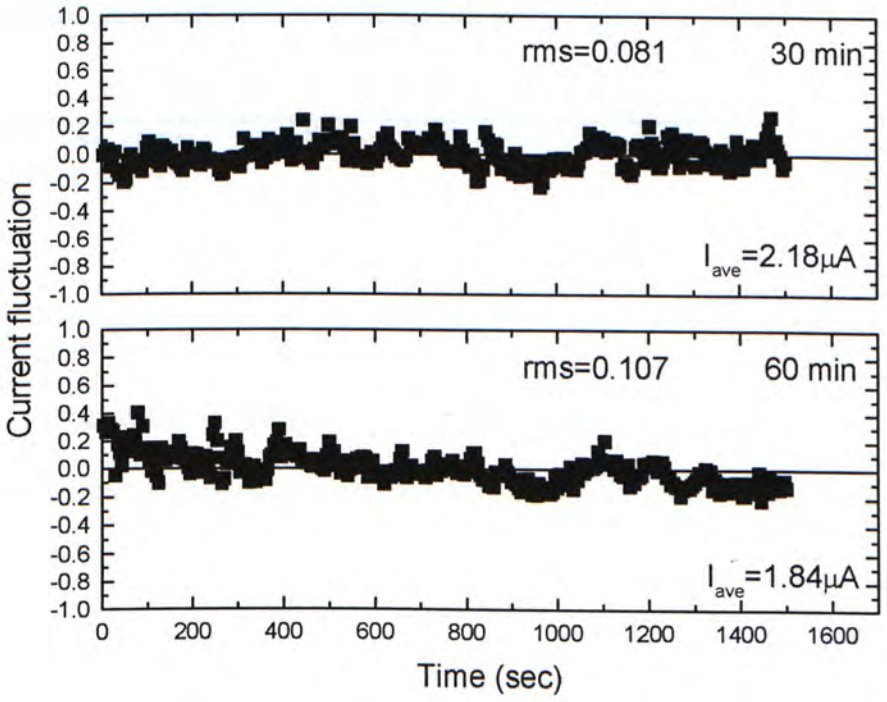

Figure 5.1.3 Fluctuation of the emission current of a-C by sputtering times of 30 min and 60 min

The improvement by the a-C coating on silicon is more significant in the case of emission stability as shown in figure 5.1.3. The surface stability, chemical inertness and low sputter yield of the a-C film seems to play an important role in the stability of field emission. The fluctuation defined as $(I-I_{ave})/I_{ave}$, where I is the emission current and I_{ave} the average emission current during the measurement, has been greatly improved a lot in comparison with the results in last chapter.

When the sputtering time is 30 min, the field emission current is more stable as shown in figure 5.1.3. The effect of amorphized silicon on the current fluctuation is suppressed by the a-C coating. The fluctuation of the emission current could be due to the amorphous structure of the a-C film and the thickness of a-C film. In order to control the fluctuation, therefore, it would be necessary to optimise the thickness, the sp^3/sp^2 ratio and the structure of the a-C film.

Table 5.1.2 Summary of field emission characteristic of a-C on flat silicon sample

Material	Technique	Sputtering time	Current density ($\mu A/cm^2$)	Turn-on Field (V/μm)	$\beta/\phi^{3/2}$	Stability rms
Silicon (100) n-type 0.01Ωcm	a-C coating by Sputtering	30 min	500	12	52	0.081
		60 min	300	15	46	0.107

As the sputtering time and conditions vary, the sp^2 traction in the a-C film as well as the surface roughness varies. Since both the bonding configuration and surface roughness are varied with different sputtering times, it is difficult to explain the direct relation between field emission and the sputtering time. But, this study shows an the a-C film with suitable thickness and bonding configuration will show superior field emission properties.

With the above best condition, 30 min sputtering an a-C thin film is deposited on a PS layer prepared as described in a previous chapter.

Figure 5.1.4 and 5.1.5 show typical I-V curves and F-N plots obtained from a-C coatings on PS layers with different thickness and on a reference Si substrate. The linearity of the FN plot shows that the anode current is due to electron field emission.

The turn-on voltage of a-C film coating on the porous silicon with different anodization times of 15sec, 30sec, 1min and 3min is approximately 12 V/μm, 10 V/μm, 17 V/μm and 13 V/μm respectively while the emission current density reaches $1\mu A/cm^2$. This is comparable to a turn-on field of about 12 V/μm from a-C film coating on flat silicon substrate as shown in figure 5.1.4.

From figure 5.1.5, the value of $\beta/\phi^{3/2}$ is determined to be 79, 96, 44, 79 and 89 for an a-C coated porous silicon with anodization times of 15sec, 30sec, 1min, 3min and flat silicon respectively.

The turn-on voltage is improved by coating a-C on porous silicon. This should be due to the low work function of a-C film [145-147] combined with the structure of the PS fibres [130, 132-134] that enhance the field emission properties.

In addition, the value of $\beta/\phi^{3/2}$ of these samples increase dramatically by using the a-C coating when compared with those with only a PS layer. This is mainly caused by the lower work function (ϕ) of the a-C film and the nanometer-sized tips of the porous silicon layer increase the value of β.

The overall emission current also greatly increases. The large emission current is due to the high density of nanometer-sized tips of porous silicon as emission sites.

For the a-C layer sputter-deposited for 30 min on PS, the turn-on voltage and the value of $\beta/\phi^{3/2}$ are better for PS prepared with anodization time of 30 seconds. This is due to the optimized condition on structure and thickness of the PS layer together with the bonding and thickness in the a-C coating.

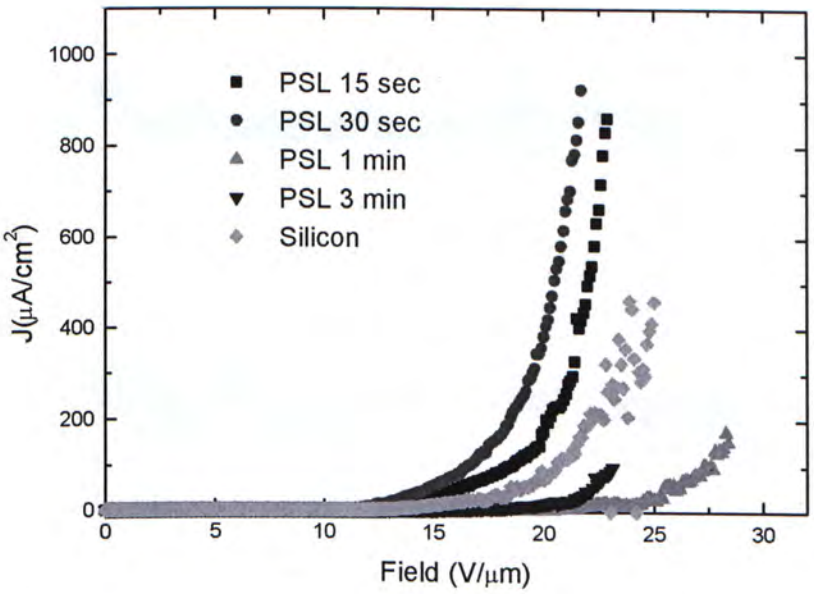

Figure 5.1.4 Current-voltage characteristic for a-C films coated on different thickness of PS layer and flat silicon substrate.

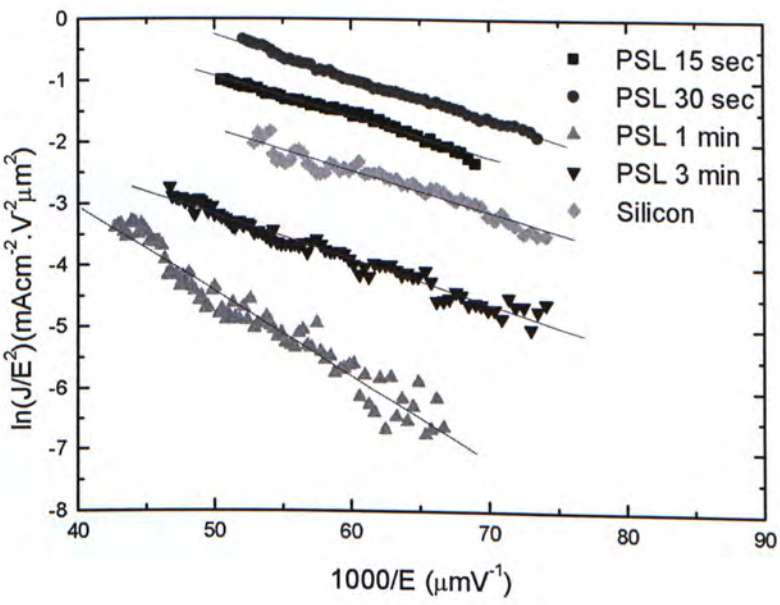

Figure 5.1.5 Data plotted in Fowler-Nordheim coordinates.

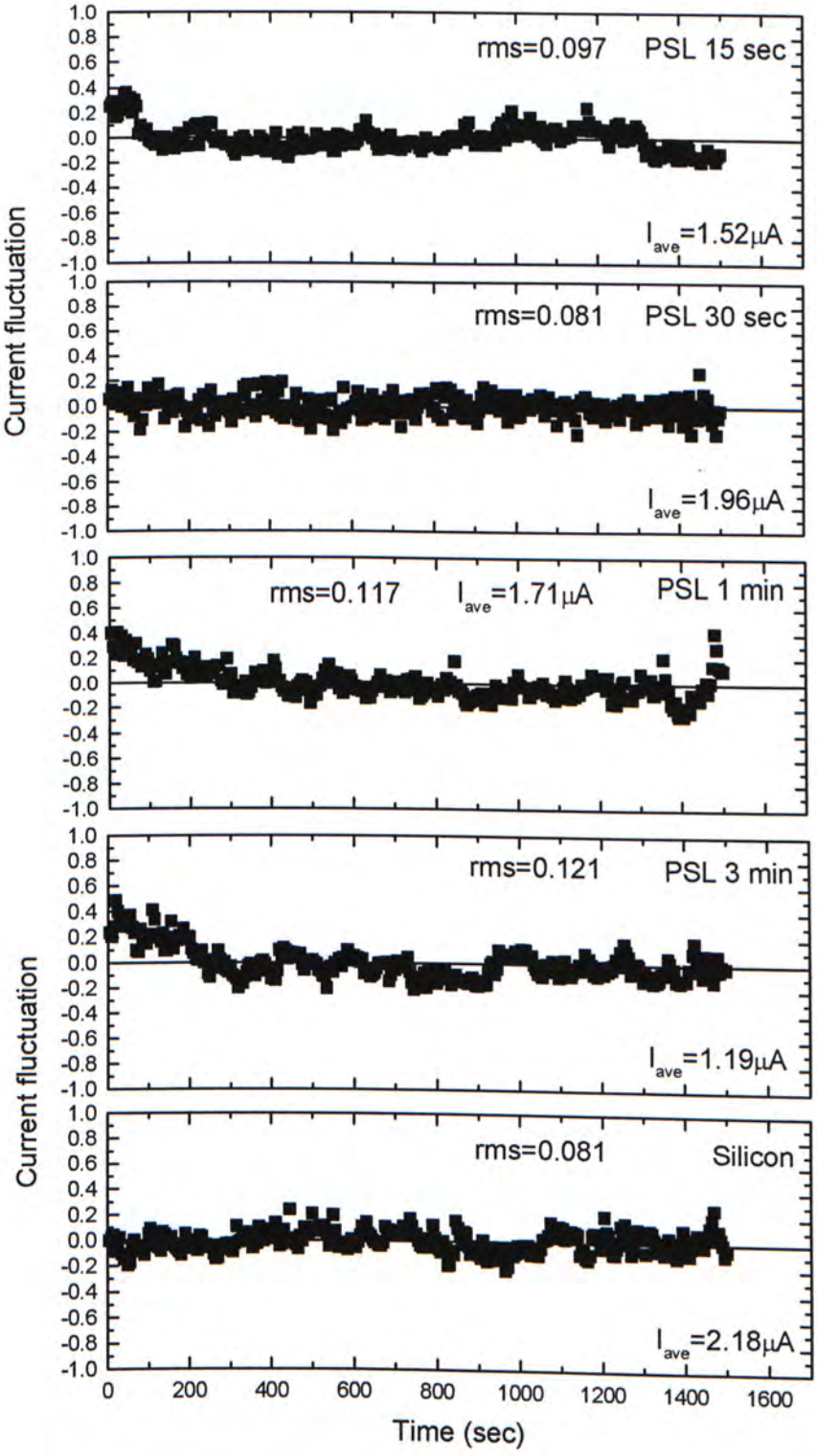

Figure 5.1.6 Fluctuation of emission current of a-C coated by sputtering 30 min on porous silicon which is anodized for 15sec, 30sec, 1min, 3min and on flat silicon only.

The improvement of emission stability arising from the a-C coating on the porous silicon is shown in figure 5.1.6. The fluctuation of field emission current of a-C film sputter deposited for 30 min on PS layer is more stable than uncoated PS layer as shown in table 4.3.2. The current fluctuation of PS is stabilized by the a-C coating. The small fluctuation of the emission current could be due to both the amorphization of the PS layer and the amorphous structure of the a-C film.

The fluctuation of field emission current of a-C film sputter deposited for 30 min on porous silicon prepared with anodization time of 30 seconds is the most stable. The RMS fluctuation can be further reduced by optimising the processing time of anodization and sputtering. A summary of field emission characteristic of a-C coating on PS layer with different anodization time is tabulated in table 5.1.3.

Table 5.1.3 Summary of field emission characteristic of a-C by sputtering 30min on porous silicon with different anodization time

Material	Technique	Experimental condition	Current density ($\mu A/cm^2$)	Turn-on Field (V/μm)	$\beta/\phi^{3/2}$	Stability Rms
Silicon (100) n-type 0.01Ωcm	a-C coating by Sputtering 30min	Flat silicon	500	12	52	0.081
	Porous silicon layer then a-C coating 30min	Anodization time is 15 sec	900	12	98	0.097
		Anodization time is 30 sec	900	10	92	0.081
		Anodization time is 1 min	200	17	49	0.117
		Anodization time is 3 min	100	13	89	0.121

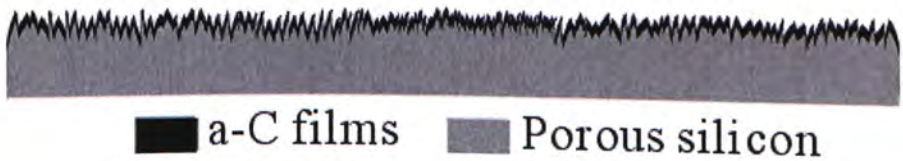

Figure 5.1.7 The schematic diagram showing a cross section of the structure of a-C films coated on porous silicon.

Figure 5.1.7 is a schematic diagram showing a cross section of the structure of the a-C film coated on PS layer field emitter. The geometric enhancement by surface morphology must be considered. To investigate the geometric effect, a Digital Instruments Nanoscope III atomic force microscope (AFM) is used to investigate the surface morphology. The surface topography of a-C coated PS layer is probed by the AFM in contact mode. Each sample is scanned at various positions and the rms roughness is determined. Typical three-dimensional AFM micrographs from samples prepared under different conditions are shown in Fig. 5.1.8 to 5.1.12. The value of rms roughness determined from the AFM image is shown in Table 5.1.4.

Table 5.1.4 Summary of roughness of a-C by sputtering 30min on porous silicon with different anodization time

Material	Technique	Experimental condition	Roughness (rms)
Silicon (100) n-type 0.01Ωcm	a-C coating by Sputtering 30 min	Flat silicon	0.715nm
	Porous silicon Layer then a-C coated by sputtering for 30min	Anodization time is 15 sec	1.074nm
		Anodization time is 30 sec	2.604nm
		Anodization time is 1 min	2.285nm
		Anodization time is 3 min	3.734nm

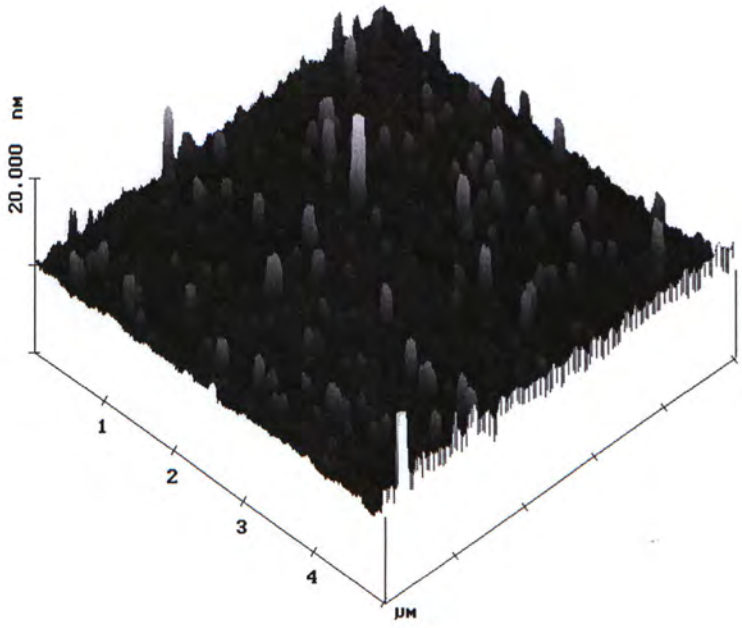

Figure 5.1.8 AFM micrographs of a-C films on flat silicon

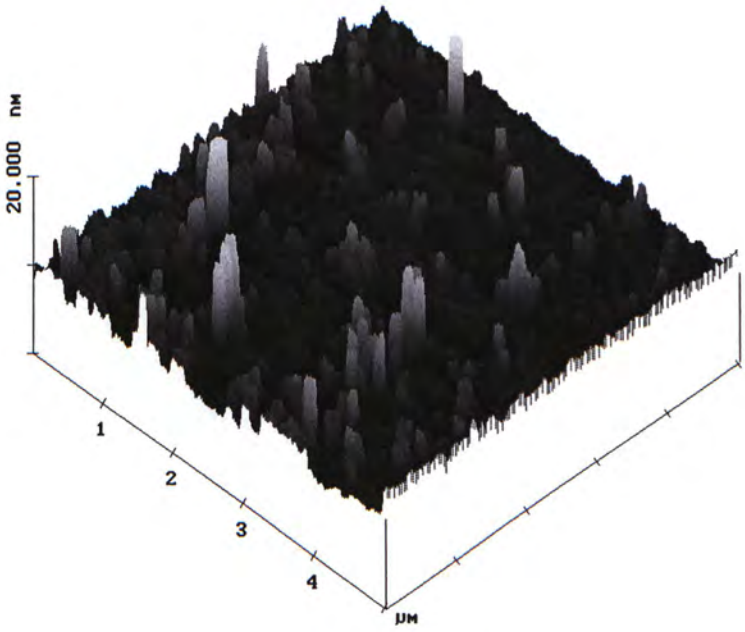

Figure 5.1.9 AFM micrographs of a-C films on PS layer anodized for 15 sec

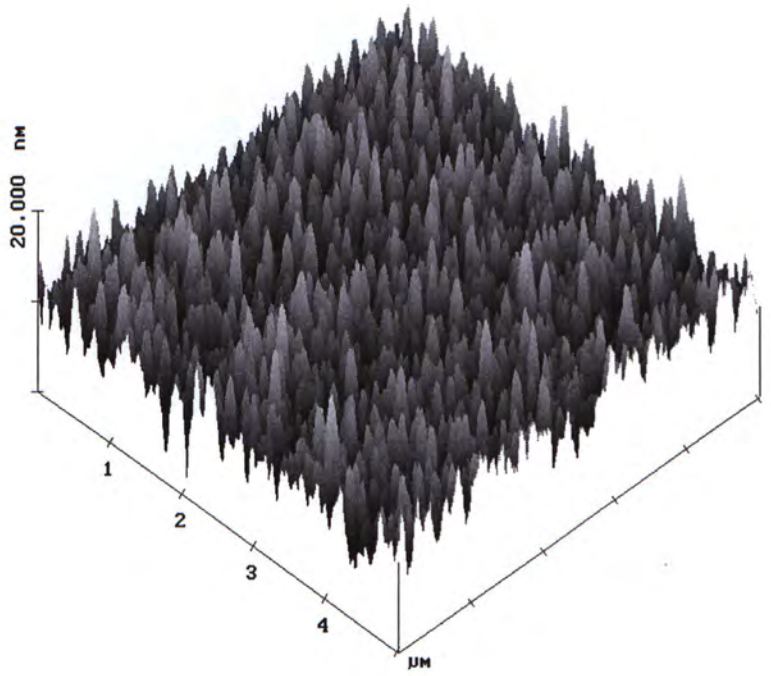

Figure 5.1.10 AFM micrographs of a-C films on PS layer anodized for 30 sec

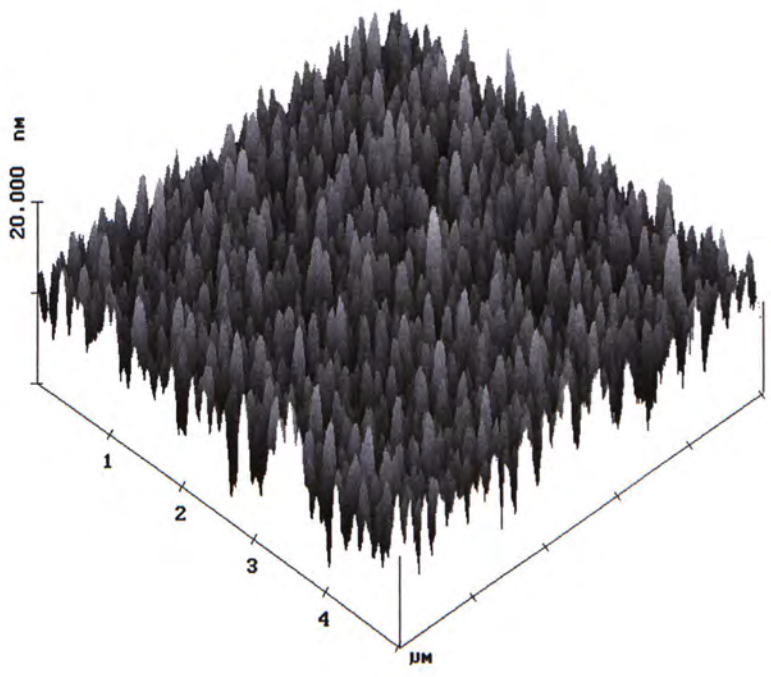

Figure 5.1.11 AFM micrographs of a-C films on PS layer anodized for 1 min

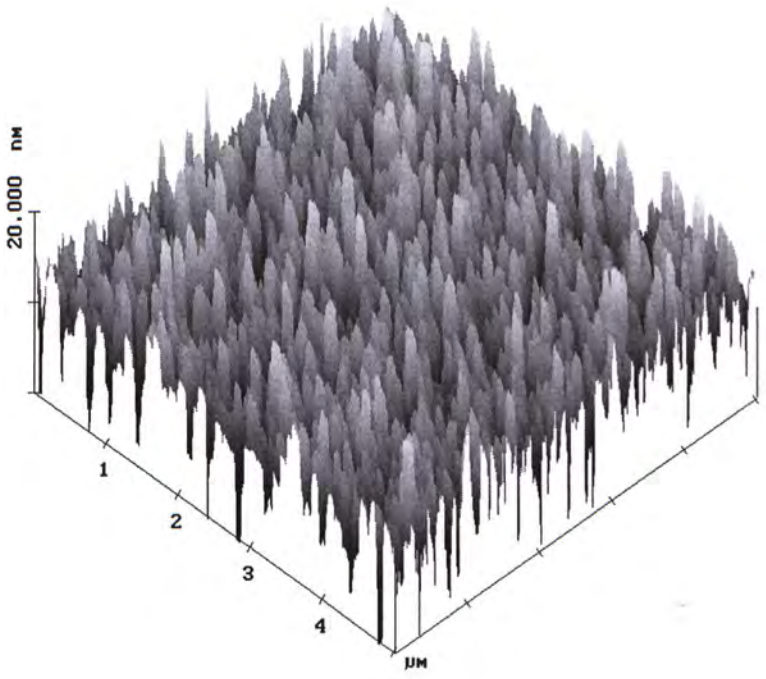

Figure 5.1.12 AFM micrographs of a-C films on PS layer anodized for 3 min

The a-C film coated flat silicon has a surface that is relatively flat with small protrusions as shown in figure 5.1.8. The root-mean-square (rms) roughness is about 0.715nm.

Figure 5.1.9 shows the AFM image of a-C film deposited on PS layer prepared by anodization for 15 sec. Denser protrusions with small average aspect ratio are seen. The root-mean-square (rms) roughness is about 1.074nm. This may be due to a larger number of nucleation sites on porous silicon.

Figure 5.1.10 shows AFM image of a-C coating on porous silicon fabricated by anodization for 30 seconds. Densely distributed small protrusions with steeper sidewalls are observed. The average aspect ratio of the protrusions formed on the surface is very high. This is one of the major factors responsible for the good emission characteristics. The root-mean-square (rms) roughness is about 2.604nm.

Similar observations are obtained for samples anodized for 1 and 3 minutes. But for the sample anodized for 3 minutes, relatively large and dense protrusions with a smaller average aspect ratio on the surface are observed. The rms roughness is about 3.734nm.

The difference in the surface morphology also contributes to the difference in the turn-on fields. A higher field enhancement factor is associated with a higher aspect ratio and higher density of the protrusions as expected. Both the shape and the density of the protrusions is responsible for the higher efficiency in electron field emission. There may be also a quantum confinement effect present in such fibrous structures which resulting in electrons that have an increased energy and thereby increasing the probability of emission.

However, the surface morphology with high aspect ratio of the protrusions is not the only factor. The thickness of the PS layer is also associated with the field emission efficiency. When the anodization time increases, it also reduces the electron emission efficiency because of the high resistivity of the PS layer. In this case, the overall emission properties can only be slightly improved in comparison with the PS layer sample without an a-C coating.

5.1.4 Conclusion

In this section, the effect of coating a-C film on flat and PS samples by DC magnetron sputtering is studied. a-C is shown to give a great improvement in the field emission performance, such as low turn-on voltage, high current density and stability. When a thin a-C film is deposited on a PS layer, the turn-on voltage and $\beta/\phi^{3/2}$ of the field emission is improved. This is due to the low work function of a-C film combined with the structure of the PS layer which improves the surface morphology of the emission surface. A thicker film appears to have a deleterious effect on the emission behavior. Atomic force microscopic (AFM) investigation of the surface reveals that the a-C film coating on porous silicon produces tips with denser higher area density and steeper sidewalls, which favours the achievement of high efficiency in field emission.

5.2 Silicon carbide coated Silicon emitter by MEVVA

This section describes silicon carbide formation on silicon field emitters by high dose carbon implantation using a metal vapor vacuum arc (MEVVA) ion source. The formation of a thin SiC layer improves the emission properties of the field emitter because of modification of the surface morphology and lowering of the work function.

5.2.1 Introduction

Silicon carbide (SiC) is a compound semiconductor with a similar structure to diamond. It has excellent physical properties such as high thermal conductivity, high breakdown field strength, high electron mobility and excellent chemical stability.

There has been a considerable amount of effort to synthesize SiC thin layers using ion implantation [92- 98]. The electron emission characteristics of SiC synthesized by carbon implantation using MEVVA ion source, has also been investigated [99-100, 145].

Dihu chen et al [99] found that for electron field emission from planar SiC/Si heterostructures there was a remarkably low turn-on field due to the improvement of the surface morphology and the work function. Also the influence of implantation on emission current density and turn-on field was reported.

Dihu chen et al [145] reported that field emission was enhanced for SiC on n-type silicon tips fabricated from the wet isotropic solution ($HF:HNO_3:CH_3COOH$) etching method. Higher emission current with a stable current density was obtained at a lower applied field.

In this study, the field emission characteristics of SiC synthesized by implantation of field emitters fabricated by using the anisotropic texturing method is studied. A schematic diagram of the sample is shown in figure 5.2.1. As described in chapter 4.2, anisotropic etching solutions with KOH and IPA are used to form the regularly shaped and repeatable high density of the silicon field emitters on the (100) Si substrate without using any masking pattern. After the silicon field emitters are formed, a high dose of carbon is implanted into the surface.

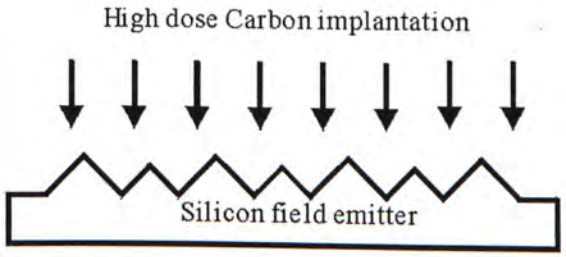

Fig 5.2.1 High dose carbon implantation into silicon field emitter by using MEVVA.

5.2.2 Experimental details

In this work, a two step fabrication process is used. Firstly, the field emitter is fabricated by using the anisotropic texturing method as described in chapter 4.2. Secondly, high dose carbon is implanted into the silicon field emitter by using MEVVA ion source with a high-purity graphite rod (99.999%) as the cathode material. Carbon implantation is performed with MEVVA ion source at an energy of 35keV to a dose of $1.0 \times 10^{18} cm^{-2}$. Thermal annealing is performed at 1200°C for 2 hours in an Ar ambient by using a tube furnace.

Table 5.2.1 Experimental Detail of field emitter preparation			
Material	2nd process	1st process	
		Etching solution	Etching time
Silicon (100) n-type 0.01Ωcm	SiC implanted by MEVVA 35keV doses of $1.0x10^{18}$	3% IPA 5% KOH at 80°C	10 min
			20 min
		6% IPA 5% KOH at 80°C	10 min
			20 min

5.2.3 Results and Discussions

Figure 5.2.2 and 5.2.3 show a typical I-V curve and F-N plot obtained from SiC formed by implantation on emitters fabricated by the using texturing process. The linearity of the FN plot shows that the anode current is due to electron field emission.

With the same implantation and annealing conditions, the turn-on voltage of SiC on emitters fabricated in 3% and 6% IPA solution with etching times of 10 minutes is approximately 19 V/μm and 15 V/μm respectively at a emission density of 1μA/cm^2. Similarly, the turn-on voltage of SiC on emitters fabricated in 3% and 6% IPA solution on with etching time of 20 minutes is approximately 17 V/μm and 10 V/μm respectively. The turn-on voltage is improved by implanted SiC on field emitter. This is probably due to both the improvement of the surface morphology and improvement of the work function [99, 145].

When etching time is 10 minutes, the value of $\beta/\phi^{3/2}$ of SiC on emitters fabricated by using texturing process in 3% and 6% IPA solution is determined to be

46 and 51 respectively. When the etching time is 20 minutes, the value of $\beta/\phi^{3/2}$ is determined to be 47 and 88 respectively.

The value of $\beta/\phi^{3/2}$ is higher than the value for the un-implanted silicon field emitter which is discussed in chapter 4.2. This is because the work function ϕ and the value of β are improved by the high dose carbon implantation [99].

As described in the chapter 4.2, the size of the field emitters increases when the concentration of IPA increases. When the concentration of IPA increases from 3% to 6%, the turn-on voltage and the value of $\beta/\phi^{3/2}$ of field emitter is also improved. When the field emitter is fabricated in 3% of IPA solution, the size of field emitters is small. Therefore, the sharpness of these small field emitters may be destroyed by the MEVVA implantation.

From figure 5.2.3, there is improvement in the turn-on voltage and the value of $\beta/\phi^{3/2}$ of the field emitter when the etching time during fabrication is longer. When the etching time is longer, the size and density of field emitters increases. In this case, the total area and number of emitters for implanted SiC is also increased. The field emission of SiC field emitters that are prepared by etching for 20 minutes is larger when compared with the emitter prepared an etching for 10 minutes.

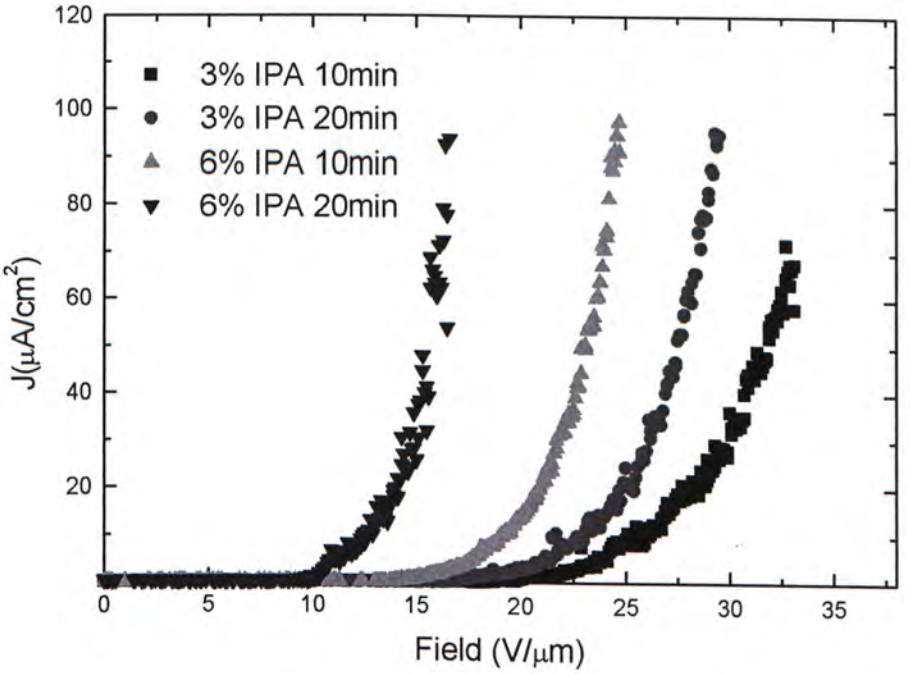

Figure 5.2.2 Field emission properties of emitter prepared by etching in 3% and 6% IPA with 5% KOH solution at 80°C for 10 min and 20 min. The SiC prepared by implantation with MEVVA ion source at an energy of 35keV to a dose of $1.0x10^{18}cm^{-2}$

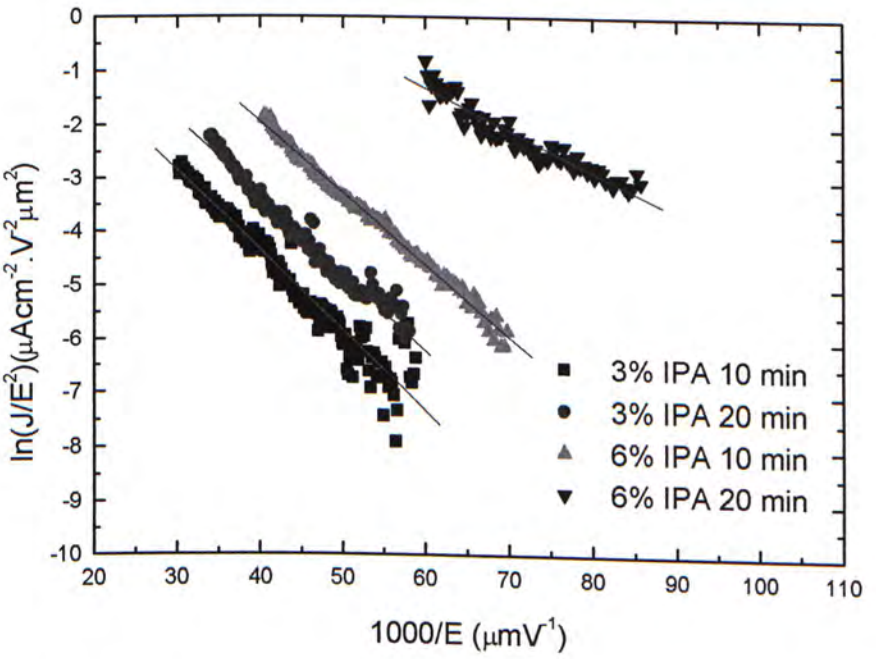

Figure 5.2.3 F-N properties of emitter prepared by etching in 3% and 6% IPA with 5% KOH solution at 80°C for 10 min and 20 min. The SiC prepared by implantation with MEVVA ion source at an energy of 35keV to a dose of $1.0x10^{18}cm^{-2}$

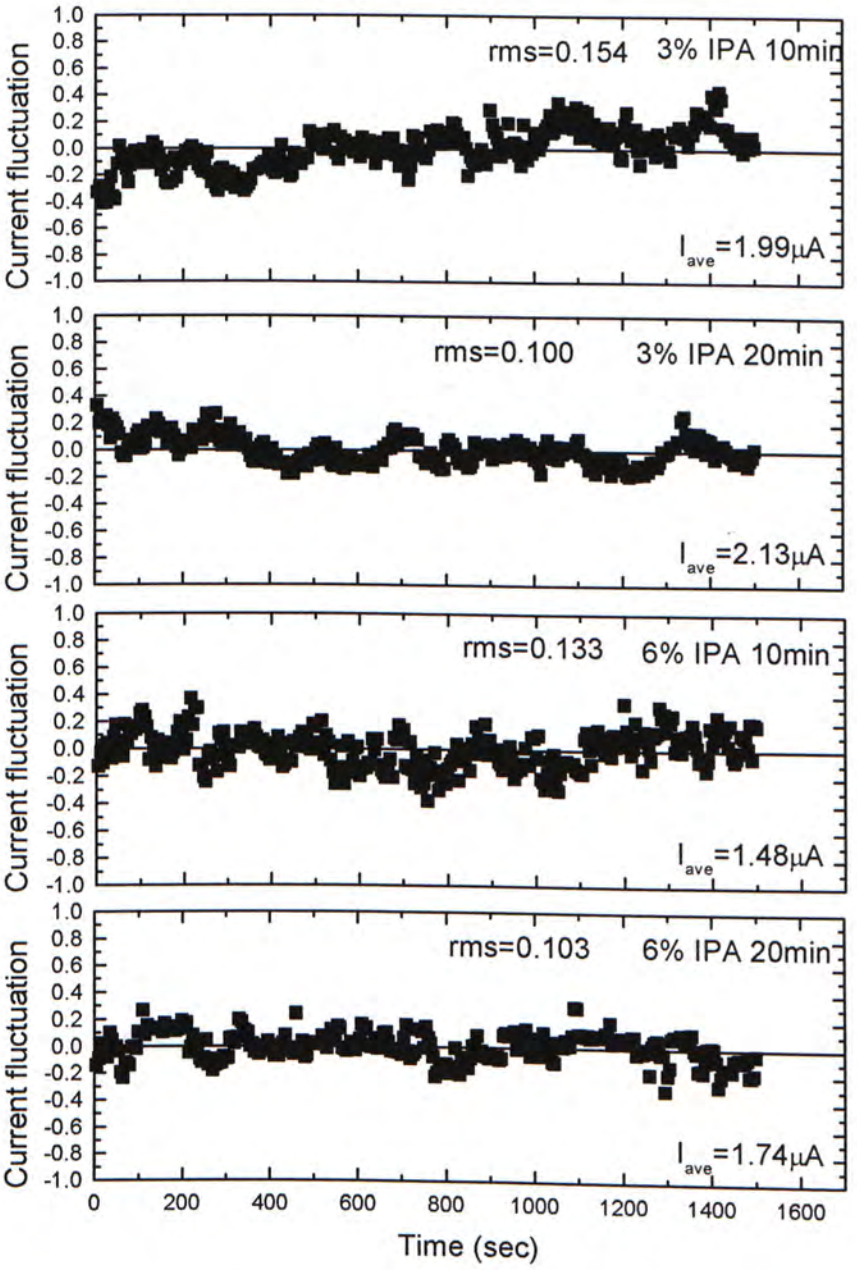

Figure 5.2.4 Fluctuation of emission current of FEA with SiC capping layers by MEVVA implantation

Figure 5.2.4 shows that the fluctuation of field emission current is improved when the etching time during processing is increased. The fluctuation of field emission current of field emitter should be due to the high dose carbon implantation into silicon. When the etching time is increased, the density and the size of field emitters increases and the field emission currents become more stable.

Table 5.2.2 Summary of field emission characteristic of field emitter with different concentration of IPA and etching time. SiC implanted by MEVVA ion source at an energy 35keV to doses of $1.0x10^{18}$

Material	Technique	Experimental condition	Current density ($\mu A/cm^2$)	Turn-on Field (V/μm)	$\beta/\phi^{3/2}$	Stability rms
Silicon (100) n-type 0.01Ωcm	SiC implanted by MEVVA 35keV doses of $1.0x10^{18}$	3% IPA, etching time 10 min	80	19	46	0.154
		3% IPA, etching time 20 min	100	17	47	0.100
		6% IPA, etching time 10 min	100	15	51	0.133
		6% IPA, etching time 20 min	100	10	88	0.103

5.2.4 Conclusion

Silicon field emitters with SiC/Si heterostructures formed by high dose carbon implantation into Si field emitters prepared by texturing are studied. The improvement in the field emission characteristics is correlated with the surface morphology of densely distributed small protrusions and the work function of SiC layer on the surface of the silicon field emitter.

Chapter Summary

In this chapter, field emitters coated with materials with different work functions was studied. In the first study, amorphous carbon (a-C) was coated on to flat silicon and porous silicon (PS) by using DC magnetron sputtering. In the second, silicon carbide (SiC) is formed by implantation of carbon into silicon field emitters using a MEVVA ion source.

We found that a-C coated Si and PS had improved field emission properties over silicon. There was a dramatic improvement in the turn-on voltage, the value of $\beta/\phi^{3/2}$, the stability of a-C coated Si and PS. In a-C coated PS layer, the emission current and the stability are also greatly improved. With the PS layer the roughness of a-C film is increased leading to an increased value of $\beta/\phi^{3/2}$. The overall current density and turn-on voltage of an a-C coated PS layer is about 900$\mu A/cm^2$ and 10-17V/μm respectively.

Silicon carbide (SiC) can improves the field emission properties of textured surfaces. SiC was prepared by high dose carbon implantation using a MEVVA ion source. The SiC layer improved the stability, turn-on voltage and the value of $\beta/\phi^{3/2}$ of textured surface. This is because the SiC surface layer improves both the surface morphology and work function of textured surface. The overall current density and turn-on voltage is about 100$\mu A/cm^2$ and 10-19V/μm respectively.

Chapter 6 Conclusions

The aim of this work is to fabricate silicon field emitters by using different methods to decrease the fabrication time and increase the field emission efficiency. Materials with different work function are coated onto different substrates to improve the field emission properties such as the current density, the turn-on voltage, the value of $\beta/\phi^{3/2}$ and stability. Table 6.1 is the summary of emission characteristics of field emitters fabricated for this study.

Table 6.1 Summary of field emission characteristic

Material	Technique	Experimental condition	Current density ($\mu A/cm^2$)	Turn-on Field (V/μm)	$\beta/\phi^{3/2}$	Stability Rms
Silicon (100) n-type 0.01Ωcm	Wet isotropic etching	Circle mask	130	35	15	0.216
	Two Step Anodization	Circle mask	100	27	19	0.119
		Square mask	100	28	19	0.122
		Chess mask	130	26	18	0.159
		Negative circle mask	100	33	19	0.143
Silicon (111) n-type 0.01Ωcm	Two Step Anodization	Circle mask	180	26	19	0.137
		Negative circle mask	70	27	22	0.106
Silicon (100) n-type 0.01Ωcm	5% Wet KOH etching	3% IPA, etching time 5 min	50	38	14	0.170
		3% IPA, etching time 10 min	500	24	21	0.141
		3% IPA, etching time 20 min	100	25	27	0.137
		6% IPA, etching time 5 min	200	27	20	0.180
		6% IPA, etching time 10 min	200	26	20	0.161
		6% IPA, etching time 20 min	300	24	22	0.145

Silicon (100) n-type 0.01Ωcm	Porous silicon layer Prepared by a Anodization current density is 10mA/cm^2	Anodization time is 15 sec	400	16	45	0.160
		Anodization time is 30 sec	500	12	28	0.119
		Anodization time is 1 min	100	25	45	0.219
Silicon (100) n-type 0.01Ωcm	a-C coating on planar Si by Sputtering	Sputtering time is 30 min	500	12	52	0.081
		Sputtering time is 60 min	300	15	46	0.107
Silicon (100) n-type 0.01Ωcm	Porous silicon layer then a-C coating 30min	Anodization time is 15 sec	900	12	98	0.097
		Anodization time is 30 sec	900	10	92	0.081
		Anodization time is 1 min	200	17	49	0.117
		Anodization time is 3 min	100	13	89	0.121
Silicon (100) n-type 0.01Ωcm	SiC implanted by MEVVA 35keV doses of 1.0x10^{18}	3% IPA, etching time 10 min	80	19	46	0.154
		3% IPA, etching time 20 min	100	17	47	0.100
		6% IPA, etching time 10 min	100	15	51	0.133
		6% IPA, etching time 20 min	100	10	88	0.103

The best values of emission currents at low electric field depends on the work function of the emitter surface material, nanometric size of the apex tip radius, micrometric size of the emitter (h/R >>1) and density of the field emitters.

In part I of this thesis, three fabrication methods are studied to improve the field emission properties by improving the field enhancement factor. First is the two-step anodization method. Second is anisotropic texturing method. Third is porous silicon formation. In chapter 4.1, the anodization of silicon with different concentrations of HF solutions is performed by a two step anodization method. High aspect ratio silicon field emitter arrays are fabricated on n-type silicon with a

resistivity of 0.01Ωcm. The turn-on voltage of field emitters fabricated by using this method is lower than the turn-on voltage the field emitters fabricated by using the conventional wet etching method. This arises from the increase in the surface roughness by the anodization process. Different shapes of silicon field emitters with good uniformity and reproducibility are fabricated on both <111> and <100> silicon.

There is slight improvement in the overall current density and the value of $\beta/\phi^{3/2}$ of these silicon field emitters. For further improvement, the size of the emitter apex has to be reduced and the density of the emitters has to be increased. The anisotropic texturing process is found to improve the size and density of silicon field emitters.

In chapter 4.2, the anisotropic texturing process is used to form randomly distributed silicon field emitters on the (100) crystallographic plane without using any masking pattern. The field emitter size and density strongly depends on the concentration of IPA and the etching time. Base size and height of field emitter is very small, about $1\mu m^2$ and $1\mu m$ respectively. The value of $\beta/\phi^{3/2}$ of the field emitters is also larger because of the larger density of field emitters. The overall current density of these field emitters is about $100\mu A/cm^2$. And the overall turn-on voltage is about 24-38 V/μm.

In chapter 4.3, the formation of porous silicon layer is studied. PS has high density of very sharp asperities, each of which can behave as a site for field emission. A dramatic improvement in the emission properties of PS is observed. The turn-on voltage of the PS layer is greatly improved to about 12-25 V/μm. The value of $\beta/\phi^{3/2}$ of porous silicon is also greatly improved due to the denser and sharper asperities. The stability of porous silicon as a field emitter is not very good because of the

change in resistance of amorphous porous silicon caused by continuous burning out of porous silicon fibres during field emission.

In part II of this thesis, materials with different work function are coated onto field emitters and the field emission characteristics are studied. First, amorphous carbon (a-C) is coated on flat silicon and porous silicon by using D.C. magnetron sputtering. Second, silicon carbide (SiC) is formed by implantation of carbon into silicon field emitters using a MEVVA ion source.

In chapter 5.1, Amorphous carbon (a-C) coated on flat silicon is found to have improved the field emission properties compared with planar silicon. The a-C film coating improves the stability, turn-on voltage and the value of $\beta/\phi^{3/2}$ for silicon. It also enhances the surface morphology for field emission. The stability of the a-C coating on silicon as the emitting surface is improved compared with uncoated silicon. The overall current density of a-C coated silicon is not very good because of low roughness.

A dramatic improvement in the turn-on voltage and the value of $\beta/\phi^{3/2}$ of a-C coated porous silicon as a field emitter is observed. The emission current and the stability of the field emitter are also greatly improved.

In chapter 5.2, silicon carbide (SiC) coating on randomly distributed silicon field emitters is studied. SiC is prepared by high dose carbon implantation by using a MEVVA ion source. The SiC layer improves the stability, turn-on voltage and the value of $\beta/\phi^{3/2}$ of the randomly distributed silicon field emitter. This is due to an improvement in the surface morphology and work function of the silicon field emitter.

Discussion of prior work on FEA made of Si and other materials

Emitter materials must have good mechanical, thermal, and electrical characteristics, and also be vacuum compatible. Another important consideration in choosing the right material is the suitability for fabricating high-aspect-ratio structures with well-established microfabrication techniques.

Silicon constitutes the primary material from which FEAs are fabricated with a turn-on field at about 30-35V/μm. The advantage of silicon FEA is that the existing micro-fabrication and coating facilities can be used.

Other materials with lower turn-on field have been coated on Si FEA. Single element metals, such as potassium, lithium, cesium, platinum, gold, nickel, metallic compounds such refractory metal nitrides and carbides, and various types of diamond, diamond-like-carbon films or carbon nanotube have been examined as coatings.

Transition metals such as Mo, Nb, Hf, and their metal carbides such as ZrC and HfC, are mechanically stable, and have high melting points. They have been fabricated onto high-aspect-ratio FEAs to achieve lower turn-on field and higher emission stability [151].

Noble metals such as Pd, Ir, and Pt have been used in the fabrication of emitters for field emission because of their chemical stability. Pd films show high efficiency of cold electron emission with a turn-on field at about 10V/μm [152].

The fabrication of FEAs using elemental metals such as Mo and Nb is well-established, but they are susceptible to oxidation. To avoid problems from the degradation of the tips, several alternate materials are being studied. Refractory metal carbides have lower work functions than refractory metals and also less

susceptible to oxidation. Other materials such as gallium nitride and various forms of carbon are being investigated as potential materials.

More recently, there has been a considerable amount of research on using carbon nanotubes in FEAs as they provide very high aspect ratios and exceptionally high field enhancement factors.

Comparison of the performance and characteristics of FEA fabricated with the state-of-the-art FEA

The most commonly used materials for FED studies are: Si, DLC and PS. The main emission characteristics for Silicon are about 10-30V/μm with a current density of about 10^{-6} to 10^{-9}A/cm^2. They have good stability in field emission characteristics [153]. In this thesis, the base size and the height of the emitter fabricated by using anisotropic texturing process is of about 1μm^2 and 1μm respectively and the density of emitters is very high. The overall current density of these field emitters is about 100μA/cm^2. The overall turn-on voltage is about 24-38 V/μm.

The turn-on voltage of DLC on Silicon is about 4-40V/μm with current density about 10^{-3}A/cm^2 [154, 155]. In this thesis, amorphous carbon (a-C) coated on porous silicon is also found to have improved the field emission properties. It also enhances the surface morphology for field emission. The turn-on voltage of the PS layer is improved to about 10-17 V/μm.

Porous Silicon formed on p-type silicon wafer can be used as a field emission enhancement method due to its nano-scale physical structure. The turn-on field of PS is about 1-10V/μm with current density about 10^{-3} to 10^{-6}A/cm^2. But they have not good field emission stability. The turn-on field of PS on a silicon tip array

is approximately 8V/μm [156]. In this thesis, the formation of porous silicon layer on n-type silicon is studied. PS on n-type silicon substrate has high density of very sharp asperities when compare with p-type silicon substrate. The turn-on voltage of the PS layer is improved to about 12-25 V/μm.

Further improvement

The fabrication of field emitters still has much room for improvement. Much work is needed to improve the stability and reliability of FEA emission in order to setup an imaging cell for investigating the distribution of the emission sites. This is needed in order to realize fabrication of a device.

In future, coating of n-type porous silicon layer with SiC nanorods by using CVD can be investigated. Nanorods as field emitters have high chemical stability and high mechanical strength comparison with carbon related materials such as diamond and amorphous carbon [157]. The nanorods can grow on small nano-sized holes in the porous silicon surface. In this case, the uniformity and the aspect ratio of SiC nanorods may be better.

Studies of various carbides on textured and porous silicon surfaces can be further investigated.

References

Chapter 1

[1] K.R. Shoulders, Adv. Computers 2 (1961) 135-293.
[2] C.A. Spindet, J. Appl. Phys. 39 (1968) 3504-3505.
[3] R.N. Thomas, H.C. Nathanson, Appl. Phys. Lett. 21 (1972) 384.
[4] D.O. Smith, J.S. Judge, M. Trongello, P.R. Thornto, US Patent 3,970,887.
[5] H.F Gray, Proc. Colloquium on Advances in Electron Emission, (1982) 24.
[6] H.F Gray, Proc. The 29th Int. Field Emission Symposium, (1982) 111.
[7] H.F Gray, Proc. G.J. Campisi, R.F. Greene, Technical Digest of the Int. electron Devices Meeting IEDM-86, (1986) 776.
[8] H.F Gray, Proc. G.J. Campisi, Mat. Res. Soc. Symp. Proc., vol. 76 (Materials Research Society, 1987) 25.

Chapter 2

[9] F.N. Barry, "Receiving tubes," in Components Handbook (MIT Radiation Laboratory Series), J.F. Blackburn, Ed. New York; McGraw-Hill, 1949, p. 517
[10] E.C. Kemble, The Fundamental Principles of Quantum Mechanics, 1st ed. New York: McGraw-Hill, (1937), sec. 21j
[11] I. Brodie and C.A. Spindt, Adv. Electron. Electron Phys., vol. 83 (1992) 1
[12] S.M. Sze, Physics of Semiconductor Devices. Wiley, New York, (1981)
[13] R. Gomer, "Field Emission and Field Ionization" Cambridge, MA; Harvard Univ. Press, (1961)
[14] I. Brodie, P.R. Schwoebel, Proceedings of the IEE 82 (1994) 1006
[15] R.H. Fowler, D.L. Nordheim, Roy. Soc. Proc. A 119 (1928) 173
[16] L.M. Baskin, O.I. Lvov, G.N. Fursey, Phys. Stat. Sol. 47 (1971) 49
[17] N.A. Cade, R. Johnston, Proc. 3rd Int. Vacuum Microelectronics Conf., Monterey, CA, 1990
[18] R.Greene, H.F. Gray, Proc, 1st Int. Vacuum Microelectronics Conf., Williamsburg, VA, 1998
[19] H.F. Gray, G.J. Campisi, R.F. Greene, Technical Digest of the Int. Electron Devices Meeting IEDM-86, (1986) 776
[20] S. Kanemaru, T. Hirano, H. Tanoue, J. Itoh, J. Vac. Sci. Technol. B 14 (1996) 1885
[21] F. Levy, R. Meyer, Proc. Int. Display Research Conf., San Diego, CA, (1991) 20
[22] R. Meyer, Proc. Int. Display Research Conf., Strasbourg, France, (1993) 189
[23] R. Meyer, A.Ghis, P.Rambaud and F.Muller, Proc. Japan Display Conf. (1995) 153
[24] C.E.Holland, C.A.Spindt, I.Brodie, J.B.Mooney and E.R.Westerberg, Reported at the Int. Display Conf. (London, UK, 1987)
[25] N. Kumar, et. al., Proc. of Society for Information Displays, Seattle, WA, USA, May (1993) 1009
[26] C.T. Sune, G.W. Jones, D. Vellenga, J. Vac. Sci. Technol. B 10 (1992) 2984
[27] Y.J. Yoon, Y Lu, B. Lalevic, R.J. Zeto, J. Vac. Sci. Technol. B 12 (1994) 648
[28] C.M. Park, M.S. Lim, M.K. Han, Y.I. Choi, Proc. 10th Int. Vacuum Microelectronics Conf, Kyongju, Korea, (1997) 176
[29] R.D. Underwood, S. Keller, U.K. Mishra, D. Kapolnek, B.Y. Keller, S.P. DenBaars, J. Vac. Sci. Technol. B 16 (1998), 822.

[30] C.A. Spindt, et. al., J. Appl. Phys., vol 47, (1976) 5248
[31] A. Ghis, et. al., J. Appl. Phys., vol 47, (1976) 5248
[32] A. Ghis, et. al., 3rd IVMC, Monterey, USA, July 1990
[33] J. Huang, US patent 5404070
[34] C.A. Spindt, et. al., IEEE trans. on Electron Devices, vol.36, (1989) 225
[35] A. Palevsky,el at., SID 94 Digest, P55
[36] F. Courreges, Information Display 11/96, (1996) 10
[37] J. D. Levine, 7th IVMC'94, Grenoble, France.
[38] C. Xie, IDRC'94, (1994) 444
[39] R. Meyer, Technical Digest of IVMC 91, Nagahama 1991
[40] P.H. Holloway, J. Sebastian, T. Trottier, H. Swart, R. Petersen, Solid State Technology 8/95, (1995) 47
[41] C.E Hunt, A.G. Chakhovskoi, J. Vac. Sci. Technol. B 15 (1997) 516
[42] R.T. Smith, Information Display 2/98, (1998) 12
[43] J.B. Price, H.R. Huffand, R.R. Burgess, The Electrochem. Soc. Softbound Proc. Series (1973) 339
[44] K. Okano, K. Hoshina, M. lida, Appl. Phys. Lett. 64 (1994) 2742
[45] S.J. Kim, B.K. Ju, Y.H. Lee, B.S. Park, Y.J. Baik, S.K. Lim, M.H. Oh, J. Vac. Sci. Technol. B 15 (1997) 499
[46] H. Robbins and B. Schwartz, J. Electrochem. Soc. 106 (1959) 505
[47] H. Robbins and B. Schwartz, J. Electrochem. Soc. 107 (1960) 108
[48] B. Schwartz and H. Robbins, J. Electrochem. Soc. 108 (1961) 365
[49] B. Schwartz and H. Robbins, J. Electrochem. Soc. 123 (1976) 1903
[50] S.S. Choi, S.H. Lim, D.W. Kim, M.Y. Jung and H. Jeon, J. Vac. Sci. Technol. B 17 (1999) 583
[51] Akihiko Hosono, Shinji Kawabuchi, Shinji Horibata, Soichiro Okuda, Hiroshi Harada, and Mikio Takai, J. Vac. Sci. Technol. B 17 (1999) 583
[52] Ted J. Hubbard, Erik K. Antonsson, J. Microelectromechanical Systems, vol. 3, March 1994.
[53] A.A. Talin, T.E. Felter, D.J. Devine, J. Vac. Sci. Technol. B 13 (1995) 448
[54] J.L. Shaw, D. Temple, H.E Gray, Proc. 7th Int. Vacuum Microelectronics Conf., Grenoble, France, (1994) 358
[55] S.L. Skala, D.A. Offiberg, A.A. Talin, T.E. Felter, Proc. Spring Meeting of the Materials Research Society, Pittsburgh, PA, (19a96) 387
[56] T. Xie, W.A. Mackie, P.R. Davis, J. Vac. Sci. Technol. B 14 (1996) 2090
[57] W.A. Mackie, R.L. Hartman, M.A. Anderson, PR. Davis, J. Vac. Sci. Technol. B 12 (1994) 722
[58] A.F. Myers, S.M. Camphausen, JJ. Cuorno, JJ. Hren, J. Liu, J. Bruley, J. Vac. Sci. Technol. B 14 (1996) 2024
[59] R. Schlesser, M.T. McClure, W.B. Choi, JJ. Hren, Z. Sitar, Appl. Phys. Lett. 70 (1997) 1596
[60] G. Wojak, V Zhirnov, W.B. Choi, J. Cuorno, J. Hren, Proc. 10th Int. Vacuum Microelectronics Confl, Kyongju, Korea, (1997) 146
[61] W.B. Choi, JJ. Cuorno, VY Zhirnov, A.F. Myers, JJ. Hren, Appl. Phys. Lett. 68 (1996) 720
[62] W.B. Choi, M.Q. Ding, VY Zhirnov, A.F. Myers, JJ. Hren, JJ. Cuorno, Proc. 10th Int. Vacuum Microelectronics Conf., Kyongju, Korea, (1997) 527

[63] T.G. McCauley, T.D. Corrigan, A.R. Krauss, O. Auciello, D. Zhou, D.M. Gruen, D. Temple, R.P.H. Chang, S.English, R.J. Nemanich, Proc. the Covalently Bonded Disordered Thin Film Materials Symposium, Material Research Society 1997 Fall Meeting, Boston, MA, 1997.
[64] M.W. Geiss, J.C. Twitchell, T.M. Lyszczarz, J. Vac. Sci. Technol. 14 (1996) 2060
[65] Z.H. Huang, P.H. Cutler, N.M. Miskovsky, T.E. Sullivan, J. Vac. Sci. Technol. B 13 (1995) 526
[66] R Lerner, P.H. Cutler, N.M. Miskovsky, J. Vac. Sci. Technol. B 15 (1997) 337
[67] P. Lerner, P.H. Cutler, N.M. Miskovsky, Proc. 10th Int. Vacuum Microelectronics Conf., Kyongju, Korea, (1997) 24
[68] R. Schlesser, B.L. McCarson, M.T. McClure, Z. Sitar, J. Vac. Sci. Technol. B 16 (1998) 689
[69] M.W. Geiss, J.C. Twitchell, T.M. Lyszczarz, J. Vac. Sci. Technol. 14 (1996) 2060
[70] A. Badzian, B.L. Weiss, R. Roy, T. Badzian, W. Drawl, P. Mistry, M.C. Turchan, Proc. 10th Int. Vacuum Microelectronics Conf., Kyongju, Korea, (1997) 546
[71] J.H. Jung, B.K. Ju, YH. Lee, J. Jang, M.H. Oh, MEE Electron Dev. Lett. 18 (1997) 197
[72] Q.A. Huang, M. Qirt, B. Zhang, J.K.O. Sin, Proc. 10th Int. Vacuum Microelectronics Conf., Kyongju, Korea, (1997) 300
[73] W.P. Kang, A. Wisitsora-at, LL. Davidson, M. Howell, DX Kerns, Q. Li, LE Xu, C.K. Kim, J. Vac. Sci. Technol. B 16 (1998) 732
[74] S.H. Kim, I.T. Han, N. Lee, LW Kim, J.H. Choi, J.M. Kim, Proc. 10th Int. Vacuum Microelectronics Conf., Kyongju, Korea, (1997) 480
[75] N. Kumar, H.K. Schmidt, M.H. Clark, A. Ross, B. Lin, L. Fredin, B. Baker, D. Patterson, W. Brookover, C. Xie, C. Hilbert, R.L. Fink, C.N. Potter, A. Krishnan, D. Elchman, Proc. SID Int. Symposium, San Jose, CA, 1994 (Society for information Display).
[76] S1 Kwon, Y.H. Shin, D.M. Aslam, J.D. Lee, J. Vac. Sci. Technol. B 16 (1998) 712
[77] C.M. Lin, F.Y. Chuang, LT. Lai, C.H. Wang, T.Y. Hsiu, M. Yokoyarna, I.N. Lin, LT. Tsai, C.M. Huang, W.C. Wang, Proc. 10th Int. Vacuum Microelectronics Conf., Kyongju, Korea, (1997) 151
[78] Y. Li, D.M. Aslam, S.J. Kwon, Proc. 10th Int. Vacuum Microelectronics Conf., Kyongju, Korea, (1997) 509
[79] K. Okano, T. Yamada, H. Ishihara, S. Koizurni, J. Itoh, Appl. Phys. Lett. 70 (1997) 2201
[80] A.N. Stepanova, E.I. Givargizov, L.Y Bormatova, V.V. Zhirnov, E.S. Mashkova, A.V. Molchanov, J. Vac. Sci. Technol. B 16 (1998) 678
[81] K.H. Park, S. Lee, K.-H. Song, J.1. Park, K.J. Park, S.Y Han, S.J. Na, N.Y. Lee, K.H. Koh, J. Vac. Sci. Technol. B 16 (1998) 724
[82] T. Sugino, S. Kawasaki, Y. Yokota, Y. lwasaki, J. Shirafuji, J. Vac. Sci. Technol. B 16 (1998) 720
[83] A.A. Talin, L.S. Pan, K.E McCarty, T.E. Felter, H.J. Doerr, R.F. Banshah, Appl. Phys. Lett. 69 (1996) 3842
[84] T.Y. Kosolapova, Handbook of High Temperature Compounds, Hemisphere Publishing Corporation, 1990.
[85] A. Uhlir, Bell Syst. Tech. J. 35, (1956) 333

[86] D.R. Turner, J. Electrochem. Soc. 105, (1958) 402
[87] M.I.J. Beale, N.G. Chew, M.J. Uren, A.G. Cullis, and J.D. Benjamin, Appl. Phys. Lett. 46, (1985) 86
[88] W.K. Yue, D.L. Parker, and M.H. Weichold, Tech. Dig. Int. Electron Devices Meet. 1990, (1990) 167
[89] M. Takai, M. Yamashita, H. Wille, S. Yura, S. Horibata, and M. Ototake, Appl. Phys. Lett. 66, (1995) 422
[90] E. Boswell, T.Y. Seong, and P.R. Wilshaw, J. Vac. Sci. Technol. B 13, (1995) 437
[91] J.R. Jessing, D.L. Parker, and M.H. Weichold, J. Vac. Sci. Technol. B 14, (1996) 1899
[92] K.J. Reeson, J. Stoemenos, and P.L.F. Hemment, Thin Solid Films 191, (1990) 147
[93] P. Martin, B. Baudin, M. Dupuy, A. Ermolieff, M. Olivier, A.M. Papon, and G. Rolland, J. Appl. Phys. 67, (1990) 2908
[94] A. Nejim, P.L.F. Hemment, and J. Stoemenos, Appl. Phys. Lett. 66 (1995) 2646.
[95] J.K.N. Lindner, B. Gotz, A. Frohnwieser, and B. Stritzker, Mater. Res. Soc. Symp. Proc. 396 (1996) 877
[96] H. Yan, R.W.M. Kwok, and S.P. Wong, Appl. Surf. Sci. 92 (1996) 61
[97] H. Yan, R.W.M. Kwok, and S.P. Wong, Diamond Relat. Mater. 5 (1996) 556
[98] S.P. Wong, L.C. Ho, Dihu Chen, W.S. Guo, H. Yan, and R.W.M. Kwok, Mater. Res. Soc. Symp. Proc. 438 (1997) 277
[99] Dihu chen, S.P. Wong, W.Y. Cheung, W. Wu, E.Z. Luo, J.B. Xu, I.H. Wilson and R.W.M. Kwok, Appl. Phys. Lett. 72 (1998) 1926
[100] Dihu chen, W.Y. Cheung, S.P. Wong, Nucl. Instr. And Meth. B 148 (1999) 589
[101] C.A. Spindt, C.E. Holland, P.R. Schwoebel, I. Brodie, J. Vac. Sci. Technol. B 16 (1998) 758
[102] C.A. Spindt, C.E. Holland, RR. Schwoebel, I. Brodie, J. Vac. Sci. Technol. B 14 (1996) 1986
[103] C.O. Bozler, C.T. Harris, S. Rabe, D.D. Rathman, M.A. Hollis, H.I. Smith, J. Vac. Sci. Technol. B 12 (1994) 629
[104] W.D. Goodhue, P.M. Nitishin, C.T. Harris, C.O. Bozler, D.D. Rathman, G.D. Johnson, M.A. Hollis, J. Vac. Sci. Technol. B 12 (1994) 693
[105] S. Itoh, T. Watanabe, K. Ohtsu, M. Taniguchi, S. Uzawa, N. Nishimura, J. Vac. Sci. Technol. B 13 (1996) 487

Chapter 3

[106] I.G. Brown and J.E. Galvin, Nucl. Instr. And Meth. B A245 (1986) 217

Chapter 4.1

[107] D.R. Turner, J. Electrochem. Soc. 105 (1958) 402.
[108] R.L. Smith, S.D. Collins, J. Appl. Phys. 71 (1992) R1.
[109] K. Imai, Solid-State Electronics, 24 (1981) 159.
[110] R.C. Frye, Proc. Material Res. Soc. Symp., 33 (1984) 53.
[111] R.C. Anderson, R.S. Muller and C.W. Tobias, J. of Electroelectromechanical Systems, 3 (1994) 10.
[112] K. Higa, K. Nishii and T. Asano, J. Vac. Sci. Technol. B16 (1998) 651.

[113] J.R. Jessing, H.R. Kim, D.L. Parker and M.H. Weichold, J. Vac. Sci. Technol. B16 (1998) 777.
[114] B. Hamilton, Semicond. Sci. Technol. 10 (1995) 1187.
[115] T.J. Hubbard, E.K. Antonsson, J. of Electroelectromechanical Systems, 3 (1994) 19
[116] A. van der Ziel, Solid State Physical Electronics (Prentice-Hall, Engle-wood Cliffs, NJ, (1968) 164.
[117] Y.M. Fung, W.Y. Cheung, I.H. Wilson, J.B. Xu and S.P. Wong, Mat. Res. Soc. Symp. Proc. 621 (2000) R 5.4

Chapter 4.2

[118] E. Vazsonyi, K. De Clercq, R. Einhaus, E. Van Kerschaver, K. Said, J. Poortmans, J. Szlufcik, J. Nijs, Solar Energy Materials & Solar Cells 57 (1999) 179.
[119] H. Seidel, J. Electrochem. Soc. 137 (1990) 3612.
[120] M. Declercq, J. Electrochem. Soc. 122 (1975) 545.
[121] H. Seidel, L. Csepregi, A. Heuberger, H. Baumgartel, J. Electrochem. Soc. 137 (1990) 3612.
[122] C. Moldovan, R. Iosub, D. Dascalu, G. Nechifor, Sensors and Actuators B58 (1999) 438.
[123] D.L. King, M.E. Buck, 22nd IEEE Photovoltaics Specialists Conf., (1991) 303.

Chapter 4.3

[124] P.R. Wilshaw and E.C. Boswell, J. Vac. Sci. Technol. B12, (1994) 662.
[125] E.C. Boswell and P.R. Wilshaw, J. Vac. Sci. Technol. B11, (1993) 412.
[126] E.C. Boswell, and P.R. Wilshaw, J. Vac. Sci. Technol. B14, (1996) 1895.
[127] Q. Mei, T. Tamagawa, C. Ye, Y. Lin, S. Zurn and D.L. Polla, J. Vac. Sci. Technol. B11, (1993) 493
[128] I. Kleps, D. Nicolaescu, C. Lungu, G. Musa, C. Bostan, F. Caccavale, Appl. Surf. Sci. 111(1997) 186.
[129] M. Takai, M. Yamashita, H. Wille, S. Yura, S. Horibata and M. Ototake, Appl. Phys. Lett. 66, (1995) 422.
[130] D. Nicolaescu, V. Filip, Peter R. Wilshaw, Appl. Surf. Sci. 94/95 (1996) 79.
[131] J.R. Jessing, H.R. Kim, D.L. Parker, and M.H. Weichold, J. Vac. Sci. Technol. B16, (1998) 777.
[132] A. Uhlir, Bell Syst. Tech. J. 35, (1956) 333.
[133] D.R. Turner, J. Electrochem. Soc. 105, (1958) 402.
[134] M. I. J. Beale, N.G. Chew, M. J. Uren, A.G. Cullis, and J.D. Benjamin, Appl. Phys. Lett. 46, (1985) 86.
[135] W.K. Yue, D.L. Parker, and M. H. Weichold, Tech. Dig. Int. Electron Devices Meet. 1990, (1990) 167.
[136] J.R. Jessing, D.L. Parker, M.H. Weichold, J. Vac. Sci. Technol. B14, (1996) 1899.
[137] M.I.J. Beale, J.D. Benjamin, M.J. Uren, N.G. Chew, and A.G. Callis, J. Cryst. Growth 73, (1985) 622.
[138] A.A. Evtukh, V.G. Litovchenko, R.I. Marchenko, and N.I. Klyui, J. Vac. Sci. Technol. B14, (1996) 2130.
[139] P.C. Searson, Appl. Phys. Lett. 56, (1990) 236.

Chapter 5.1

[140] J. Robertson, Diam. Rel. Mater 5 (1996) 7997.

[141] O. Groning, O.M. Kuttel, P. Groning, L. Schlapbach, Appl. Surf. Sci. 111 (1997) 135.

[142] D.W. Han, Y.H. Kim, D.J. Choi, E.J. Chi, W.Y. Yoon, H.K. Baik, Thin Solid Films 355 (1999) 199.

[143] E.J. Chi, J.Y. Shim, H.K. Baik, J. Vac. Sci. Technol. B17 (1999) 728.

[144] E.J. Chi, J.Y. Shim, H.K. Baik, J. Vac. Sci. Technol. B16 (1998) 1219.

[145] J. Liu, V.V. Zhirnov, A.F. Myers, G.J. Wojak, W.B. Choi, J.J. Hren, S.D. Wolter, M.T. McClure, B.R. Stoner, LT. Glass, J. Vac. Sci. Technol. B13 (1995) 442.

[146] W.P. Kang, LL. Davidson, M. Howell, B. Bhuva, D.L. Kinser, DY Kerns, Q. Li, LF. Xu, J. Vac. Sci. Technol. B14 (1996) 2068.

[147] V.V. Zhirnov, A.B. Voronin, E.I. Givargizov, A.L. Meshcheryakova, J. Vac. Sci. Technol. B14 (1996) 2034.

Chapter 5.2

[145] Dihu chen, W.Y. Cheung, S.P. Wong, Y.M. Fung, J.B. Xu, I.H. Wilson and R.W.M. Kwok, J. Vac. Sci. Technol. A17 (1999) 2019.

Chapter 6

[146] K. Higa and T. Asano, Jpn. J. Appl. Phys., Part 1 35, 6648 (1996).

[147] K. Higa, K. Nishii, and T. Asano, Technical Digital of Microprocess and Nanotechnology Conference, 1997, p.108.

[148] K. Higa, K. Nishii, and T. Asano, Appl. Phys. Lett. 71 (1997) 983.

[149] K. Higa, K. Nishii, and T. Asano, Technical Digest of 10th International Vacuum Microelectronics Conference, 1997, p.78.

[150] K. Higa, K. Nishii, and T. Asano, J. Vac. Sci. Technol. B 16 (1998) 651.

[151] W.A. Mackie, T. Xie, J. E. Blackwood, S. C. Williams, and P. R. Davis, J. Vac. Sci. Technol. B 16 (1998) 1215.

[152] E. Czerwosz, P. Dluzewski, W. Gieraltowski J. Vac. Sci. Technol. B 18 (2000) 1064.

[153] M. Yoshiki, N. Furutake, J. Vac. Sci. Technol. B 17(2) (1999) 567.

[154] F. J. himpsel, J. A. Knapp, Phys. Rev. B. B20 (1979) 624.

[155] F. Lacher, C. Wild, Diamond Relat. Mater. 6 (1997) 1111.

[156] J. R. Jessing, J. Vac. Sci. Technol. B 14 (1996) 1899.

[157] K. H. Chen, J. –J. Wu, Diamond Related Material. 9 (2000) 1249.

List of publications

1. Dihu Chen, W.Y. Cheung, S.P. Wong, Y.M. Fung, J.B. Xu, and I. H. Wilson, " Field Emission Characteristics of SiC Capped Si Tip Array by Ion Beam Synthesis", J. Vac. Sci. Technol. A 17 (1999) 2109-2112.

2. Y.M. Fung, W.Y. Cheung, I.H. Wilson, J.B. Xu and S.P. Wong, "Silicon Field Emitter Array BY Fast Anodization Method", Mat. Res. Soc. Symp. Proc. Vol. 621. (2000) R 5.4

3. Y.M. Fung, W.Y. Cheung, I.H. Wilson, Dihu Chen, J.B.Xu, S.P. Wong, "Electron Field Emission Characteristics of Textured Silicon Surfaces", J. Vac. Sci. Technol. May/Jun (2001) .